SEMICONDUCTOR LASER DIODE MODELING AND LINEARIZATION BY PREDISTORTION

A Thesis

Submitted to the College of Graduate Studies and Research

in Partial Fulfillment of the Requirements

for the Degree of Master of Science

in the Department of Electrical Engineering

University of Saskatchewan

by

Mike Sieben

Saskatoon, Saskatchewan

August 1994

COPYRIGHT

UNIVERSITY OF SASKATCHEWAN

Electrical Engineering Abstract 94A405

SEMICONDUCTOR LASER DIODE MODELING AND LINEARIZATION BY PREDISTORTION

Student: Mike Sieben Supervisor: David Dodds

M. Sc. Thesis Presented to the

College of Graduate Studies and Research

August, 1994

ABSTRACT

Fiber optic transmission systems are expected to become viable options for delivery of telephone, data and cable television to subscribers. Semiconductor lasers have been used as transmitters in digital applications for many years, however, new analog applications are now being proposed. The inhibiting factor for analog applications such as cable television or common antennae television (CATV) distribution is the inherent nonlinearity exhibited by semiconductor lasers. These nonlinear characteristics result in harmonic distortion and intermodulation distortion which degrade the system performance and limit the number of CATV channels that can be multiplexed on a fiber. Understanding the nature of these nonlinearities in semiconductor lasers is essential to designing compensation circuits to linearize the laser and improve its performance. This thesis

presents predistortion as an appropriate linearization technique for semiconductor lasers. The predistortion block is incorporated prior to the laser and its ideal characteristics are the inverse of the laser characteristics. Two models of a single-mode Fabry-Perot semiconductor laser have been developed in order to predict the laser's analog transmission performance. The first model is based on an analysis of the single-mode semiconductor laser rate equations in the frequency domain. The laser and predistorter blocks have been modeled with Volterra kernels. This thesis also presents a second laser model based on a time domain simulation of the rate equations using a circuit simulation software package. The time domain model for the predistorter was developed from its Volterra kernels. The performance of the Volterra based predistorter was then evaluated by simulating the time domain predistorter model together with the time domain model of the Fabry-Perot semiconductor laser. Finally, performance of this compensation design was tested by building a hardware prototype. All results show that nonlinear distortion levels, as measured by harmonic distortion and intermodulation distortion, decrease when predistortion is employed prior to the laser.

ACKNOWLEDGMENTS

The author thanks Professor David E. Dodds for his guidance and instruction throughout the course of this work. His advice and assistance in the preparation of this thesis are gratefully appreciated.

The author also thanks Mr. Garth Wells and Mr. Greg Erker of TR Labs for their advice and comments during the assembly of the hardware circuits used in the research.

This research was partially supported by Telecommunication Research Laboratories (TR Labs) and the Natural Sciences and Engineering Research Council of Canada (NSERC).

TABLE OF CONTENTS

LIST OF TABLES

LIST OF FIGURES

LIST OF ABBREVIATIONS

AM-VSB	Amplitude Modulation-Vestigial Sideband
AT&T	American Telegraph and Telephone
BISDN	Broadband Integrated Services Digital Network
BOSS	Block Oriented System Software
CATV	Common Antennae Television
CSO	Composite Second Order
CTB	Composite Triple Beat
dBc	Decibels with respect to the carrier
DFB	Distributed Feedback
ECA-2	Electronic Circuit Analysis-2
FFT	Fast Fourier Transform
FM	Frequency Modulation
FTTC	Fiber to the Curb
FTTH	Fiber to the Home
HD	Harmonic Distortion
IM	Intensity Modulation
IMD	Intermodulation Distortion
IMP	Intermodulation Product
LD	Laser Diode
LED	Light Emitting Diode
PD	Photodetector

RD	Resonance Distortion
SCM	Subcarrier Modulation
SNR	Signal to Noise Ratio
TV	Television

1. INTRODUCTION

1.1 Historical Background

Optical communications have developed from primitive beginnings to a very sophisticated level over the past century. It is suggested [1] that Alexander Graham Bell was the first to develop a modern optical communication system in 1880. He was issued a patent for a "photo-phone" which could transmit voice over distances of several hundred meters. The photo-phone was based on modulating reflected sunlight by causing a mirror to vibrate. The receiver was a photocell. Early forms of optical transmission like this were through the atmosphere and as a result, the weather hampered many of the transmissions.

It was soon realized that an optical waveguide was needed for reliable transmission. D. Hondros and P. Debye [2] pioneered work on dielectric waveguides for the propagation of radio waves. F. P. Kapron *et al* [3] then developed a quartz fiber in 1970 with an optical attenuation of 20 dB/km. From that time on, research on materials for optical transmission has made impressive progress. Losses were reduced from 20 dB/km to 4 dB/km in 1973 and to 0.2 dB/km in 1979.

One of the major steps in developing modern optical communication systems was the development of the laser in 1960. Later, in 1962, the first semiconductor laser was developed. Research continued in the area of developing semiconductor lasers for optical fibers. Some of the first lasers developed were at 0.83 μm wavelength. The prospect for

lower fiber losses at longer wavelengths led to intensive research for lasers and photodetectors at 1.3 μm and later 1.55 μm wavelengths.

Modern optical communication systems have developed into three principal subsystems: the transmitter, the channel, and the receiver. The optical transmitter usually consists of a forward biased semiconductor junction diode. It can be either a light emitting diode (LED) or a laser diode (LD). The channel is an optical fiber and the receiver is a photodetector (PD) consisting of a reverse-biased semiconductor junction diode.

New and more sophisticated systems are being developed and proposed for the future. New fiber materials and fabrication methods can increase the available bandwidth and decrease losses. Further development in the area of semiconductor lasers will increase the linearity of the laser's input/output characteristic and increase the capacity for data transmission.

1.2 Fiber Optic Applications

Fiber optics have a number of advantages which make them attractive in a wide range of applications. Very low attenuation and large bandwidth are two major ones. In addition, optical fibers are smaller and lighter than trunking coaxial cable and have no problems with ground loops.

To date, the most extensive application of fiber optics has been in the telephone industry. The rapid advances in the 1970's led to a series of field experiments and early applications in North America [4]-[6], Europe [7], and Japan [8],[9]. The first commercial long distance optical fiber telephone system was put into service by the American Telephone and Telegraph Company (AT&T) in 1983 [10]. Today, many major cities throughout North America are linked by an optical fiber system. In addition, many

developed countries are linked by transatlantic and transpacific optical systems. Fiber optic systems in the telephone industry are exclusively digital due to the digital switching, multiplexing and transmission technology currently in use.

More recently, fiber optic systems are becoming popular for video applications as well. The limited amount of radio bandwidth and the high loss of coaxial cable has limited the growth of video transmission to customers. Fiber optics with its low loss and high bandwidth is a prime alternative. Several video distribution systems have been proposed using digital modulation [11]-[14] or frequency-modulated (FM) [15]-[21] subcarrier modulation (SCM). These techniques however, have major drawbacks in the fact that they require very large bandwidths (30 to 100 MHz per channel) and require a conversion from analog to digital or FM and back again. The ideal solution to these problems is to eliminate the format conversion and transmit the same multicarrier video spectrum used by the cable television industry [22]-[24].

The current CATV format is Amplitude Modulation-Vestigial Sideband (AM-VSB) and it is expected to remain this way even if the current coaxial cable systems are replaced with fiber optic systems. The prime reason is economic. Almost every television (TV) set in North America is built for AM-VSB format and as such, people are reluctant to purchase a new digital TV receiver. As a result, the easiest way to implement a fiber optic system in the current cable television network is to make the fiber system transmit AM-VSB analog signals.

Current CATV systems have a tree and branch architecture. At the headend of the system, signals are locally generated or they are brought in via radio or satellite. From this point, multiple channel TV signals are transmitted to remote locations in the community over trunk coaxial cables. These long coaxial cables run from the headend to the "neighborhood." From this point, feeder cables run from the trunking system drop-off point to the tap outside the subscriber's home. The last element in the transmission path is

the subscriber drop which is the residential wiring portion of the system connecting the feeder drop-off point to the subscriber's TV set.

In Fiber to the Curb (FTTC) architectures, the trunk and feeder coaxial cables of the CATV network are replaced with fiber optics [25]. The lower transmission losses in fiber permit a greater area of coverage. The coverage of coaxial CATV systems is limited not by the coaxial cables themselves but by the accumulation of noise from the cascaded amplifiers that drive the system. Amplifiers are required on these cables at intervals of 2000 feet. After approximately 27 to 30 amplifiers, the signal quality is rendered unsatisfactory for viewing.

In Fiber to the Home (FTTH) architecture's, the fiber optic cable is extended to the subscribers home. As previously stated, fiber optics offer a larger bandwidth than coaxial cable thus increasing the potential number of video channels transmitted to the subscriber.

As previously stated, the current CATV format for transmitting video is AM-VSB. This is an analog format and as such, the linearity of the transmission system is important in maintaining the Signal to Noise (SNR) at the receiver. In current FTTC and FTTH systems, the limiting sub-system for linearity is the semiconductor laser. Consequently, much research is being carried out on the linearity of semiconductor lasers [26]-[48]. Currently, laser diodes are being built which are linear enough to transmit up to 60 video channels and still meet the CATV distortion requirements. Improved fabrication techniques, device structures and geometries have had some success. However, this linearity comes with cost. An alternative is to use circuit techniques to linearize inexpensive lasers which have poor linearity.

Integration of telephone and video on to one fiber optic line is the next step being considered by communications researchers. Combining video, telephone and further items such as e-mail lines, alarms and meter readings on to one line can be proven to have large

economic advantages since the optical line can replace all of the individual subscriber lines currently used except power ones. Field trials of fiber optic broad-band integrated systems are also being carried out with the emphasis on combining CATV and Broadband Integrated Services Digital Network (BISDN) services on to one fiber [49]-[51]. Proposed future applications in this area look promising; however, the linearity of the laser will be an important factor in determining the data transmission capabilities for these systems as well.

1.3 Thesis Objectives

There were four main objectives of the research described in this thesis. The first objective was to review the linearization techniques available for improving the linearity of semiconductor lasers in analog applications. Based on this review, a selection of the most appropriate scheme for this research has been made. The second objective was to model the rate equations which describe the interaction of current and light in the semiconductor laser. This modeling attempts to demonstrate the frequency dependence of the lasers nonlinearities. The third objective was to develop the linearization scheme selected for this research. The linearization scheme is to compensate for the laser's nonlinearities over a broad frequency range. The fourth and final objective was to attempt to build and test a prototype of the linearization circuit with a laser diode. The hardware circuit should cost less than the laser it is correcting.

1.4 Thesis Organization

Chapter 2 presents a brief review of the general principles of lasers and the basics of semiconductor laser diodes. In addition, the basics of laser nonlinearity in analog applications and the rate equations describing the semiconductor laser are presented.

Chapter 3 presents a review of the different types of compensation techniques that are available for improving the linearity of semiconductor lasers. Based on this review, the best technique for this research was selected. This technique is predistortion.

Chapter 4 presents an analysis of the single-mode rate equations and introduces the Volterra transfer functions that model the dynamic behavior of the laser. A Volterra model is developed for the laser diode and the predistorter.

Chapter 5 presents results of a harmonic analysis of the Volterra model of the laser with and without predistortion.

Chapter 6 presents details of how the time domain model of the laser was created. The development of the time domain model of the predistorter is also included.

Chapter 7 presents results of the distortion measurements of the time domain model of the laser with and without predistortion. The nonlinear performance is measured in terms of harmonic and intermodulation distortion levels.

Chapter 8 presents details of how a predistorter circuit was constructed in hardware. Again, the harmonic and intermodulation distortion levels at the output of the laser with and without predistortion are included.

Chapter 9 contains the conclusions of this work and some suggestions for future research.

2. LASER DIODES

The semiconductor laser is the dominant laser in optical fiber communications. The spectral and temporal properties of the laser are significantly better than those of the LED and, thus, make it more popular in optical communication systems. These lasers are of the same order size as optical fibers and this general similarity in size makes coupling the light wave from the laser into the optical fiber more efficient than would be possible with lasers of much larger physical dimensions such as gas lasers. Further, solid state lasers are rugged and do not draw a lot of power like gas and liquid lasers.

2.1 General

The operation of most lasers can be described by considering the electron transitions which may occur between two energy levels of a hypothetical atomic system. As described in [52], the higher energy level can be called E_h and the lower energy level E_l. When an electron in an atom undergoes transitions between these two energy states it either emits or absorbs a photon which can be described in terms of a wave of frequency f for which $E_h - E_l = hf$, where $h = 6.626 \times 10^{-34}$ Js (Plank's constant).

If the electron is in the lower level E_l, then in the presence of photons of energy $(E_h - E_l)$ it may be excited to the upper level E_h by absorbing a photon. Alternatively, if the electron is in the level E_h, it may return to the ground state with the emission of a photon. The emission process may occur in two distinct ways. These are: (1) the spontaneous emission process in which the electron drops to the lower energy level in an

entirely random way and (2) the stimulated emission process in which the electron is "triggered" to undergo the transition by the presence of photons of energy $(E_h - E_l)$. The absorption and emission processes are illustrated in Figure 2.1 (a), (b) and (c).

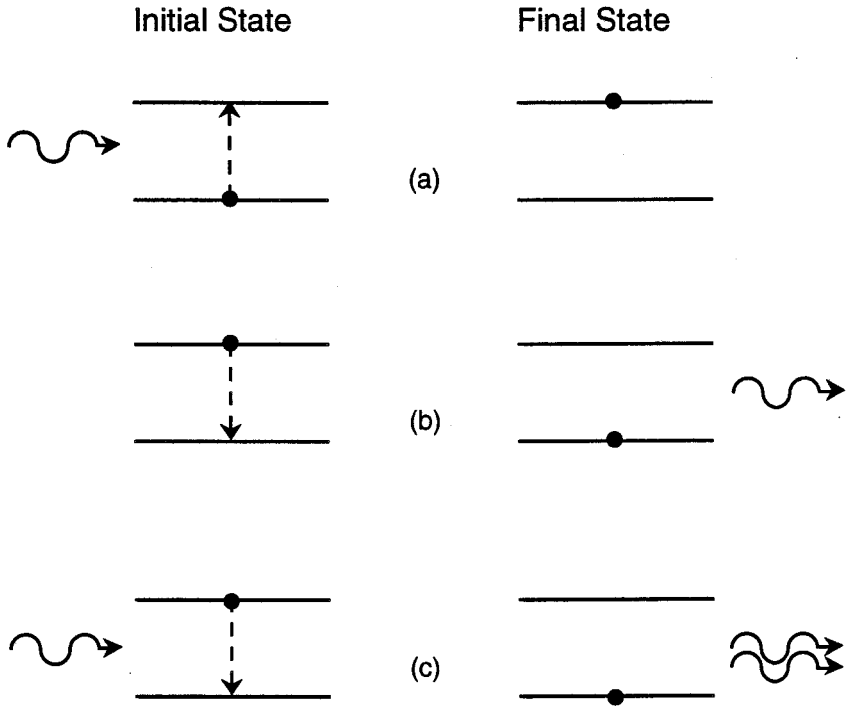

Figure 2.1 Energy level diagrams illustrating (a) absorption, (b) spontaneous emission and (c) stimulated emission. The black dot indicates the state of the atom before and after the transition.(Adapted from [52])

When a number of atoms are considered, stimulated emission is balanced by absorption in thermal equilibrium. In this state, the density of the electrons in the lower energy level is more than the density of the electrons in the upper energy level. The light amplification or lasing condition only happens when the density of the electrons in the upper state is larger than the density in the lower state. This condition is called population inversion. This inversion is obtained by pumping electrons into the upper energy level.

Since the spontaneous radiation from any atom is emitted at random, the radiation emitted by a large number of atoms will be incoherent. In contrast to this, the stimulated emission process results in coherent radiation as the waves associated with the stimulating and stimulated photons have identical frequencies, are in phase and have the same state of polarization. This means that with stimulated emission the amplitude of an incident wave can grow as it passes through a collection of atoms in what becomes an amplification process.

2.2 Basics of Semiconductor Lasers

As described in [52], semiconductor lasers work on this principle of interaction between light and electrons in elevated energy states. The p-n junction provides the active medium, so to obtain laser action, the requirements of population inversion and optical feedback must be met. To obtain stimulated emission there must be a region of the device where there are many excited electrons and vacant states (holes) present together. This is achieved by forward biasing a junction formed from very heavily doped n and p materials. In n^+ type material, the Fermi level lies within the conduction band and similarly for p^+ type material, the Fermi level lies in the valence band. The equilibrium and forward biased energy diagrams for a junction formed from such materials is shown in Figure 2.2. When the junction is forward biased with a voltage that is nearly equal to the energy gap voltage E_g, electrons and holes are injected across the junction in sufficient numbers to create a population inversion in a narrow zone called the active region. Figure 2.3 shows the active region in a p-n junction.

The thickness of the active region can be approximated by using the diffusion length of the electrons injected into the p region, assuming that the doping level of the p region is less than that of the n region so that the junction current is carried substantially by electrons.

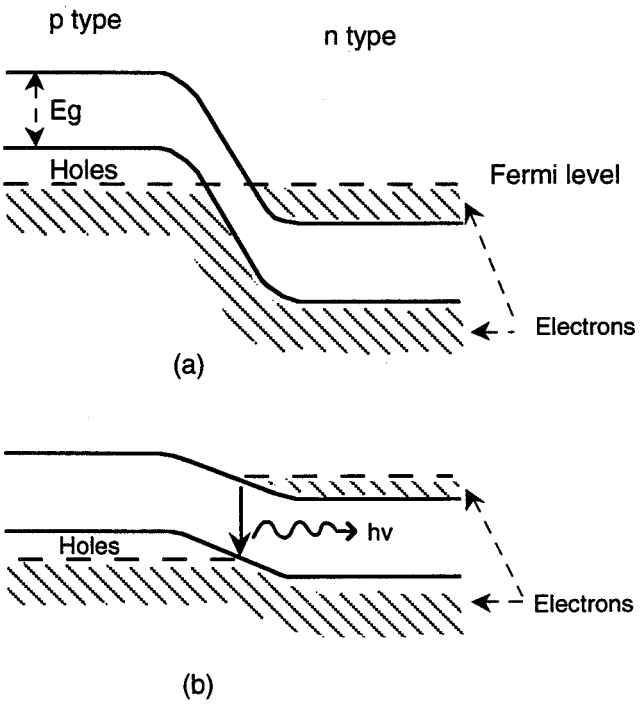

Figure 2.2 Doped p-n junction (a) in equilibrium and (b) with forward bias (Adapted from [52])

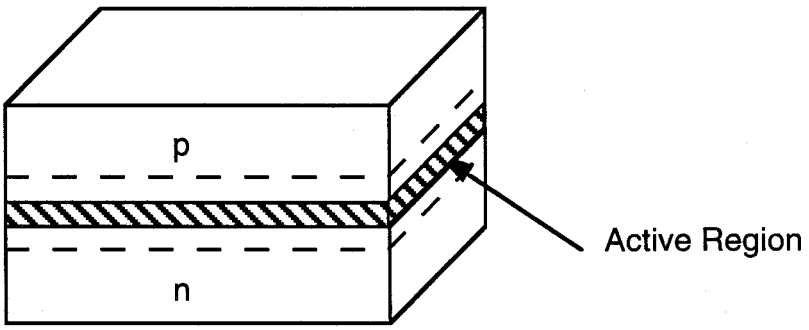

Figure 2.3 Diagram showing the active region of a semiconductor laser (Adapted from [52])

If the injected carrier concentration becomes large enough, the stimulated emission can exceed the absorption so that optical gain can be achieved in the active region. Laser

oscillations occur when the round trip gain of the photon within the cavity exceeds the total losses over the same distance. In semiconductors, the principal losses are due to scattering at optical inhomogeneities in the semiconductor material and free carrier absorption. The latter results when electrons and holes absorb a photon and move to higher energy states in the conduction band or valence band respectively. The carriers then return to lower energy states by nonradiative processes.

In larger lasers, mirrors are placed at the ends of the amplifying medium to maintain the lasing condition. The optical cavity thus plays the role of an oscillator as it provides a positive feedback for the photons by reflection on the mirrors at the end of the cavity. In the case of diode lasers, it is generally not necessary to use external mirrors to provide positive feedback. The high refractive index of the semiconductor material provides a reflectance at the material/air interface that is sufficient in most cases. If higher reflectance is required, a dielectric layer can be added to one end and to the sides to confine the active region. A general structure in shown in Figure 2.4.

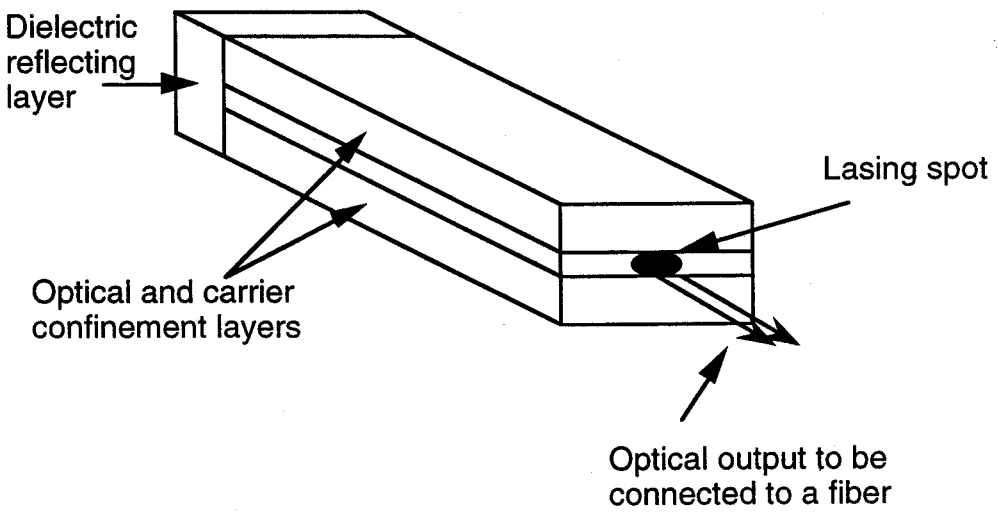

Figure 2.4 Resonator cavity for a semiconductor laser (Adapted from [53])

The onset of laser action at the threshold current density is detected by an abrupt increase in the radiance of the emitting region, as shown in Figure 2.5.

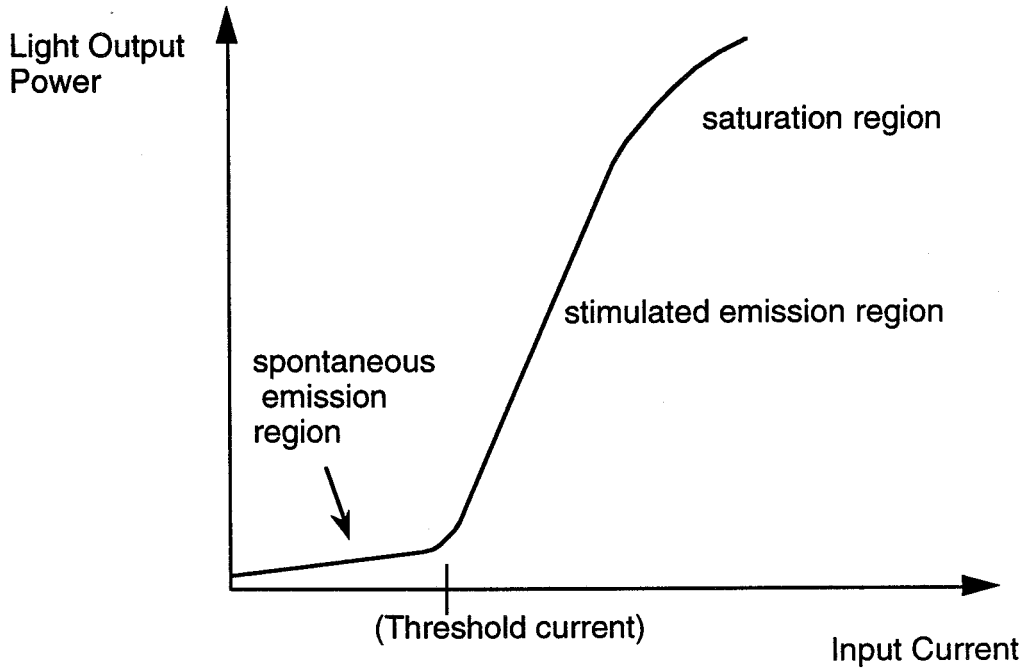

Figure 2.5 Light-current characteristic of a semiconductor laser

2.3 Laser Modes

The frequencies or wavelengths at which a laser will operate are determined by the resonant frequencies of the optical cavity and the frequency range over which stimulated emission can provide sufficient gain. As described in [1], resonant frequencies are determined by satisfying the phase condition for oscillation. If the phase condition is satisfied at multiple frequencies, then all of those for which there is adequate gain will oscillate. Each such oscillation is called a mode. The second requirement for oscillation is that the gain at the frequency of oscillation must be greater than the cavity losses at that frequency.

If the gain versus wavelength and the losses of the laser are known, then the range of frequencies for which the gain exceeds the loss can be determined. The laser will operate at any frequency within this range for which the phase condition is satisfied. Figure 2.6 shows a typical spectrum of a laser with more than one oscillating mode having sufficient gain and Figure 2.7 shows a laser with only one oscillating mode.

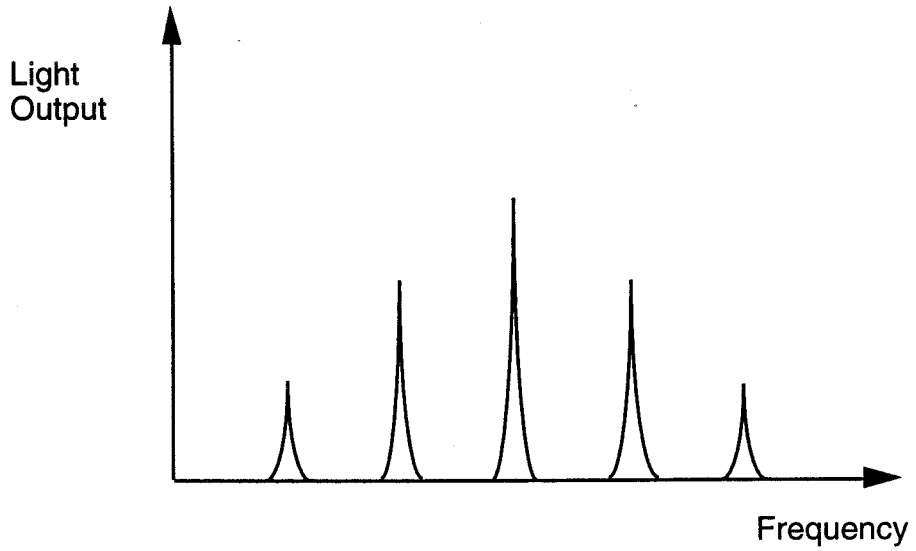

Figure 2.6 Spectrum of the output of a multimode laser

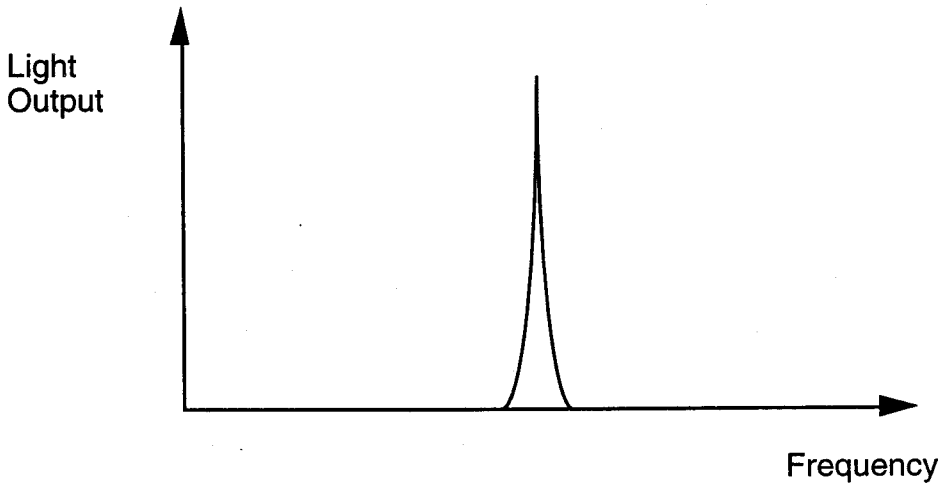

Figure 2.7 Spectrum of the output of a singlemode laser

Lasers with more than one mode propagating are called multimode lasers and ones with only one mode propagating are called singlemode lasers. In optical fiber communications, the light wave from a multimode laser has greater spectral width and therefore greater intermodal dispersion than a single mode laser. Consequently, single mode lasers are used more frequently and are used in the applications discussed in this thesis.

2.4 Laser Diode Nonlinearity

As previously mentioned, laser diodes are well-suited optical sources for optical communication systems. Current optical communication systems can be digital or analog in nature. When laser diodes are used as optical sources for wide-band analog applications, the linearity of the laser diode is an important factor.

In an analog system, the time-varying electric analog signal $s(t)$ is used to modulate directly an optical source about a bias point I_b, as shown in Figure 2.8. The optical output power is expressed as [53]:

$$P(t) = P_b[1 + ms(t)] \tag{2.1}$$

where:

P_b = optical output power when there is no signal
$s(t)$ = analog signal
m = modulation depth

The modulation index is defined as:

$$m = \frac{\Delta I}{I_b - I_{th}} \tag{2.2}$$

where:

ΔI = zero to peak modulation variation in current
I_{th} = threshold current
I_b = bias current

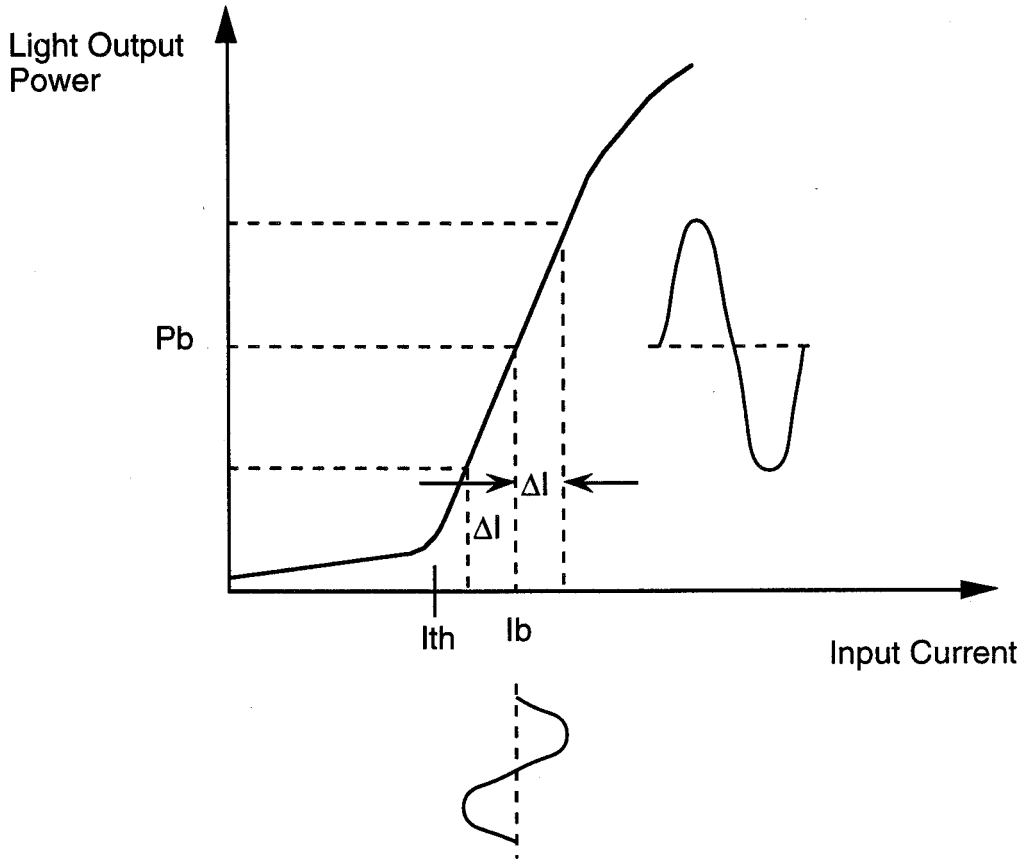

Figure 2.8 Bias point and amplitude modulation range for analog applications (Adapted from [53])

To prevent distortions in the output signal, the modulation must be confined to the linear region of the curve for optical output versus drive current. Furthermore, if ΔI is greater than $I_b - I_{th}$ (that is m is greater than 100 percent), the lower portion of the signal can be cut off and severe distortion can result. Typical m values for analog applications range from 0.2 to 0.5.

In analog applications, any device nonlinearities will create frequency components in the output signal that were not present in the input signal. Two important nonlinear terms of measurement described in [53] are harmonic distortion (HD) and intermodulation

distortion (IMD). If the signal input to a nonlinear device is a simple sine wave $x(t) = A\sin\omega t$, the output will be:

$$y(t) = A_o + A_1 \sin\omega t + A_2 \sin 2\omega t + A_3 \sin 3\omega t + \cdots \tag{2.3}$$

That is, the output signal will consist of a component at the frequency ω plus spurious components at zero frequency, at the second harmonic frequency 2ω, at the third harmonic frequency, and so on. This effect is known as harmonic distortion. The distortion in decibels for an *n-th* order term is:

$$\textit{n-th order harmonic distortion} = 20\log_{10}\left|\frac{A_n}{A_1}\right| \tag{2.4}$$

To determine intermodulation distortion, the modulating signal of a nonlinear device is taken to be the sum of two sine waves $x(t) = A_1 \sin\omega_1 t + A_2 \sin\omega_2 t$. The output signal is then:

$$y(t) = \sum_{m,n} B_{mn} \sin(m\omega_1 + n\omega_2) \tag{2.5}$$

where m and $n = 0, \pm1, \pm2, \cdots$. This signal includes all of the harmonics of ω_1 and ω_2 plus cross-product terms such as $\omega_2 - \omega_1$, $\omega_2 + \omega_1$, $\omega_2 - 2\omega_1$, $\omega_2 + 2\omega_1$, etc. The sum and difference frequencies give rise to the intermodulation distortion. The sum of the absolute values of the coefficients m and n determines the order of the intermodulation distortion. For example, second-order intermodulation products (IMP) are at $|\omega_1 \pm \omega_2|$ with amplitude B_{11}; the third-order intermodulation products are at $|\omega_1 \pm 2\omega_2|$ and $|2\omega_1 \pm \omega_2|$ with amplitudes B_{12} and B_{21}; and so on. Harmonic distortions are also present for $m \neq 0$ with $n = 0$ and $m = 0$ with $n \neq 0$. The corresponding amplitudes are B_{m0} and B_{0n}, respectively. In general, the odd order intermodulation products having $m = n \pm 1$ cause the most problems because they may fall within the bandwidth of the channel. Of these, only the third and possibly the fifth order terms are usually important, since the amplitudes

of higher order terms tend to be significantly smaller. Second order terms are important if the application is broadband.

In laser diodes there can be nonlinearities in the curve for optical power output versus diode current, as illustrated in Figure 2.9. These nonlinearities are a result of inhomogenieties in the active region of the device and also arise from power switching between the dominant lateral modes in the laser. These nonlinearities are commonly referred to as "kinks" and are generally not seen in modern laser diodes. Power saturation occurs at high output levels. This nonlinearity is indicated by a downward curving of the light output versus current curve. Power saturation exists in all semiconductor laser diodes.

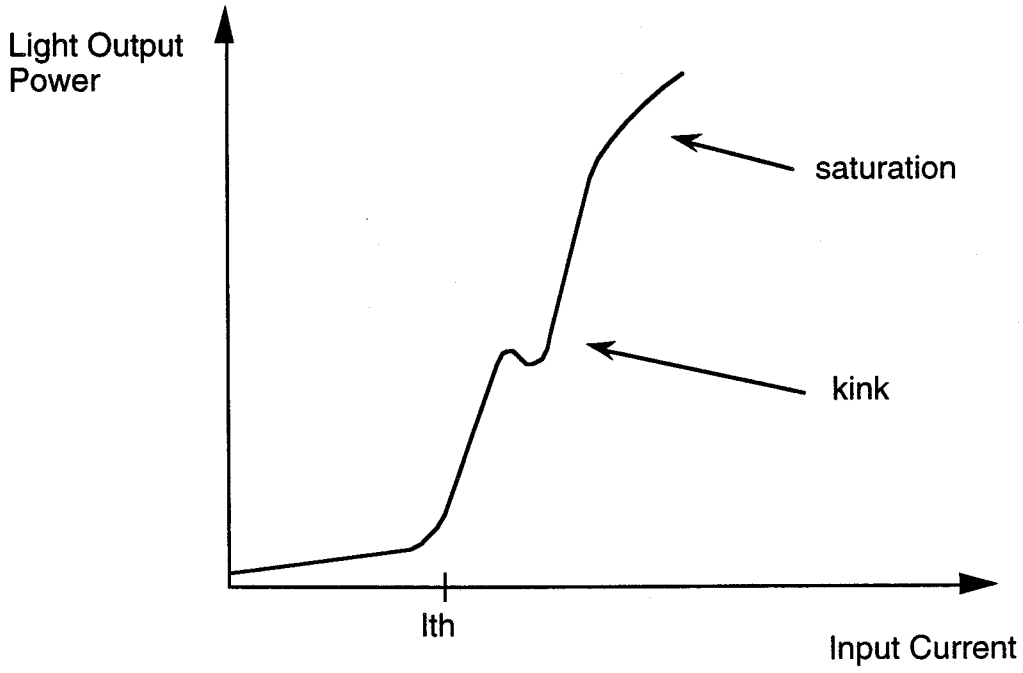

Figure 2.9 Example of kink and power saturation in the curve for light output power versus input current for a laser diode (Adapted from [53])

As was previously mentioned, the total harmonic distortion is high when the bias current is near threshold. As the bias is increased, relatively low distortion is observed. For much higher bias currents, distortion increases again since the operating point is near the laser saturation region. There is a bias current that gives the minimum distortion that is approximately half way between the threshold current and the current for which the power saturation starts. The lowest levels of distortion are generally measured at this bias point.

Additional nonlinearity effects become prominent when the input signal frequency becomes comparable to the resonant frequency of the optical cavity. At higher frequencies, usually above 500 MHz, frequency components of the modulation signal experience further degradation of linearity. This frequency dependent distortion is the dominant nonlinearity at higher frequencies and results from the nonlinear coupling between the photons and the injected carriers [24]. This nonlinear coupling is also responsible for the relaxation oscillation that limits the modulation bandwidth of the laser. This type of distortion is called resonance distortion (RD).

There can also exist other mechanisms which cause nonlinearity of the laser [24]. Some suggested reasons are spatial hole burning [54]-[56], carrier heating [57], or spectral hole burning [26], [58]. Others include current leakage, intervalence band absorption and free-carrier absorption. Two types of current leakage can occur. Imperfections in the locking structure can lead to shunt current leakage wherein the current through the active layer is reduced to a nonlinear fraction of the total injected current. Leakage also occurs when carriers escape from the heterojunction by diffusion from the edges of the active region to the cladding layers. Intervalence band absorption causes nonlinearities because of the strong dependence of absorption on carrier density.

A final type of distortion, which appears to be a problem in all lasers, is distortion which results from optical reflections or feedback. Optical reflections may cause nonlinearity within the laser itself [59] or may produce interferometers within the fiber that

interact with laser chirp to convert frequency modulation (FM) to intensity modulation (IM).

2.5 Dynamic Response

The dynamic behavior of single-mode semiconductor lasers can be modeled by two rate equations [1]. These two quantum rate equations describe the electron density within the active cavity and the density of photons being emitted. Further, they can provide information about the time development of the photon amplitude, frequency and phase.

The rate equations listed below describe the transient behavior of a single-mode semiconductor laser.

$$\frac{dN}{dt} = \frac{I}{V} - \frac{N}{\tau_s} - g(N - N_o)S \tag{2.6}$$

$$\frac{dS}{dt} = \Gamma g(N - N_o)S - \frac{S}{\tau_p} + \Gamma\beta\frac{N}{\tau_s} \tag{2.7}$$

The variable parameters in equations (2.6) to (2.9) are:

S = density of photons in lasing mode
N = density of electrons in the conduction band of the semiconductor
I = injection current

The constant parameters in equations (2.6) to (2.9) are:

Γ = optical confinement factor
τ_s = spontaneous electron lifetime
τ_p = photon lifetime
N_o = transparent carrier density

g = optical power gain

ε = power gain compression parameter

β = probability of spontaneous emission of a photon in phase with the lasing mode

V = volume of active laser region times electronic charge

Equations (2.6) and (2.7) are simple versions of the rate equations describing the operation of a single-mode semiconductor laser. To provide greater accuracy in predicting the nonlinear response of single-mode semiconductor lasers, (2.6) and (2.7) were modified [37],[60] to include a gain compression factor, ε. The modified rate equations are shown below.

$$\frac{dN}{dt} = \frac{I}{V} - \frac{N}{\tau_s} - g(N - N_o)(1 - \varepsilon S)S \tag{2.8}$$

$$\frac{dS}{dt} = \Gamma g(N - N_o)(1 - \varepsilon S)S - \frac{S}{\tau_p} + \Gamma\beta\frac{N}{\tau_s} \tag{2.9}$$

These rate equations are appropriate when the following assumptions are valid:

1) The laser is operating in a single-mode state.

2) The electron and photon population are homogeneous throughout the cavity.

3) The gain coefficient is a constant.

It should also be noted that the parameter V, the volume of active laser region times electronic charge, is established in [41], [47], [73], and [77].

The terms in these equations are justified by accounting for all factors that affect the number of photons and electrons. In equation (2.8), the derivative of N with respect to time, $\frac{dN}{dt}$, is the rate of change of carrier density. The next term, $\frac{I}{V}$, indicates that the electron concentration in the conduction band is increased by current flow in the diode. The next term, $-\frac{N}{\tau_s}$, represents the decrease in electrons due to spontaneous emission.

The last term, $-g(N-N_o)(1-\varepsilon S)S$, is the loss of electrons due to stimulated emission; this term gives rise to the nonlinear effects of the laser diode because it is a product of the values related to the input and the output.

In the second rate equation, (2.9), the rate of change of photon density is $\frac{dS}{dt}$. The stimulated emission term $\Gamma g(N-N_o)(1-\varepsilon S)S$ is a source of photons. The next term, $-\frac{S}{\tau_p}$, is the decay in the number of photons due to losses in the optical cavity. The last term, $\Gamma\beta\frac{N}{\tau_s}$, is the fraction of photons produced by spontaneous emission that adds to the energy of the lasing mode.

The rate equations can be solved for steady state values of I, S and N by setting the derivative terms to zero and solving the two equations for S and N given I.

The rate equations in (2.8) and (2.9) mathematically describe the interaction between electrons and photons within the laser cavity and consequently, some of the nonlinearities that exist in the input/output relationship between current and light. It has become common practice to include the phenomenological constant ε, which is called the power gain compression parameter, in the rate equations to help account for the nonlinear relationship that exists between the input current and the output photons in real single-mode semiconductor lasers. However, all of the nonlinearities exhibited by single-mode semiconductor lasers are not included in the rate equations and cannot be accounted for by simply including them in the parameter ε. For example, nonlinearities present from coherent reflected waves from the laser mirror facet and from a pigtail are not included in these rate equations. Despite this, the rate equations in (2.8) and (2.9) are good mathematical models for single-mode Fabry-Perot semiconductor lasers.

3. REVIEW OF LINEARIZATION TECHNIQUES

Although a lot of emphasis in optical fiber communications has been on digital transmission, there is a growing interest in the use of optical systems in broadband analog communications. Analog optical systems are now economical in CATV and other broadband distribution networks.

For transmitting these analog signals on optical fibers, direct intensity modulation of laser diodes is the simplest method. Problems arise from the nonlinearity of the optical source. Often, this nonlinearity limits the bandwidth of optical video transmission systems.

There are two potential applications for AM-VSB CATV lightwave systems, each with slightly different requirements. CATV companies are looking to fiber to improve the quality, capacity and reliability of the trunk systems that connect their head-end facilities to remote distribution nodes. Telephone companies are aggressively pursuing FTTH systems to meet the expected future demand for expanded video capacity. For either application, the transmission quality can be described by three parameters [24], carrier-to-noise ratio (CNR), composite triple beat (CTB), and composite second-order (CSO) distortion. The CNR is the ratio of the carrier to total noise power in 4 MHz bandwidth. The CSO and CTB are the ratios of the carrier to the total power within the largest accumulation of second and third order distortion products, respectively, within each channel. Typical values for trunk and FTTH systems are listed in Table 3.1. The term dBc represents decibels with respect to the carrier.

These distortion requirements limit the number of video channels that can be multiplexed. Currently, laser diodes are being built which are linear enough in themselves to transmit up to 60 video channels and still meet the CATV CSO and CTB requirements. Improved fabrication techniques and device structures have lead to this successful application. However, fabricating linear lasers is an expensive task. Consequently, linearizing inexpensive lasers with poor linearity by circuit techniques to compensate for the inherent non-linearity of the light sources to the point where they perform as well as expensive lasers is an alternative. Further, linearization methods could be used on even highly linear laser systems since no laser diode is perfectly linear. For example, the Ortel Corporation [61] linearizes an already good linear laser to the point where the laser, along with its compensating drive circuitry, can transmit up to 80 channels. The price of the system is around $10,000.

Table 3.1
Fiber to the Home and Trunk System Requirements (Adapted from [24])

	Trunk	FTTH
Distance(km)	10-20	1-2
Number of channels	40-80	30-40
CNR(dB)	55	48
CTB(dBc)	-65	-55
CSO(dBc)	-55	-50

A number of different linearization techniques have grown from this quest for laser diode linearity. These include electro-optical feedback, phase shift modulation, optical feedforward, quasi-feedforward, postdistortion, predistortion, and adaptive predistortion.

3.1 Opto-Electronic Feedback

The opto-electronic feedback method involves the use of a monitoring photodiode and a feedback network to provide negative electrical feedback to the drive circuitry. The nature of the signal changes from electrical to optical and then back to electrical as it travels around the feedback loop. The feedback signal adjusts the drive circuitry so as to improve the linearity of the output signal. Figure 3.1 shows a simplified block diagram of a opto-electronic feedback system.

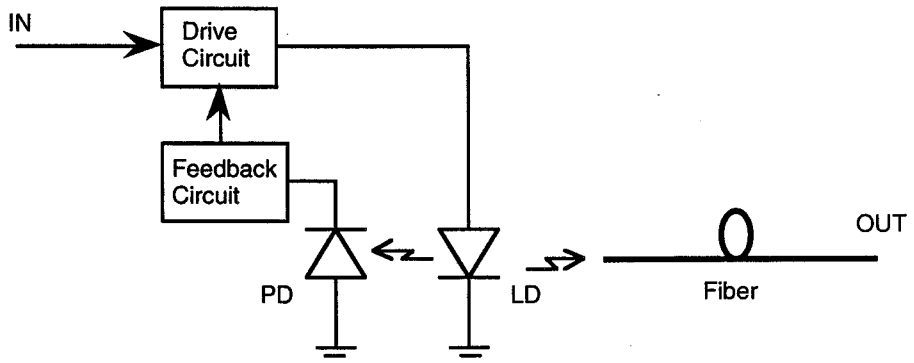

Figure 3.1 Opto-electronic feedback system

Sampling of the optical output can be done by using a photodiode packaged along with the source that monitors the output of the rear facet of the laser diode as is shown in Figure 3.1. Another alternative is to sample the optical output by using a tee coupler in the optical fiber.

A number of experiments have been carried out using the feedback technique. M. Sekita *et al.* [62] reported a 20 dB reduction of the second harmonic by using opto-electronic feedback in a single channel TV transmission experiment. Also, A. Van de Grijp *et al.* [63] reported a reduction in the 2nd and 3rd harmonics of 10 dB to -51 dBc

and a reduction of the noise level of 12 dB for a 6 MHz channel. Ueno and Kajitani [64] achieved improvements of 12 dB and 4 dB in second and third order distortion respectively.

All of these experiments where carried out in the 1970's and the 1980's and proved that opto-electronic feedback is useful for single-channel TV transmission.

3.2 Phase Shift Modulation

A phase shift modulation technique for the selected cancellation of harmonic components of any order was demonstrated by J. Strauss and O. I. Szentesi [65] in 1977. The experiment utilized two LEDs but the principle could also be applied to LDs. Consider two LD transmitters whose optical outputs are summed in an optical coupler as shown in Figure 3.2.

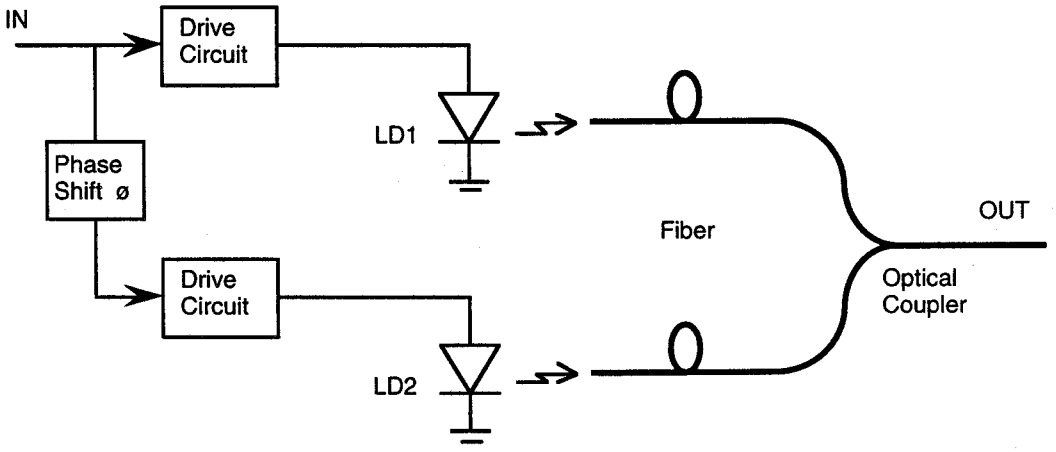

Figure 3.2 Phase shift modulation system (Adapted from [65])

For the phase difference ø equal to 90°, the second order distortions are out of phase and cancel each other. Strauss and Szentesi reported a 25 dB improvement in the second order distortion at 3.1 MHz for a resultant of -62 dBc.

A *n-th* order distortion product can be canceled when the phase angle between the two modulating signals is equal to 180°/n. Thus, to eliminate the third order distortion, the signal phase shift between the pairs is 60°. Simultaneous cancellation of both second and third-order distortion can thus be achieved by using two pairs of matched laser diodes.

3.3 Quasi-Feedforward

This technique was demonstrated by Patterson *et al.* [66] in 1979. They used LEDs in their experiments, but again, this technique could be applied to laser diodes as well. The block diagram of this compensation method is illustrated in Figure 3.3.

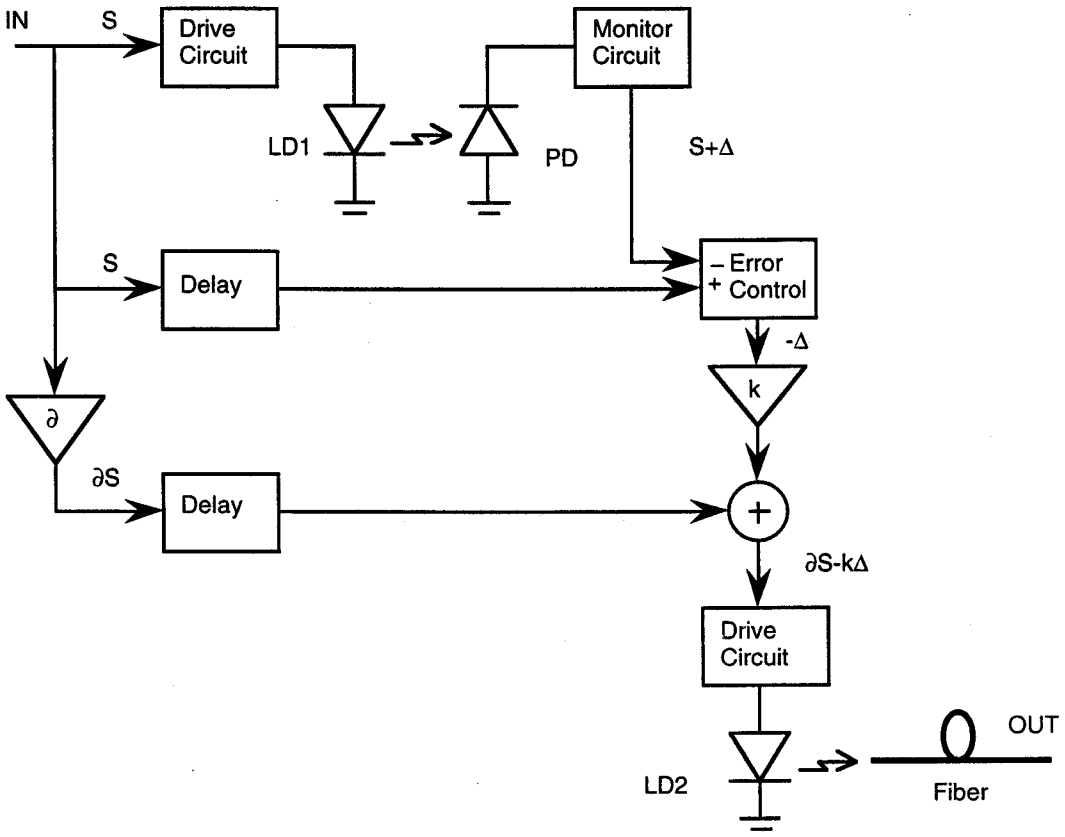

Figure 3.3 Quasi-feedforward system (Adapted from [66])

The incoming signal S modulates two LDs of similar characteristics (LD1 and LD2), both of which generate an equal amount of distortion Δ. With the aid of the reference signal path the distortion from LD1 is isolated, inverted and brought to the level required to create a compensating signal equal in amplitude and opposite in sign to the distortion generated by LD2.

With this technique, Patterson *et al.* , utilizing two LEDs as light sources, observed a reduction in the second and third order distortion of 35 dB and 20 dB respectively to figures below -55 dBc in a three tone test. To achieve this degree of effectiveness, very precise time delays and amplifiers with very flat amplitude and linear phase response over the frequency range of interest were required. In addition, the success of this technique is improved when the characteristics of the two optical sources are closely matched.

3.4 Optical Feedforward

The optical feedforward compensation technique shown in Figure 3.4 is similar to the quasi-feedforward scheme just described.

Distortion compensation using feedforward is achieved through isolation of the distortion produced in a nonlinear circuit and by a subsequent injection of the processed error signal back into the circuit. The main difference between this scheme and the quasi-feedforward one is that the injection of the error signal occurs in the optical domain in the optical feedforward technique and occurs in the electrical domain in the quasi-feedforward technique. In addition, in the optical feedforward scheme, a single source is used for both signal transmission and for error monitoring. Compensation is achieved by coupling the light emitted from a second source to the main optical signal path with an optical coupler.

One advantage the optical feedforward scheme has over the quasi-feedforward scheme is that it can reduce laser noise in the optical signal. In the optical feedforward scheme, the error signal is injected in the optical domain. Since the laser noise is part of the error signal, the laser noise in the output is reduced.

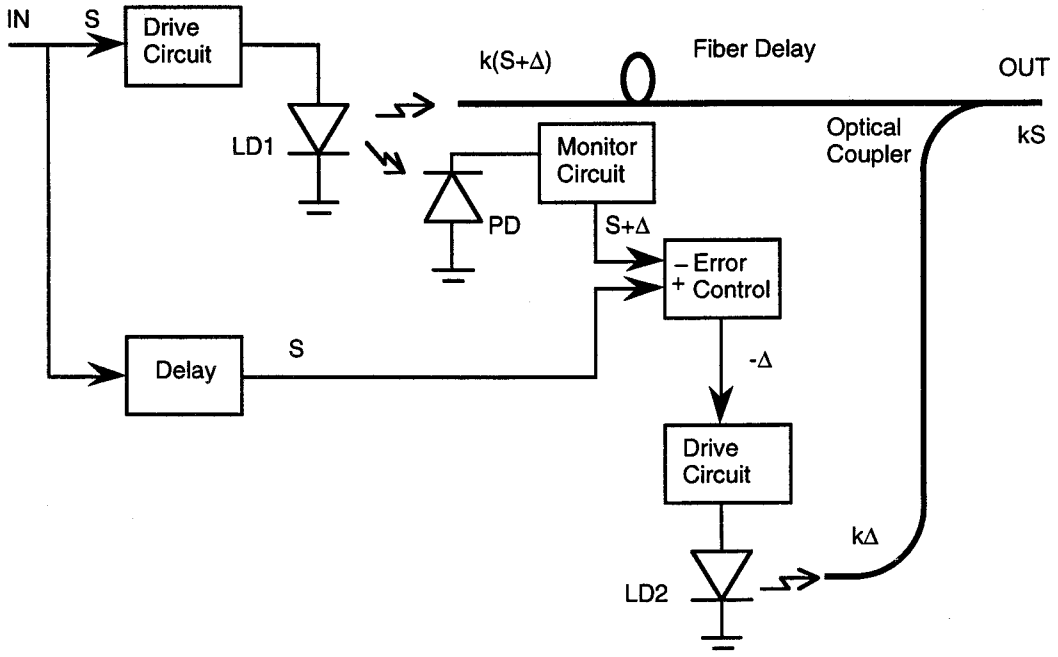

Figure 3.4 Optical feedforward system (Adapted from [66])

Current experiments implementing this technique have shown significant results. D. Hassin and R. Vahldieck [67] reported a reduction of the second and third harmonics by 20 dB each on the average over a bandwidth of 850 MHz. They also reported that the system bandwidth was mainly limited by the RF amplifiers used in the circuit which exhibited significant phase nonlinearities above 800 MHz. A second experiment was carried out by L. S. Fock and R. S. Tucker [68]. They reported a reduction in noise of more than 10 dB over the frequency range 1.7-3.0 GHz, a reduction of second harmonic

distortion of 25 dB to -55 dBc at 2.4 GHz, and a reduction of third order harmonic distortion of more than 10 dB to -30 dBc over the frequency range 2.1-3.0 GHz.

Feedforward compensation is an effective technique for improving the linearity of optical transmitters, however the two optical signals being coupled must be stable, especially in wideband applications.

3.5 Postdistortion

Postdistortion is a direct compensation technique that has no feedback or feedforward path. In this scheme, complementary distortion is introduced into the signal after it has modulated the laser. The induced distortion cancels as nearly as possible the distortion introduced by the optical source.

Postdistortion can be added to the signal in one of two different domains, the optical domain or the electrical domain. If the signal is postdistorted in the optical domain, the distortion is added to the optical path before the light is photodetected as shown in Figure 3.5.

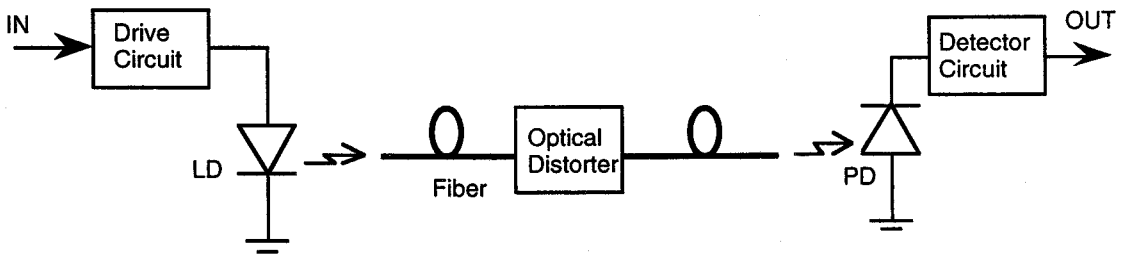

Figure 3.5 Postdistortion system in the optical path

If the signal is postdistorted in the electrical domain, the distortion is added to the path after the light has been photodetected with circuitry as shown in Figure 3.6.

Some success has been predicted with optical postdistortion [69] but significant practical implementations of both types of postdistortion are rare.

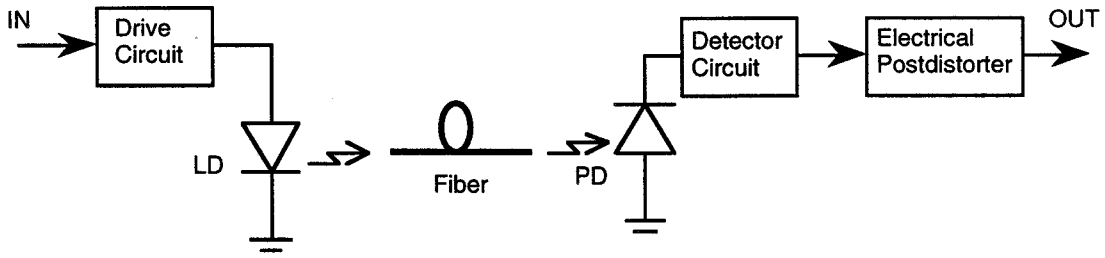

Figure 3.6 Postdistortion system in the electrical path

3.6 Predistortion

Predistortion is another direct compensation technique that has no feedback or feedforward paths. In this scheme complementary distortion is introduced into the signal before it modulates the laser such that when the modified input signal is applied to the nonlinear transmitting laser, an undistorted signal results. A block diagram of the predistortion apparatus is shown in Figure 3.7.

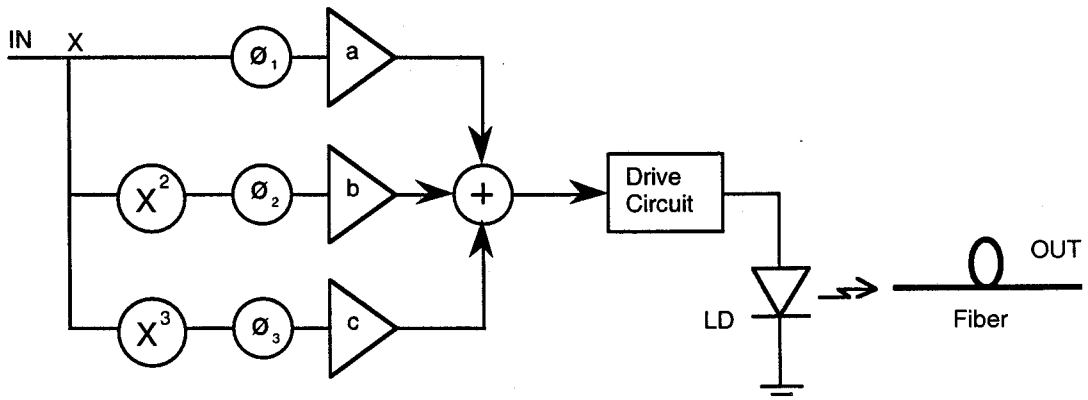

Figure 3.7 Predistortion system

The input x is normally transmitted from the laser such that the light output is a nonlinear function of x. If it is assumed that the inverse function can be represented by a

polynomial series $ax + bx^2 + cx^3$, then this circuit adds nonlinear terms to the modified input so that the output is linear in x up to fourth order. In most lasers, the fourth, fifth and higher order harmonics are usually negligible. The ø terms represent phase adjustment since it is essential that the second and third order distortion terms being added are 180° out of phase with the terms generated by the laser.

A number of predistortion circuits have been demonstrated. K. Asatani and T. Kimura [70] developed a predistorter for a LED. Their results showed an improvement in second and third-order harmonic distortions of 19 dB and 21 dB respectively for a 3.58 MHz carrier signal. R. Childs and V. A. O'Byrne [71] developed a predistortion circuit for a directly modulated Distributed Feedback (DFB) laser. Their results showed a reduction in the CSO of 12 dB but no reduction in the CTB term. The resultant figures for CSO and CTB after predistortion were both below -60 dBc. S. Mysore [72] developed a predistortion circuit that reduced the second and third order IM products by 15 dB and 11 dB respectively over a bandwidth of 40 MHz. T. Darcie and G. Bodeep [24] constructed a second order predistorter and succeeded in achieving a net reduction of CSO without increasing CTB. In a 60 channel system, the CSO was reduced by 17, 11, and 7 dB at channels 3, 11, and 40 respectively with no change in the CNR or CTB. N. Tayebi [73] performed theoretical calculations of how well a predistorter could work. His results showed that if all of the nonlinearities in the laser are accounted for in the semiconductor rate equations, a perfect predistorter could be built that would all but eliminate the second and third order harmonic and intermodulation products to figures below -800 dBc.

One of the main differences between Tayebi's predistorter and those previously mentioned is that he incorporated into the design a way to compensate for the frequency dependence of the laser nonlinearities. As will be shown later, the nonlinear distortions created in the laser increase with frequency. Consequently, a predistorter which compensates for this effect would appear to be more successful.

3.7 Adaptive Predistortion

One of the problems with the predistortion technique previously described is that it cannot compensate for changes in the laser characteristics. Laser diode characteristics can change as a result of temperature fluctuation and aging. One of these characteristics that changes is the level of nonlinear distortion. If the predistorter is built for the laser when it is new, it may not be as effective after a long period of operation. As well, the predistorter may not be as effective if the temperature of the laser continually changes.

M. Bertelsmeier and W. Zschunke [74] showed how this problem could be eliminated by developing an adaptive predistorter. A block diagram of this technique is shown in Figure 3.8.

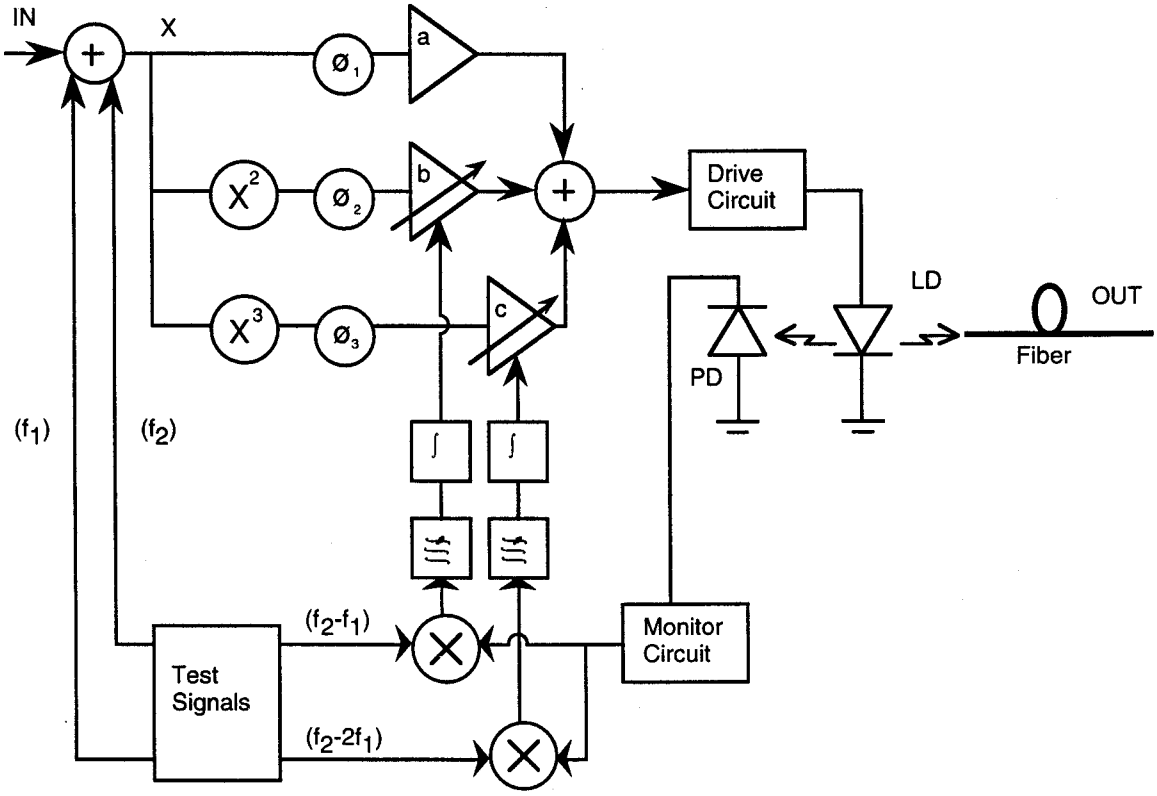

Figure 3.8 Adaptive predistortion system (Adapted from [74])

In this technique, second and third order harmonics of the input signal are generated by the square law and cube law circuits. They are weighted and added to the undistorted signal to create a predistorted signal that will drive the optical source. This portion of the circuit is the same as the predistorter in the previous section.

To correct for the changes in the laser diode distortion as a result of temperature change and aging, the gain coefficients of the square and cube paths must be adjustable. This is carried out by the addition of two test signals with frequencies f_1 and f_2 to the transmitted signal in an unused frequency band. Distortions of these test signals are minimized by correlating the IMD products in the output signal with sinusoidal reference signals of frequencies f_2-f_1 and f_2-$2f_1$. Based on this comparison, the gains in the predistorter square and cube paths are adjusted accordingly. Bertelsmeier and Zschunke have shown that this method can reduce second and third order IMD by approximately 15 dB and 10 dB respectively for frequencies up to 300 MHz.

This adaptive strategy does have a feedback path but it is important to note that it is only to monitor the distortion levels of the pilot tones and does not carry any information from the input signal like a pure feedback correction technique would. Consequently, the adaptive predistorter scheme is not bandlimited like the pure feedback strategy is.

3.8 Summary and Discussion

As can be seen in the previous sections, linearization of optical transmitters has been studied for some time and a variety of linearization schemes have been proposed and tested. One aspect common to all of the linearization schemes is the need to identify how and to what degree the laser diode generates nonlinearities. In other words, in order to correct the problem, you have to know what the nature of the problem is.

In order to determine which linearization scheme is the best for our application it is suitable to briefly restate the application. One of the goals of this research is to develop a linearization scheme which costs less than the laser it is correcting. If the laser is moderately linear, the predistorter and laser diode system should perform about as well as an expensive laser diode. The application is for AM analog transmission of television signals over the frequency range 50 to 700 MHz.

On re-examination, it can be seen that most of the proposed techniques suffer from practical disadvantages. Electrical feedback is limited with today's technology to a bandwidth of around 30 MHz due to the loop delay. As a result, opto-electronic feedback is useful only in narrowband applications and would not meet the current wideband requirements of 700 MHz.

Phase shift modulation works for selective harmonic compensation but, in general, is not feasible because an additional source is required for cancellation of each harmonic. As well, precisely matched sources, high quality couplers and identical coupling between the source into the fibers are all necessary to achieve an effective distortion reduction.

Optical feedforward schemes require an additional laser diode and an optical power combiner. If the laser diode is expensive, the cost of the scheme can become critical because two laser diodes are required. Further, distortion compensation depends greatly on the exact signal superposition in the optical combiner.

Quasi-feedforward compensation is similar to straight optical feedforward compensation in that a second laser diode is required. This linearization scheme is sensitive to mismatches in the laser diodes. The two laser diodes must have very similar characteristics.

One of the primary downfalls of postdistortion is that the transmission path introduces additional distortion on top of the source distortion complicating the correction

process. The path distortion varies with the optical path length thus changing the postdistortion requirements for systems with varying transmission lengths. Further, it is not possible to use adaptive distortion based on a pilot tone or other feedback technique.

Predistortion does not fall victim to the loop delay problem like the electrical feedback scheme does and is applicable to broadband multicarrier systems. In addition, the predistorter hardware circuitry can generally be built for a minimal cost (*i.e.* less than the cost of the laser). Although the predistortion scheme avoids some of the downfalls it still has some drawbacks. Laser diodes are affected to a large degree by aging and temperature variations. If the laser diodes nonlinear distortion changes with these parameters, a straight predistorter will not compensate for the change. In addition, if there are variations in the laser diodes from a production run, each predistorter has to be tuned to the particular laser diode.

Consequently, the linearization scheme which appears to have the best potential is adaptive predistortion. This scheme has all the benefits of regular predistortion, but by also being adaptive, can adjust to variations in the laser diode's distortions whether they are from aging, temperature change or variations in the product line.

It is apparent that predistortion and adaptive predistortion are viable techniques for linearizing laser diodes for broadband applications. The tradeoff for moving from predistortion to adaptive predistortion is compensation for aging, temperature variations, and product to product variations for the price of increased system complexity.

The objectives in this thesis include modeling the laser diode, demonstrating the frequency dependence of the nonlinearities and trying to linearize the laser diode over a broad frequency range. The objectives do not include trying to determine the change in nonlinear distortion as a function of temperature, time, or product variation. It has been concluded that predistortion is the best linearization scheme for this research and is

pursued in the remainder of this thesis. Adaptive predistortion appears to be the best practical linearization technique for broadband applications where the laser is subject to aging and temperature fluctuations.

4. VOLTERRA TRANSFER FUNCTIONS

4.1 Volterra Series

The output of a linear system, $w(t)$, is obtained by the fundamental convolution integral of the impulse response of the system and the input:

$$w(t) = \int_{-\infty}^{\infty} h(\tau)x(t-\tau)d\tau \tag{4.1}$$

where $h(t)$ is the impulse response and $x(t)$ the input.

Equation (4.1) is valid only for linear circuits and systems. If the system is nonlinear, the relation between the output and the input can be expressed in a Volterra series form as shown in [75] and [76].

$$\begin{aligned} w(t) = &\int_{-\infty}^{\infty} h_1(\tau_1)x(t-\tau_1)d\tau_1 + \int_{-\infty}^{\infty}\int_{-\infty}^{\infty} h_2(\tau_1,\tau_2)x(t-\tau_1)x(t-\tau_2)d\tau_1 d\tau_2 + \\ &\cdots + \int_{-\infty}^{\infty}\cdots\int_{-\infty}^{\infty} h_n(\tau_1,\tau_2,\cdots\tau_n)x(t-\tau_1)\cdots x(t-\tau_n)d\tau_1 d\tau_2\cdots d\tau_n \end{aligned} \tag{4.2}$$

In (4.2), the multidimensional function $h_n(\tau_1,\tau_2,\cdots\tau_n)$ is called the *n-th order nonlinear impulse response*. Just as the linear frequency domain transfer function $H(\omega)$ is the Fourier transform of $h(t)$, the nonlinear transfer function $H_n(\omega_1,\omega_2,\cdots\omega_n)$ is the n-dimensional Fourier transform of $h_n(t_1,t_2,\cdots t_n)$.

One way of representing the Volterra operator is by $H_n[x(t)]$ where:

$$H_n[x(t)] = \int_{-\infty}^{\infty} \cdots \int_{-\infty}^{\infty} h_n(\tau_1, \tau_2, \cdots \tau_n) x(t-\tau_1) \cdots x(t-\tau_n) d\tau_1 d\tau_2 \cdots d\tau_n \tag{4.3}$$

Thus, a nonlinear system can be represented as:

$$w(t) = H[x(t)] = H_1[x(t)] + H_r[x(t)] \tag{4.4}$$

where H_1 is the first order Volterra operator of the system:

$$H_1[x(t)] = \int_{-\infty}^{\infty} h(\tau) x(t-\tau) d\tau \tag{4.5}$$

and H_r represents the remaining terms of the Volterra series representation of the system.

To find the nonlinear impulse response from the frequency domain nonlinear transfer function, the inverse Fourier transform is performed.

$$h_n(\tau_1, \tau_2, \cdots \tau_n) = \frac{1}{(2\pi)^n} \int\int \cdots \int_{-\infty}^{\infty} H_n(\omega_1, \omega_2, \cdots \omega_n) e^{[j(\omega_1\tau_1 + \omega_2\tau_2 + \cdots + \omega_n\tau_n)]} d\omega_1 d\omega_2 \cdots d\omega_n \tag{4.6}$$

In order to determine the coefficients of the nonlinear transfer functions, a technique called *harmonic-input* or *probing* is used. This method is similar to the process of finding the frequency domain transfer function $H(\omega)$ of a linear circuit. First, assume the circuit has the simplest possible excitation, then find the response, and finally solve algebraically for $H_n(\omega_1, \omega_2, \cdots \omega_n)$. The first order Volterra transfer function of a system is determined by applying an input tone $e^{j\omega t}$. The output is manipulated into the form of $H(\omega)e^{j\omega t}$. The ratio of the input and output yields the transfer function $H(\omega)$. A second order Volterra transfer function is determined by applying the sum of two frequency tones as inputs $e^{j\omega_1 t} + e^{j\omega_2 t}$. The output is manipulated into the form of $H_2(\omega_1, \omega_2)e^{j\omega_1 t + j\omega_2 t}$ to find $H_2(\omega)$. This approach can be used to obtain the *n-th* order Volterra transfer functions.

Volterra series can also be applied in order to find the inverse of a nonlinear system. The *m-th* order postinverse of a nonlinear system H is defined as a system that when cascaded with H results in another system for which the first order Volterra kernel is a unit impulse response while the second to the m order kernels are all zero.

In most practical applications, the systems are weakly nonlinear. As a result, only a few Volterra kernels are required to model the system. Semiconductor lasers that do not have kinks in their light versus current characteristic and are modulated around a bias point well above the threshold current can be considered as weakly nonlinear. As long as there are no hard limitations in the light versus current curve, semiconductor lasers can be represented by a series expansion containing the kernels h_1, h_2 and h_3. Results in [32] have shown that expansion to the third order is sufficient to predict laser behavior and distortion levels.

4.2 Volterra Model of Predistorter

As was previously mentioned, a single-mode semiconductor laser's characteristics can be expressed by a pair of rate equations which describe the light versus current relationship of the laser.

$$\frac{dN}{dt} = \frac{I}{V} - \frac{N}{\tau_s} - g(N - N_o)(1 - \varepsilon S)S \tag{4.7}$$

$$\frac{dS}{dt} = \Gamma g(N - N_o)(1 - \varepsilon S)S - \frac{S}{\tau_p} + \Gamma\beta\frac{N}{\tau_s} \tag{4.8}$$

This relationship between output light and input current is a nonlinear one. It has been shown that a memoryless model cannot be used to characterize the laser nonlinearities [41]. Thus, the proper model must include frequency dependent nonlinearities. This can be achieved by a Volterra series representation of the laser response.

It is quite a difficult task to actually solve the rate equations for the output S as a function of the input (i.e. $S = f(I)$). However, reversing the situation and solving for the input I as a function of the output S is manageable (i.e. $I = f(S)$). Based on this, if the Volterra series of the function $I = f(S)$ is determined, we are essentially finding the inverse function of the laser. In a sense, this function is a postdistorter since the output of the laser S is being used as the input. However, if the system is placed in front of the laser, it acts as a predistorter. Either way, the system will be the inverse function of the laser.

Consequently, the Volterra model of the predistorter will be determined first by solving the rate equations for I as a function of S and using the harmonic-input method to find the Volterra transfer functions [77]. Once the Volterra transfer functions for the predistorter have been determined, the inverse of these functions will be determined to obtain the Volterra model for the laser. The detailed calculation of the Volterra predistorter model from the rate equations is given in Appendix A. The calculations are summarized below.

The first step is to solve (4.8) for N:

$$N = \frac{\frac{dS}{dt} + \frac{S}{\tau_p} + \Gamma g(1 - \varepsilon S)SN_o}{\Gamma g(1 - \varepsilon S)S + \frac{\Gamma \beta}{\tau_s}} \tag{4.9}$$

Assuming a bias point (I_b, S_b), the current and the light can be written as:

$$I_b + i = I \tag{4.10}$$

$$S_b + s = S \tag{4.11}$$

where i and s are the small signal current and light respectively.

Substituting (4.11) into (4.7) and (4.9) and expanding terms gives:

$$\frac{I}{V}=\frac{dN}{dt}+\frac{N}{\tau_s}+gNS_b+gNs-gN\varepsilon S_b{}^2-2gN\varepsilon S_b s-gN\varepsilon s^2-gN_oS_b-gN_os \\ +gN_o\varepsilon S_b{}^2+2gN_o\varepsilon S_b s+gN_o\varepsilon s^2 \tag{4.12}$$

$$N=\frac{s'+\left[\frac{1}{\tau_p}+\Gamma gN_o-2S_b\Gamma gN_o\varepsilon\right]s+\left[-\Gamma gN_o\varepsilon\right]s^2+\left[\frac{S_b}{\tau_p}+S_b\Gamma gN_o-S_b^2\Gamma gN_o\varepsilon\right]}{\left[-\Gamma g\varepsilon\right]s^2+\left[\Gamma g-2\Gamma g\varepsilon S_b\right]s+\left[\Gamma gS_b-\Gamma g\varepsilon S_b^2+\frac{\Gamma\beta}{\tau_s}\right]} \tag{4.13}$$

Substituting (4.13) into (4.12) results in a single equation relating I to S. From this, $I_b+i=I$ can then be substituted and the whole expression simplified to give:

$$i=a+bs+cs'+ds''+es^2+fss'+gs's'+hss''+ks^3+ls^2s'+ms^2s''+nss's' \tag{4.14}$$

The constants $a,b,c,\cdots$ are expressed only in terms of the laser parameters and the bias current. The term a ends up being zero.

To obtain the Volterra transfer functions for the predistortion block we treat *s* or *s(t)* as the input and *i* or *i(t)* as the output of the system. The first order Volterra transfer function $P_1(\omega)$ is obtained by substituting $s(t)=Se^{j\omega t}$, where S is an arbitrary amplitude level of photons and $e^{j\omega t}$ is a unit phasor, into equation (4.14) and taking the coefficients of $e^{j\omega t}$. The term S is optional. If the input to the predistorter is photon density, the S term is not required. However, if the input to the predistorter is current, as will be the case in later simulations, the S term is required to normalize the predistorter transfer functions. It is included here.

$$P_1(\omega)=\left(b+cj\omega-d\omega^2\right)S \tag{4.15}$$

To obtain the second order Volterra transfer function, $s(t) = S\left(e^{j\omega_1 t} + e^{j\omega_2 t}\right)$ is substituted into equation (4.14) and the coefficients of $e^{j(\omega_1+\omega_2)t}$ give $P_2(\omega_1, \omega_2)$.

$$P_2(\omega_1, \omega_2) = \left(2e + fj(\omega_1 + \omega_2) - h(\omega_1 + \omega_2)^2\right)S^2 \tag{4.16}$$

In a similar way $P_3(\omega_1, \omega_2, \omega_3)$ is obtained by substituting $s(t) = S\left(e^{j\omega_1 t} + e^{j\omega_2 t} + e^{j\omega_3 t}\right)$ into (4.14) and taking the coefficients of the term $e^{j(\omega_1+\omega_2+\omega_3)t}$.

$$P_3(\omega_1, \omega_2, \omega_3) = \left(6k + 2lj(\omega_1 + \omega_2 + \omega_3) - 2m(\omega_1 + \omega_2 + \omega_3)^2\right)S^3 \tag{4.17}$$

The functions (4.15), (4.16) and (4.17) represent the Volterra model for the predistorter and are shown as a block diagram in Figure 4.1.

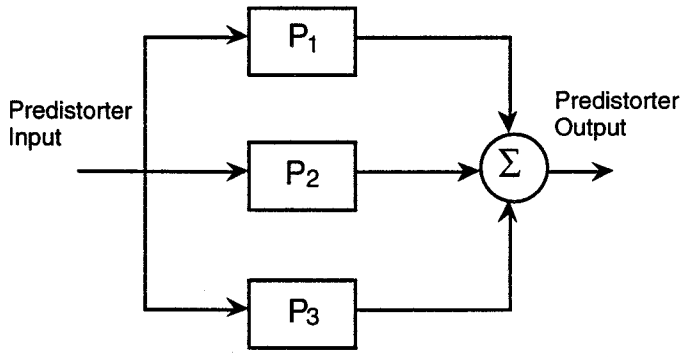

Figure 4.1 Block diagram of the Volterra model for the predistorter

4.3 Volterra Model of Laser Diode

The Volterra transfer functions for the laser are determined by finding the inverse of the predistorter functions. Assuming the transfer functions representing the laser are L_1, L_2 and L_3, the resultant block diagram of the predistorter and the laser is shown in Figure 4.2.

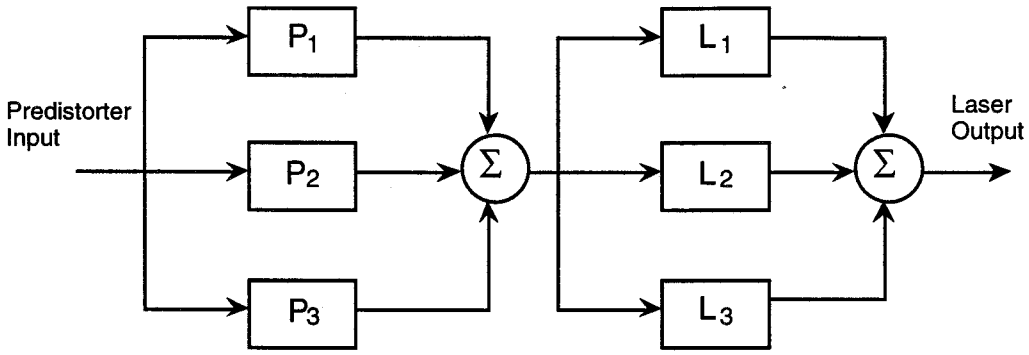

Figure 4.2 Block diagram of the Volterra models for the predistorter and laser

The two sets of transfer functions P and L will be inverse systems. The detailed calculation of the Volterra model for the laser is given in Appendix B. The calculations are summarized below.

The first order functions have a simple relation:

$$L_1(\omega) = \frac{1}{P_1(\omega)} \tag{4.18}$$

The second order function, $L_2(\omega_1, \omega_2)$, is obtained by applying an input equal to $e^{j\omega_1 t} + e^{j\omega_2 t}$ to the system and then canceling the terms of $e^{j(\omega_1+\omega_2)t}$ which correspond to the operation of the second order system.

For the second order case, the input to the predistorter is:

$$a(t) = e^{j\omega_1 t} + e^{j\omega_2 t} \tag{4.19}$$

The output of the predistorter is:

$$y(t) = P_1(\omega_1)e^{j\omega_1 t} + P_1(\omega_2)e^{j\omega_2 t} + P_2(\omega_1, \omega_2)e^{j(\omega_1+\omega_2)t} \tag{4.20}$$

Using (4.20) as the input to the laser, the output of the laser becomes:

$$\begin{aligned} x(t) = {} & L_1(\omega_1)P_1(\omega_1)e^{j\omega_1 t} + L_1(\omega_2)P_1(\omega_2)e^{j\omega_2 t} + L_1(\omega_1+\omega_2)P_2(\omega_1,\omega_2)e^{j(\omega_1+\omega_2)t} \\ & + L_2(\omega_1,\omega_2)P_1(\omega_1)P_1(\omega_2)e^{j(\omega_1+\omega_2)t} \\ & + L_2(\omega_1,\omega_1+\omega_2)P_1(\omega_1)P_2(\omega_1,\omega_2)e^{j(2\omega_1+\omega_2)t} \\ & + L_2(\omega_2,\omega_1+\omega_2)P_1(\omega_2)P_2(\omega_1,\omega_2)e^{j(\omega_1+2\omega_2)t} \end{aligned} \tag{4.21}$$

The coefficients of $e^{j(\omega_1+\omega_2)t}$ should be zero. Thus:

$$L_2(\omega_1,\omega_2) = \frac{-P_2(\omega_1,\omega_2)}{P_1(\omega_1)P_1(\omega_2)P_1(\omega_1+\omega_2)} \tag{4.22}$$

Similarly, L_3 is determined by applying an input consisting of three tones $e^{j\omega_1 t} + e^{j\omega_2 t} + e^{j\omega_3 t}$. The coefficient of the term $e^{j(\omega_1+\omega_2+\omega_3)t}$ in the final output should be zero and this way $L_3(\omega_1,\omega_2,\omega_3)$ can be determined as:

$$\begin{aligned} L_3(\omega_1,\omega_2,\omega_3) = {} & \frac{-1}{P_1(\omega_1+\omega_2+\omega_3)P_1(\omega_1)P_1(\omega_2)P_1(\omega_3)} \\ & \times \left[P_3(\omega_1,\omega_2,\omega_3) - \frac{P_2(\omega_1,\omega_2+\omega_3)P_2(\omega_2,\omega_3)}{P_1(\omega_2+\omega_3)} - \frac{P_2(\omega_2,\omega_1+\omega_3)P_2(\omega_1,\omega_3)}{P_1(\omega_1+\omega_3)} - \right. \\ & \left. \frac{P_2(\omega_3,\omega_1+\omega_2)P_2(\omega_1,\omega_2)}{P_1(\omega_1+\omega_2)} \right] \end{aligned} \tag{4.23}$$

The functions (4.18), (4.22) and (4.23) represent the Volterra transfer functions for the laser.

5. HARMONIC ANALYSIS OF VOLTERRA MODELS

The Volterra Series transfer functions for the predistorter and for the laser diode were developed in the previous chapter. The performance of the laser diode with and without the predistortion block can be evaluated by harmonic analysis.

5.1 Harmonic Analysis of Laser Diode

The performance of the laser diode alone can be evaluated by applying a single frequency tone to the input of the Volterra transfer functions derived for the laser. To proceed with the analysis, a frequency domain approach is used.

The output of a *p-th* order Volterra system in the frequency domain is:

$$Y_p(\omega) = \frac{1}{(2\pi)^{p-1}} \int_{-\infty}^{\infty} \int_{-\infty}^{\infty} \cdots \int_{-\infty}^{\infty} H_p\left(\omega - \omega_1 - \omega_2 - \cdots - \omega_{p-1}, \omega_1, \omega_2, \cdots \omega_{p-1}\right)$$
$$X\left(\omega - \omega_1 - \omega_2 - \cdots - \omega_{p-1}\right) X(\omega_1) X(\omega_2) \cdots X\left(\omega_{p-1}\right) d\omega_1 d\omega_2 \cdots d\omega_{p-1} \tag{5.1}$$

If we consider a system that is modeled with three Volterra functions: first order, second order and third order, then the output of the system is the sum of the output of each Volterra operator. In the frequency domain this can be expressed in the following form:

$$Y(\omega) = H_1(\omega)X(\omega) + \frac{1}{2\pi}\int_{-\infty}^{\infty} H_2(\omega-\omega_1,\omega_1)X(\omega-\omega_1)X(\omega_1)d\omega_1 + \frac{1}{(2\pi)^2}\int_{-\infty-\infty}^{\infty\infty} H_3(\omega-\omega_1-\omega_2,\omega_1,\omega_2)X(\omega-\omega_1-\omega_2)X(\omega_1)X(\omega_2)d\omega_1 d\omega_2 \quad (5.2)$$

If a single tone $X(\omega) = \delta(\omega-\omega_o)$ is applied to the input of the laser with Fourier transforms L_1, L_2 and L_3, the frequency domain output of the laser is:

$$Y(\omega) = L_1(\omega)\delta(\omega-\omega_o) + \frac{1}{2\pi}\int_{-\infty}^{\infty} L_2(\omega-\omega_1,\omega_1)\delta(\omega-\omega_1-\omega_o)\delta(\omega_1-\omega_o)d\omega_1 + \frac{1}{(2\pi)^2}\int_{-\infty-\infty}^{\infty\infty} L_3(\omega-\omega_1-\omega_2,\omega_1,\omega_2)\delta(\omega-\omega_1-\omega_2-\omega_o)\delta(\omega_1-\omega_o)\delta(\omega_2-\omega_o)d\omega_1 d\omega_2 \quad (5.3)$$

which becomes:

$$Y(\omega) = L_1(\omega_o)\delta(\omega-\omega_o) + \frac{1}{2\pi}L_2(\omega_o,\omega_o)\delta(\omega-2\omega_o) + \frac{1}{(2\pi)^2}L_3(\omega_o,\omega_o,\omega_o)\delta(\omega-3\omega_o) \quad (5.4)$$

L_1, L_2 and L_3 represent $L_1(\omega_1)$, $L_2(\omega_1,\omega_2)$ and $L_3(\omega_1,\omega_2,\omega_3)$ which are developed in Chapter 4 and defined in equations (4.18), (4.22) and (4.23).

The frequency domain of the output $Y(\omega)$ consists of three terms of $\delta(\omega-n\omega_o)$ with n= 1, 2 and 3. It can easily be seen that these terms represent the fundamental, the second and third order harmonics respectively.

Consequently, the coefficients of each delta function can be divided by the coefficient of the first delta function to determine the second order and third order harmonic distortion (HD).

$$HD_2 = 20\log_{10}\left|\frac{L_2(\omega_o,\omega_o)}{2\pi L_1(\omega_o)}\right| \quad (5.5)$$

$$HD_3 = 20\log_{10}\left|\frac{L_3(\omega_o,\omega_o,\omega_o)}{(2\pi)^2 L_1(\omega_o)}\right| \tag{5.6}$$

These second and third order HDs can be calculated for different frequencies and for different values of laser parameters which define L_1, L_2 and L_3.

If we recall the derivations in Chapter 4, the transfer functions for L_1, L_2 and L_3 were derived from the laser rate equations. The performance of each laser is defined by a set of laser parameters. Thus, specifying a set of parameters for a laser will determine its Volterra transfer functions.

In this thesis, two different sets of parameters are used for laser models. The first set, listed in Table 5.1, are used in work by McGee [41] and also by Way [47]. These parameters, which represent "Device A", are for a high-speed GaAlAs single-mode laser diode (Ortel LS-620). The second set, listed in Table 5.2, represent "Device B" and were used in work by Kuo [37] for a single-mode DFB laser.

Table 5.1
Laser Parameters, Device A

Parameter	Definition	Value	Units
Γ	Optical confinement factor	0.646	-
τ_s	Spontaneous electron lifetime	3.72	ns
τ_p	Photon lifetime	2	ps
N_o	Transparent carrier density	4.6E24	m^{-3}
g	Optical power gain	1E-12	$s^{-1}m^3$
ε	Power gain compression parameter	3.8E-23	m^3
β	Probability of spontaneous emission of a photon in lasing mode	0.001	-
V	Volume of active laser region times electronic charge	1.44E-35	m^3C
m	Modulation index	0.20	-

Table 5.2

Laser Parameters, Device B

Parameter	Definition	Value	Units
Γ	Optical confinement factor	0.34	-
τ_s	Spontaneous electron lifetime	3	ns
τ_p	Photon lifetime	2	ps
N_o	Transparent carrier density	1E24	m^{-3}
g	Optical power gain	3E-12	$s^{-1}m^3$
ε	Power gain compression parameter	3E-23	m^3
β	Probability of spontaneous emission of a photon in lasing mode	0.001	-
V	Volume of active laser region times electronic charge	5.76E-37	m^3C
m	Modulation index	0.30	-

Based on these two sets of parameters, the Volterra transfer functions and a Volterra model for each laser can be determined. Next, the second order HD and third order HD for each laser can be evaluated at different frequencies. The frequencies of interest are over the current CATV bandwidth which ranges from 50 MHz to approximately 700 MHz. Each signal component in the CATV band has a bandwidth of approximately 6 MHz.

Plots of the second order HD and third order HD versus frequency for laser model A, based on the Device A parameters, are shown in Figure 5.1. The bias current for laser model A is 25 mA.

Plots of the second order HD and third order HD versus frequency for laser model B, based on the Device B parameters, are shown in Figure 5.2. The bias current for laser model B is 500 μA.

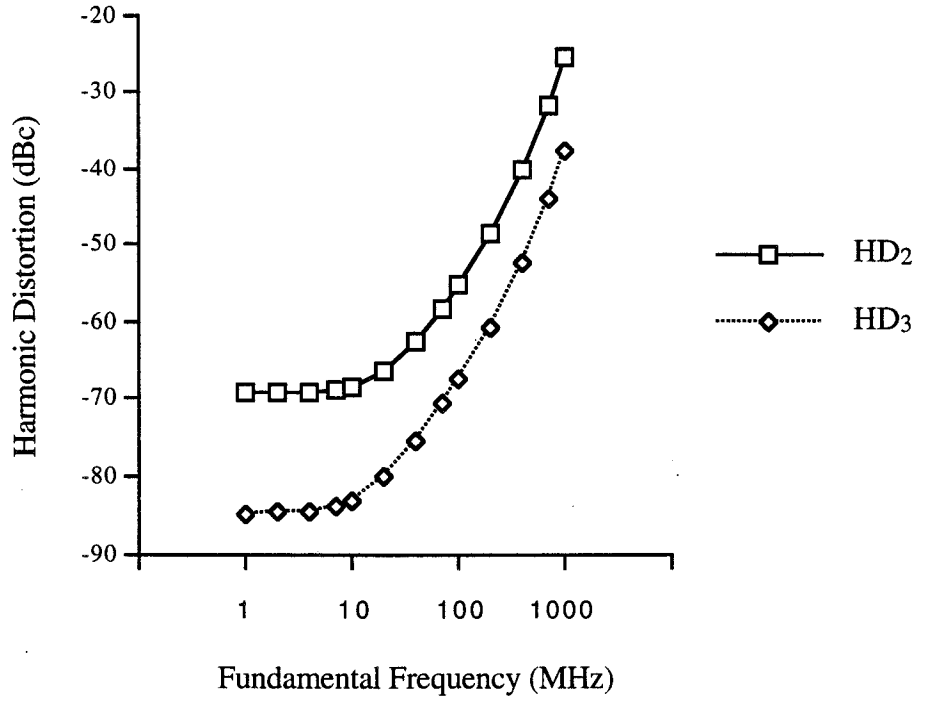

Figure 5.1 Second and third order HD of laser model A

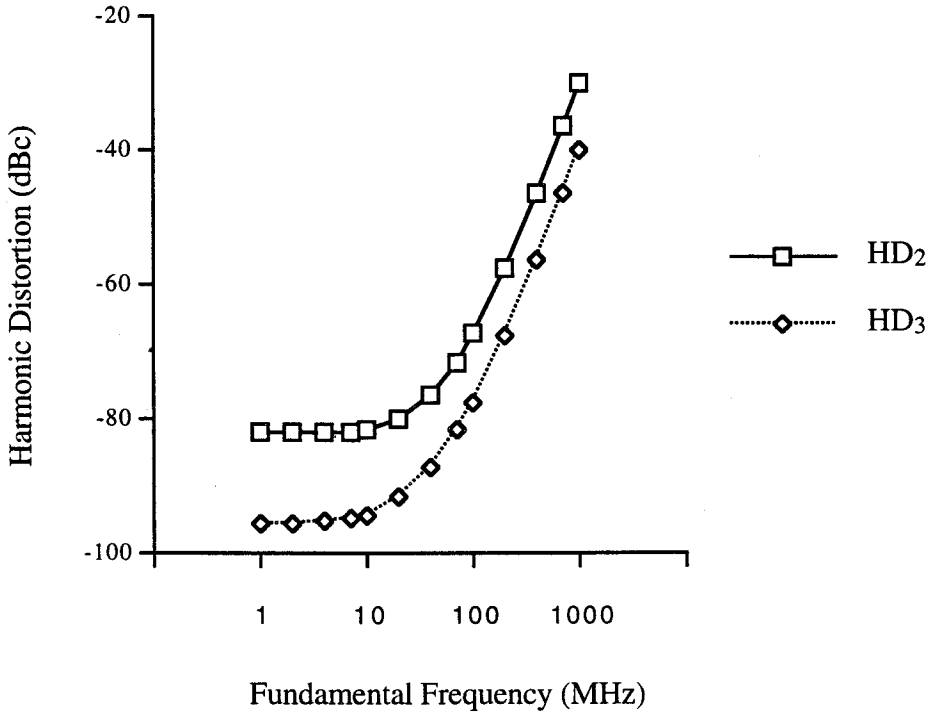

Figure 5.2 Second and third order HD of laser model B

For the purposes of comparing results to ones published by Kuo [37], the modulation index m can be changed from 0.30 to 0.04 for the laser model B. With this change, all of the parameters used in the calculation for second order HD based on Volterra series match those used in the calculations carried out by Kuo. The second order HD versus frequency is shown in Figure 5.3. The second order HD results developed from the Volterra series model generally agree with the results published by Kuo. Kuo did not publish results for third order HD.

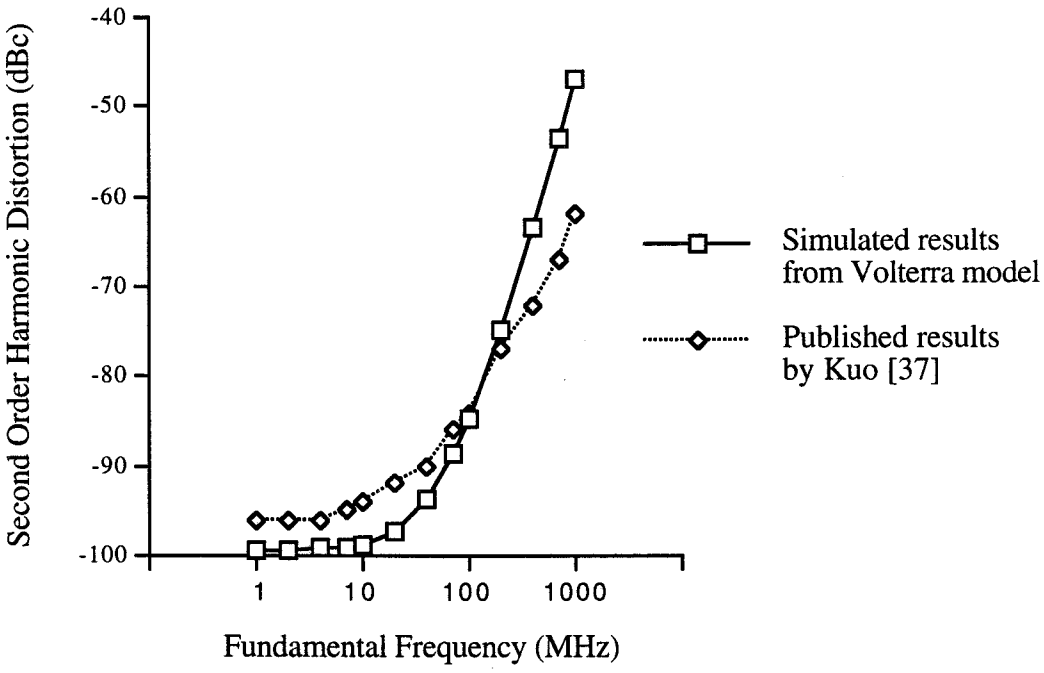

Figure 5.3 Second order HD of laser model B with modulation index 0.04

5.2 Harmonic Analysis of Laser Diode with Predistortion

The performance of the predistorter and the laser diode in cascade can also be evaluated by applying a single tone input to the system. Again, a frequency domain approach is used. The output of the predistorter and the laser is derived in detailed in Appendix C. The calculation is summarized below.

First, the output of the predistorter is calculated with the input being a delta function. Recalling equation (5.1), the output of a Volterra transfer function H_p is:

$$Y_p(\omega) = \frac{1}{(2\pi)^{p-1}} \int_{-\infty}^{\infty} \int_{-\infty}^{\infty} \cdots \int_{-\infty}^{\infty} H_p(\omega - \omega_1 - \omega_2 - \cdots - \omega_{p-1}, \omega_1, \omega_2, \cdots \omega_{p-1}) \\ X(\omega - \omega_1 - \omega_2 - \cdots - \omega_{p-1}) X(\omega_1) X(\omega_2) \cdots X(\omega_{p-1}) d\omega_1 d\omega_2 \cdots d\omega_{p-1} \tag{5.7}$$

For the predistorter with transfer functions P_1, P_2 and P_3 and input $X(\omega) = \delta(\omega - \omega_o)$, the frequency domain output is:

$$Y(\omega) = P_1(\omega_o)\delta(\omega - \omega_o) + \frac{1}{2\pi} P_2(\omega_o, \omega_o)\delta(\omega - 2\omega_o) \\ + \frac{1}{(2\pi)^2} P_3(\omega_o, \omega_o, \omega_o)\delta(\omega - 3\omega_o) \tag{5.8}$$

P_1, P_2 and P_3 represent $P_1(\omega_1)$, $P_2(\omega_1, \omega_2)$ and $P_3(\omega_1, \omega_2, \omega_3)$ which are developed in Chapter 4 and defined in equations (4.15), (4.16) and (4.17).

This output $Y(\omega)$ is now used as the input to the laser diode transfer functions L_1, L_2 and L_3. The output of the laser diode is a summation of delta functions ranging in frequencies from ω_o to $9\omega_o$. The coefficient of the ω_o term is the amplitude of the fundamental and the coefficient of the $n\omega_o$ term is the *n-th* harmonic amplitude. The terms at ω_o, $2\omega_o$ and $3\omega_o$ are:

$\delta(\omega - \omega_o)$:

$$L_1(\omega_o)P_1(\omega_o) = 1 \tag{5.9}$$

$\delta(\omega - 2\omega_o)$:

$$\frac{1}{2\pi}\left[L_1(2\omega_o)P_2(\omega_o, \omega_o) + L_2(\omega_o, \omega_o)P_1^2(\omega_o)\right] \tag{5.10}$$

$\delta(\omega - 3\omega_o)$:

$$\frac{1}{(2\pi)^2}\left[L_1(3\omega_o)P_3(\omega_o, \omega_o, \omega_o) + L_2(2\omega_o, \omega_o)P_2(\omega_o, \omega_o)P_1(\omega_o)\right. \\ \left. + L_2(\omega_o, 2\omega_o)P_1(\omega_o)P_2(\omega_o, \omega_o) + L_3(\omega_o, \omega_o, \omega_o)P_1^3(\omega_o)\right] \tag{5.11}$$

Since the amplitude of the fundamental is one, the second and third order HDs can be expressed as shown below. Again, the second and third order distortions can be calculated for the system as a function of frequency.

$$HD_2 = 20\log_{10}\left|\frac{1}{2\pi}\left[L_1(2\omega_o)P_2(\omega_o,\omega_o)+L_2(\omega_o,\omega_o)P_1^2(\omega_o)\right]\right| \tag{5.12}$$

$$HD_3 = 20\log_{10}\left|\begin{array}{l}\frac{1}{(2\pi)^2}\left[L_1(3\omega_o)P_3(\omega_o,\omega_o,\omega_o)+L_2(2\omega_o,\omega_o)P_2(\omega_o,\omega_o)P_1(\omega_o)\right.\\ \left.+L_2(\omega_o,2\omega_o)P_1(\omega_o)P_2(\omega_o,\omega_o)+L_3(\omega_o,\omega_o,\omega_o)P_1^3(\omega_o)\right]\end{array}\right| \tag{5.13}$$

Evaluation of predistorter A in cascade with Volterra laser model A were completed by calculating each term in the output expression. Plots of the second order HD and third order HD versus frequency are shown in Figure 5.4.

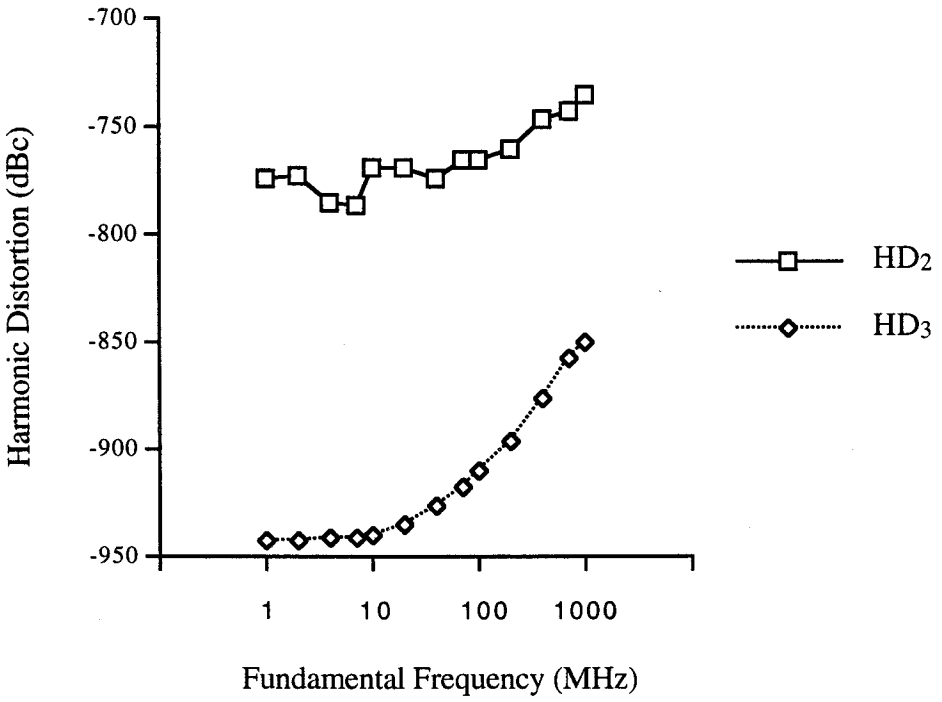

Figure 5.4 Second and third order HD of laser model A with predistortion

Plots of the second order HD and third order HD versus frequency for the model B predistorter and laser are shown in Figure 5.5. It should be noted that the Volterra model for the predistorter was truncated and then the inverse Volterra model was developed to form the laser model.

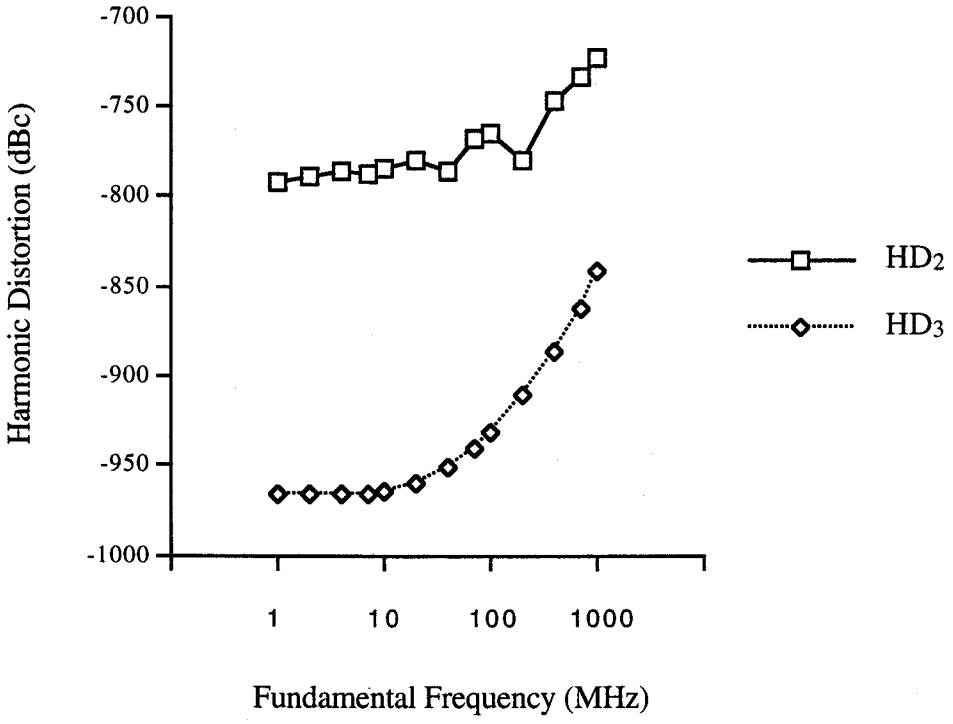

Figure 5.5 Second and third order HD of laser model B with predistortion

Comparing the results in Figure 5.1 and 5.2 with those in 5.4 and 5.5, it can be concluded that the cascading of the predistortion block in front of the laser diode block reduces the nonlinear distortion level at the output of the laser diode model over the required CATV bandwidth. These calculations were done theoretically and what the results show is that the predistorter serves as an inverse system for the Volterra model for the laser diode. Thus, -900 dBc distortion shows that this predistorter is very close to being an exact inverse of the laser diode model. Numbers like -700 dBc and -900 dBc are

unrealistic numbers in a real circuit. It should be noted that the laser diode model has also been truncated and does not exactly represent the actual laser characteristic.

5.3 Summary and Discussion

Examining the results in Figure 5.1, 5.2 and 5.3 it can be seen that the HD increases with frequency for both models. This result has been demonstrated experimentally [24], [33], [35], and [37]. As a result, the statement that lasers cannot be modeled as linear memoryless systems has been proven correct. This further demonstrates that a broadband compensation circuit has to take into consideration that the distortions increase with frequency. By modeling the predistorter with a Volterra series, this is accomplished.

There are two reasons why the performance of the predistorter and the laser as a system was not evaluated in terms of intermodulation distortion (IMD). The first is that this model will not show fifth order distortion because this model does not have a fifth order path. This model has only up to third. Third order IMD resulting from third order products (i.e. $2\omega_1 - \omega_2$) could be calculated for the predistorter; however, fifth order products with the same resultant frequencies (i.e. $\omega_1 + \omega_1 + \omega_1 - \omega_1 + \omega_2$) would not show up. The second reason is that even the calculation for the third order IMD out of the laser is too complicated. If a two tone signal is applied to the input of the predistorter, the output of the predistorter consists of 64 terms. If this signal is then applied to the input of the laser, the output of the laser will grow to 266,304 terms.

As a result, this section on Volterra series modeling is used primarily to initiate the design process for the predistorter. By testing HD with the predistorter and laser in cascade, the design for the predistorter is verified. Testing the predistorter and laser for IMD can be accomplished with time domain simulation or by laboratory experiment.

6. TIME DOMAIN MODELS

6.1 Time Domain Model of Laser Diode

In the previous chapter, the models for the laser and the predistorter were based on a frequency domain approach. The inputs, outputs and transfer functions were all analyzed in the frequency domain. In this chapter, time domain models for the laser and the predistorter are developed. The time domain model for the laser is based on a time domain simulation of the semiconductor rate equations. A similar time domain model for the predistorter was developed from the predistorter Volterra transfer functions discussed in Chapter 5.

There are a number of advantages for a time domain model of a semiconductor laser. First, this type of model facilitates the simulation of input signals which are more complicated than a pure sinusoid. For example, pulse response and multiple tone input signals can be simulated as easily as single tone signals. Second, the effect of any change in the laser parameters on the light output can be analyzed with the light versus current curve, the derivative of light versus current curve, and nonlinear distortion products. This can assist in semiconductor laser design. Finally, the model can be simultaneously tested with the circuit model of a compensation circuit to predict the improvement that a linearizer circuit would have on the laser's output distortion levels.

The time domain simulation of the laser diode is achieved through the use of the circuit simulation software package Electronic Circuit Analysis-2 (ECA-2) [78]. The two rate equations are the foundation for an equivalent circuit model for the laser. This circuit

model has the drive current as the input and a monitoring voltage represents the output photon density. A large-signal circuit model of a laser diode was first introduced and modified by Tucker [79], [80]. Tucker used the large-signal model to match the large-signal turn-on and turn-off response of InGaAsP lasers by including the chip parasitic effects. Tucker used SPICE2 circuit simulation software. Way [47] extended Tucker's work to use the new rate equations which contain ε and β. By utilizing SPICE2 software, Way successfully predicted nonlinear distortions due to intensity modulation. Neusy and McGee [41] extended Way's and Tucker's work by simulating the step response of the laser as well as harmonic and intermodulation distortion. Neusy and McGee used the Block Oriented System Software (BOSS) package.

In order to aid in the understanding of how an equivalent circuit model is derived from the rate equations, a simplified example is presented.

Consider the following differential equation:

$$C\frac{dN}{dt} = I - \frac{N}{R} \tag{6.1}$$

If the source is a current source I and the output is voltage N, the equivalent circuit is as shown in Figure 6.1.

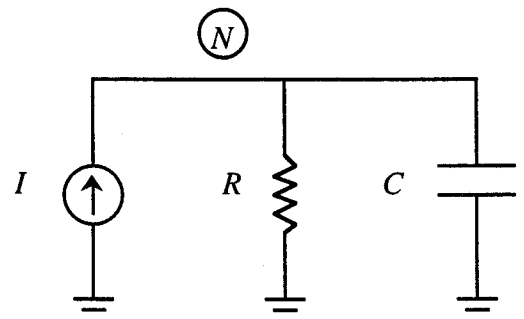

Figure 6.1 Equivalent RC circuit

Examining the first rate equation (6.2), it can be seen that the first three terms are analogous to the previous circuit with $C = 1$ and $R = \tau_s$.

$$\frac{dN}{dt} = \frac{I}{V} - \frac{N}{\tau_s} - g(N - N_o)(1 - \varepsilon S)S \tag{6.2}$$

$$\frac{dS}{dt} = \Gamma g(N - N_o)(1 - \varepsilon S)S - \frac{S}{\tau_p} + \Gamma\beta\frac{N}{\tau_s} \tag{6.3}$$

The remaining term in the rate equation (6.2) can be represented by a Zener diode and a nonlinear conductance $g[1 - \varepsilon S]S$.

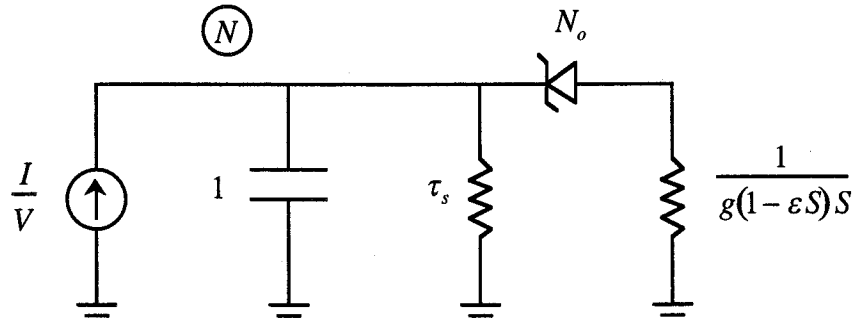

Figure 6.2 Equivalent circuit for rate equation (6.2)

The second rate equation (6.3) can be represented by an equivalent circuit that has two current sources, $\Gamma g(N - N_o)(1 - \varepsilon S)S$ and $\Gamma\beta\frac{N}{\tau_s}$.

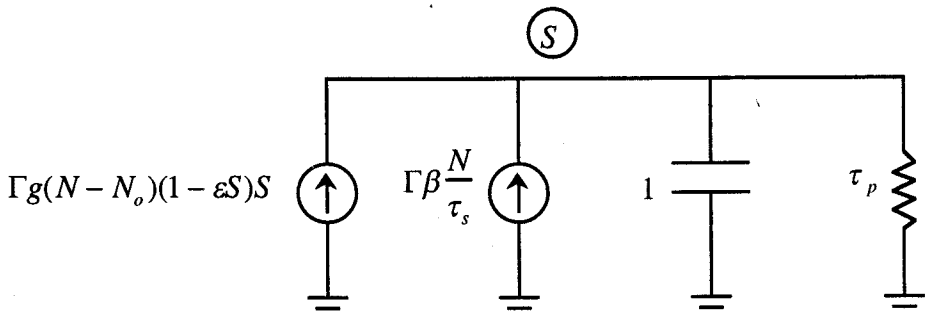

Figure 6.3 Equivalent circuit for rate equation (6.3)

Combining these two circuits into one circuit results in the circuit shown in Figure 6.4. This is the equivalent of the two rate equations combined.

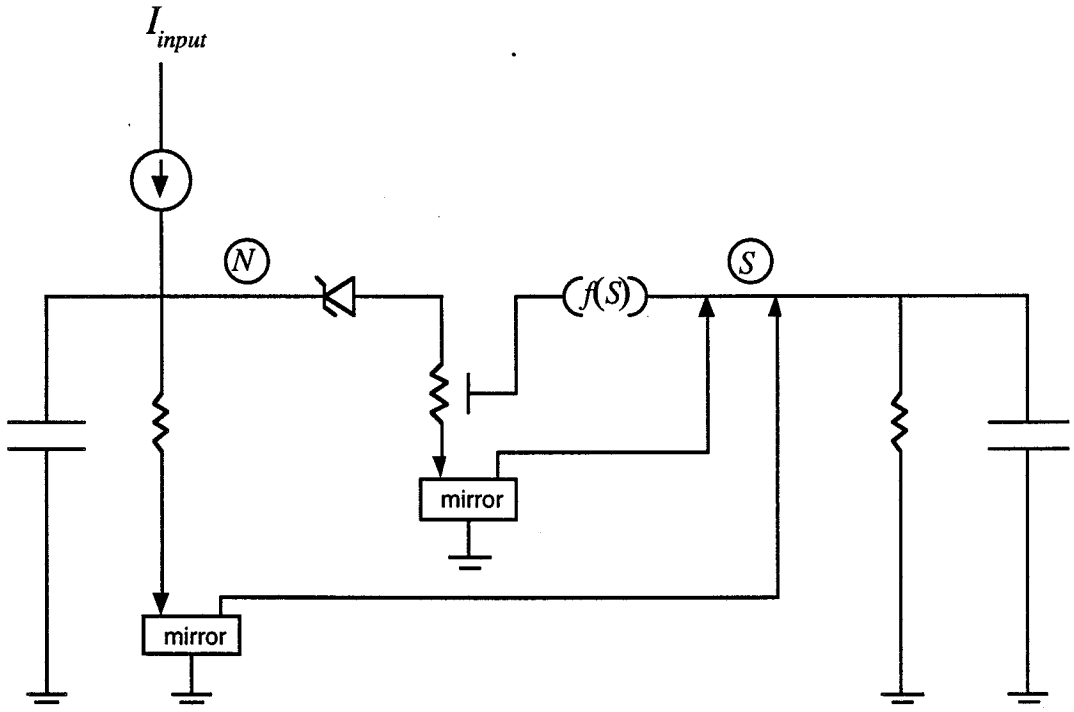

Figure 6.4 Equivalent circuit for both rate equations (6.2) and (6.3)

In this model, the injection current I is the input and the voltage S represents the density of photons output by the laser. With this model, harmonic distortion can be determined by using a single tone input, measuring the output signal and then performing a Fast Fourier Transform (FFT) on the output. Similarly, intermodulation distortion can be measured by inputting multiple tones and performing an FFT on the output. This model also facilitates the simulation of dc characteristics such as light versus current and responses to step inputs. Two ECA-2 program listings of the equivalent circuit for the laser model shown in Figure 6.4 are given in Appendix D. These listings are for the Device A and Device B laser parameters. The term $f(S)$ means that a function of S is used to modulate the resistor, that function being $[1-\varepsilon S]S$.

6.2 DC Characteristics of Laser Diode Model

One of the major advantages of the time domain model over the frequency domain model is the simulation of the laser's dc characteristics. These include plotting the light versus current curve and subsequently the derivative of this curve. Further, the response of the laser to step inputs can also be simulated.

In order to validate our circuit model for the laser, these dc simulations will be carried out for both the Device A and Device B parameters.

The light versus current curve for the laser model A is shown in Figure 6.5 and Figure 6.6. The first plot shows the curve over a large current range and demonstrates the saturation effect at high input currents. The second plot demonstrates the turn-on effect of the laser at low input currents. The same plots for the laser model B are shown in Figure 6.7 and Figure 6.8.

By differentiating these plots, the derivative of the light versus current versus current curve can be obtained. The derivative of the light versus current versus current curve for the laser model A is shown in Figure 6.9. The derivative of the light versus current versus current curve for the laser model B is shown in Figure 6.10. In Figure 6.9 and 6.10, the effect of numeric truncation in the simulation can be seen in the "noise" excursions.

The portions of the curve above 100 mA in Figures 6.5 and 6.9 and the portions of the curve above 5 mA in Figures 6.7 and 6.10 represent simulations where the term $\varepsilon S \geq 0.2$. The model is not changed for these simulations but an alternate approach for these higher currents is to represent the term $(1-\varepsilon S)$ as $\left(\frac{1}{1+\varepsilon S}\right)$.

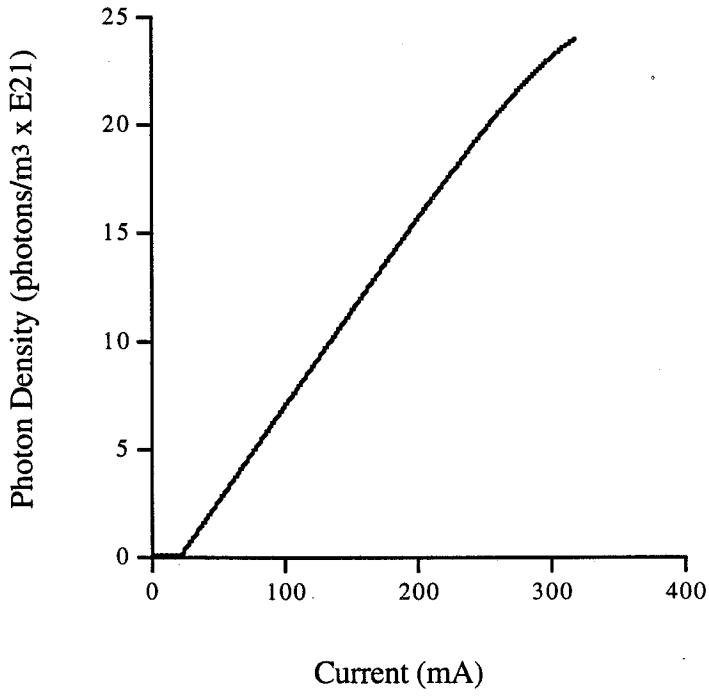

Figure 6.5 Light versus current for laser model A

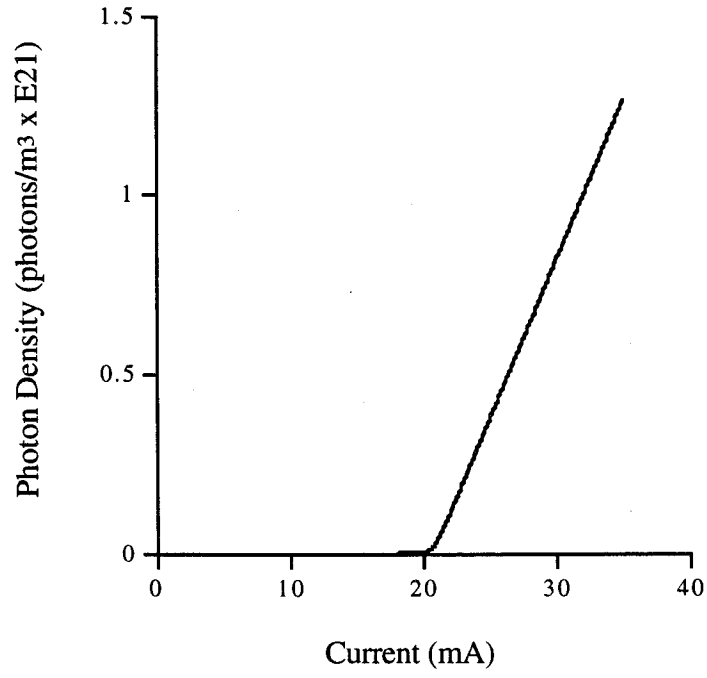

Figure 6.6 Light versus current for laser model A (turn-on range)

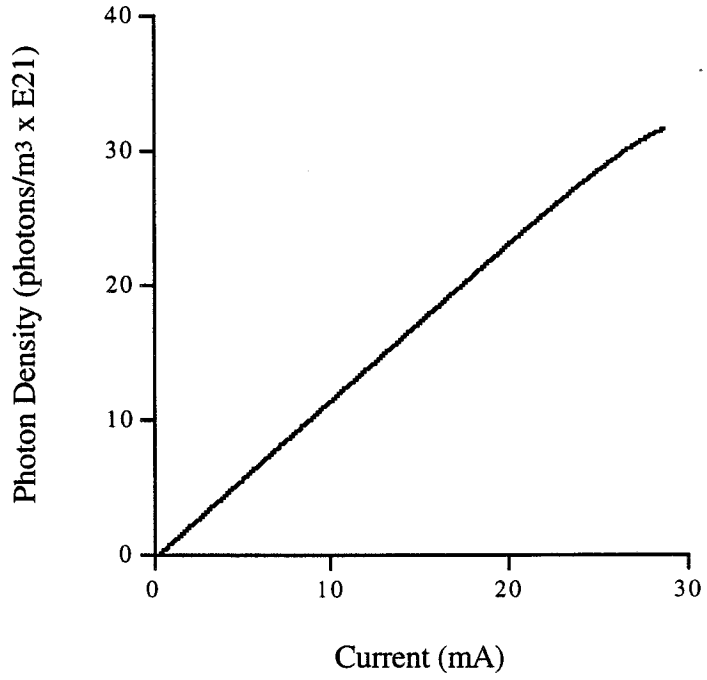

Figure 6.7 Light versus current for laser model B

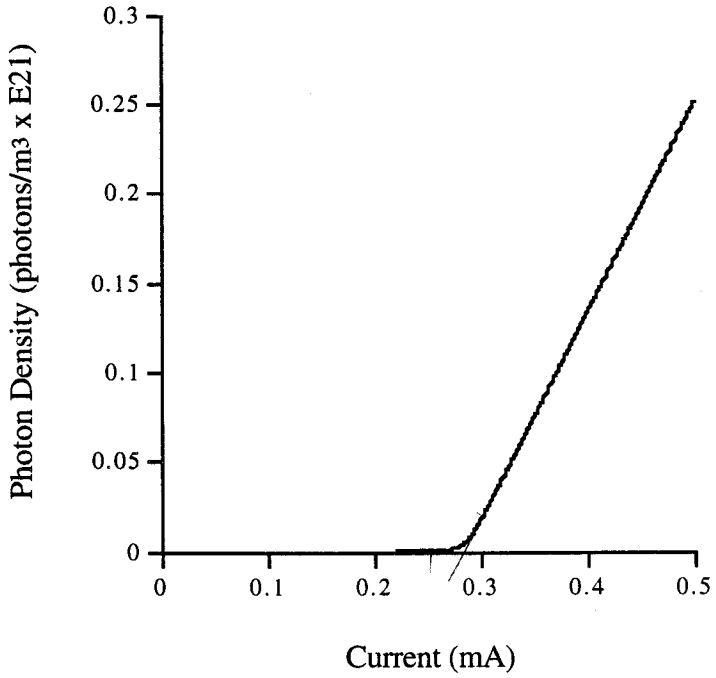

Figure 6.8 Light versus current for laser model B (turn-on range)

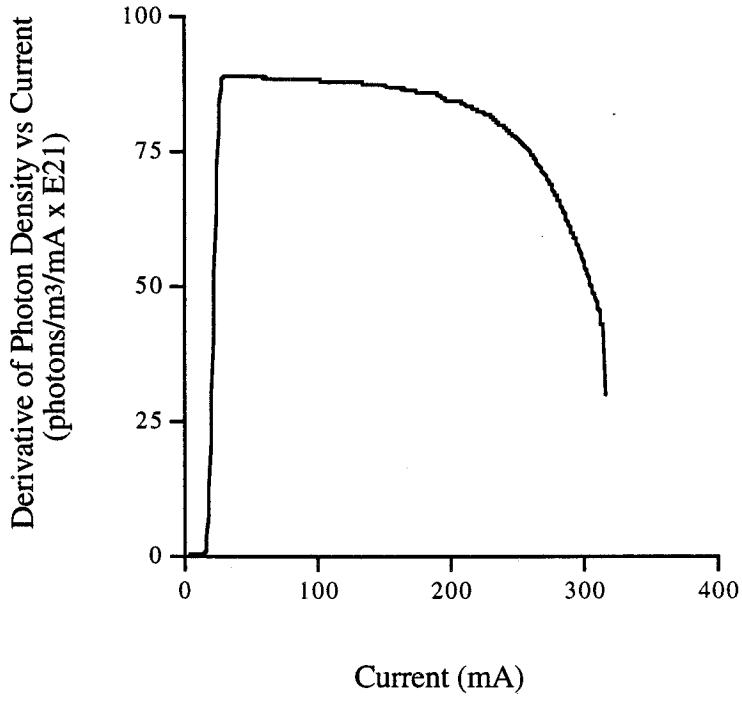

Figure 6.9 Derivative of light versus current versus current for laser model A

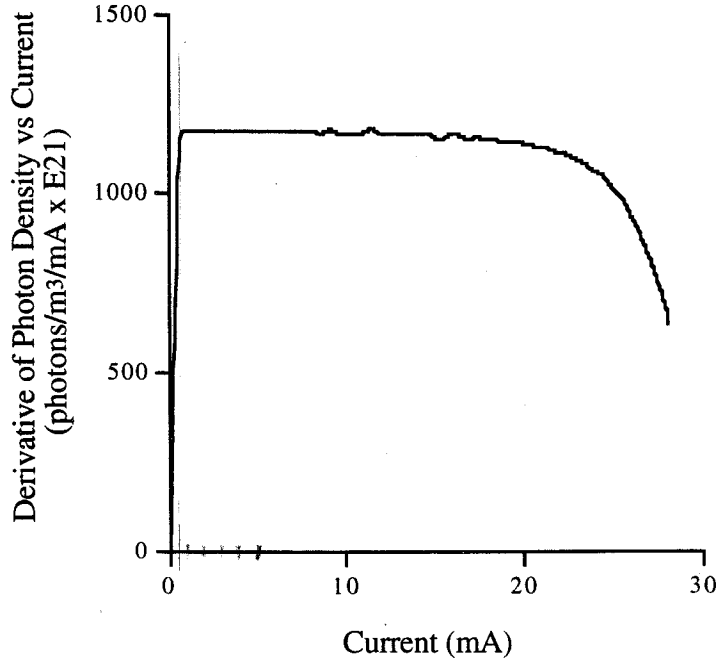

Figure 6.10 Derivative of light versus current versus current for laser model B

The last simulation is to measure the response of the laser to a step input. Most lasers exhibit an oscillatory response to a step input. The frequency with which the laser oscillates is called the resonance frequency. This frequency is important because distortions can increase significantly when the input frequency approaches this value. Both lasers are stepped from zero input to a bias level just above threshold. The laser model A is stepped from zero to 25 mA at time zero. The laser model B is stepped from zero to 500 μA at time zero. These results are shown in Figure 6.11 and Figure 6.12.

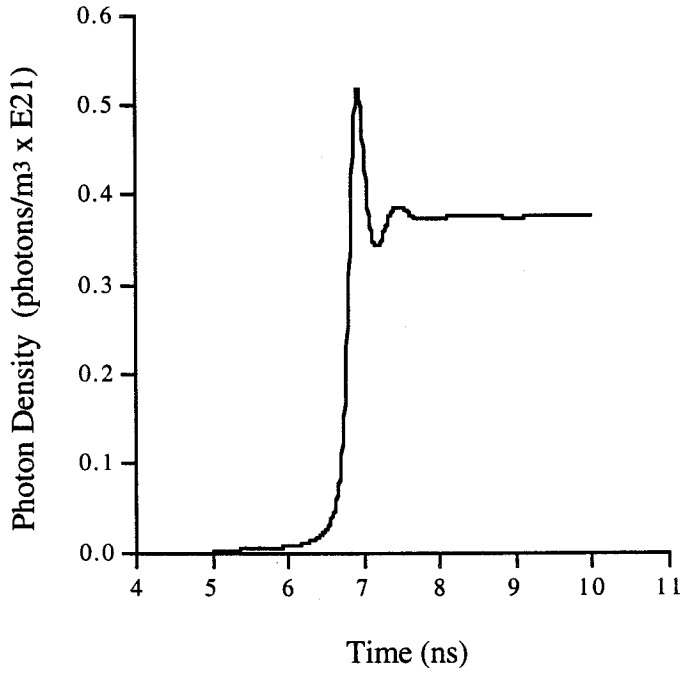

Figure 6.11 Pulse response of laser model A

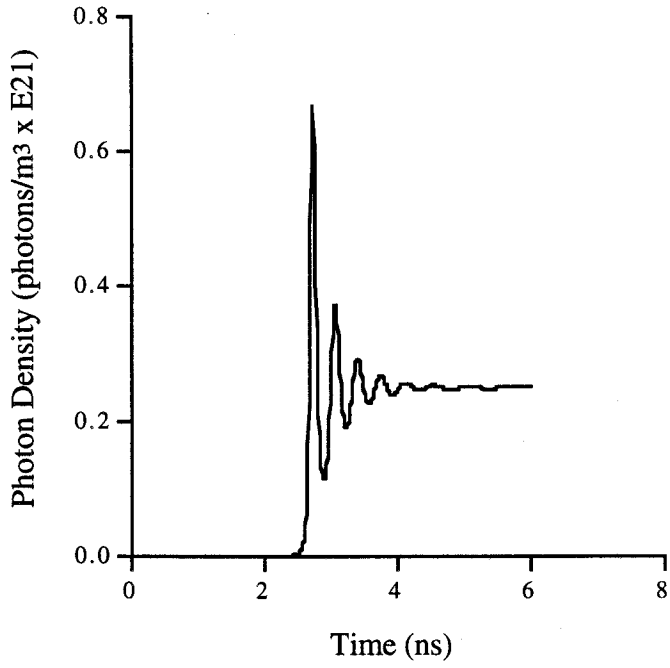

Figure 6.12 Pulse response of laser model B

6.3 Time Domain Model of Predistorter

The rate equations provide a means to create an equivalent circuit model of the laser. There are no direct rate equations which describe the operation of a predistorter. However, a time domain model for the predistorter can still be designed. Examining the Volterra model of the predistorter, it will be shown that it lends itself to a derivation of a time domain model.

Volterra systems of low order are implemented by decomposition of the system Volterra function into lower-order functions of a linear type [76]. Combination of these linear systems by multiplication and addition techniques delivers the function for the Volterra system.

If you consider a second order system with kernel $h_2(\tau_1,\tau_2)$, the Laplace transform can be written as $H_2(s_1,s_2)$:

$$H_2(s_1,s_2) = \int_{-\infty}^{\infty}\int_{-\infty}^{\infty} h_2(\tau_1,\tau_2)e^{-(s_1\tau_1+s_2\tau_2)}d\tau_1 d\tau_2 \tag{6.4}$$

In (6.4), $s_i = \sigma_i + j\omega_i$ so that the Fourier transforms previously discussed can be obtained by letting $\sigma_i = 0$. $H_2(s_1,s_2)$ can be written in the form of multiplication of linear system Laplace transforms:

$$H_2(s_1,s_2) = H_a(s_1)H_b(s_2)H_c(s_1+s_2) \tag{6.5}$$

in which

$$H(s) = \int_{-\infty}^{\infty} h(t)e^{-st}dt \tag{6.6}$$

$H_a(s)$, $H_b(s)$ and $H_c(s)$ are the system functions of the linear systems with impulse responses $h_a(t)$, $h_b(t)$ and $h_c(t)$ respectively. This can be viewed in a schematic form in Figure 6.13.

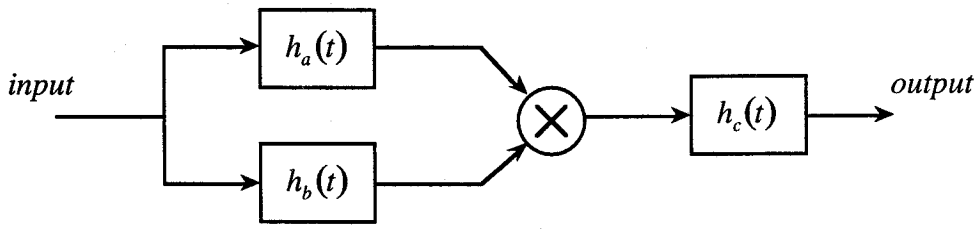

Figure 6.13 Second order Volterra system

In a similar format, a third order Volterra system is of the form:

$$H_3(s_1,s_2,s_3) = H_a(s_1)H_b(s_2)H_d(s_3)H_c(s_1+s_2)H_e(s_1+s_2+s_3) \tag{6.7}$$

and can be realized in the schematic shown in Figure 6.14.

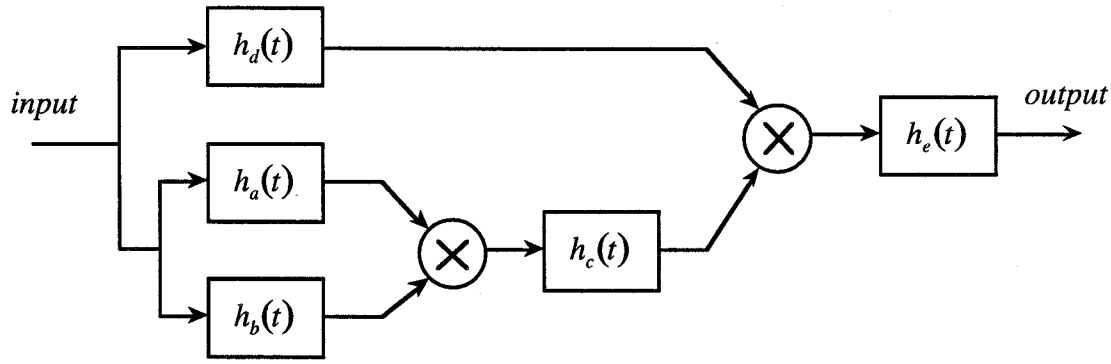

Figure 6.14 Third order Volterra system

Now, the Volterra transfer functions representing the predistorter are developed in the time domain. Recalling the three transfer functions:

$$P_1(\omega) = \left(b + cj\omega - d\omega^2\right)S \tag{6.8}$$

$$P_2(\omega_1, \omega_2) = \left(2e + fj(\omega_1 + \omega_2) - h(\omega_1 + \omega_2)^2\right)S^2 \tag{6.9}$$

$$P_3(\omega_1, \omega_2, \omega_3) = \left(6k + 2lj(\omega_1 + \omega_2 + \omega_3) - 2m(\omega_1 + \omega_2 + \omega_3)^2\right)S^3 \tag{6.10}$$

The above Fourier transforms can also be represented as Laplace transforms with the substitution of $s = \sigma + j\omega$ where $\sigma = 0$.

$$P_1(s) = \left(b + cs + ds^2\right)S \tag{6.11}$$

$$P_2(s_1, s_2) = \left(2e + f(s_1 + s_2) + h(s_1 + s_2)^2\right)S^2 \tag{6.12}$$

$$P_3(s_1, s_2, s_3) = \left(6k + 2l(s_1 + s_2 + s_3) + 2m(s_1 + s_2 + s_3)^2\right)S^3 \tag{6.13}$$

As can be seen, the Laplace transfer functions (6.12) and (6.13) are in the forms developed in (6.5) and (6.7) respectively. Examining the second order case, it can be seen that $P_2(s_1,s_2)$ is just a function of (s_1+s_2) so that $H_a(s_1)$ and $H_b(s_2)$ are equal to one. Their corresponding impulse responses are δ–functions. Figure 6.15 shows the block diagram of $P_2(s_1,s_2)$ synthesized by a multiplier and a linear system $p_2(t)$.

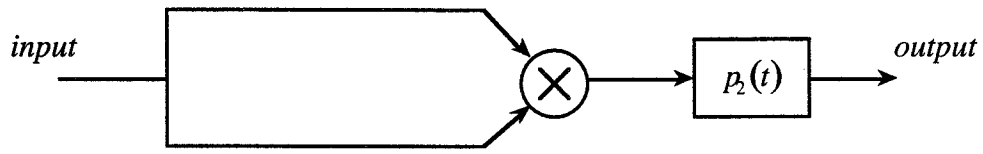

Figure 6.15 Second order Volterra system for the predistortion block

Similarly for the third order case, $P_3(s_1,s_2,s_3)$ is just a function of $(s_1+s_2+s_3)$ so that $H_a(s_1)$, $H_b(s_2)$, $H_c(s_1+s_2)$, and $H_d(s_3)$ are all equal to one. Thus, the block diagram of $P_3(s_1,s_2,s_3)$ synthesized by a multiplier and a linear system $p_3(t)$ is shown in Figure 6.16.

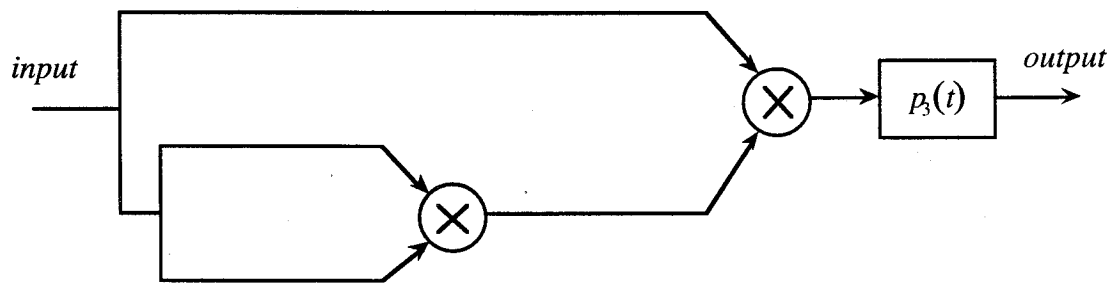

Figure 6.16 Third order Volterra system for the predistortion block

Thus, the predistorter system developed to this point is shown in Figure 6.17.

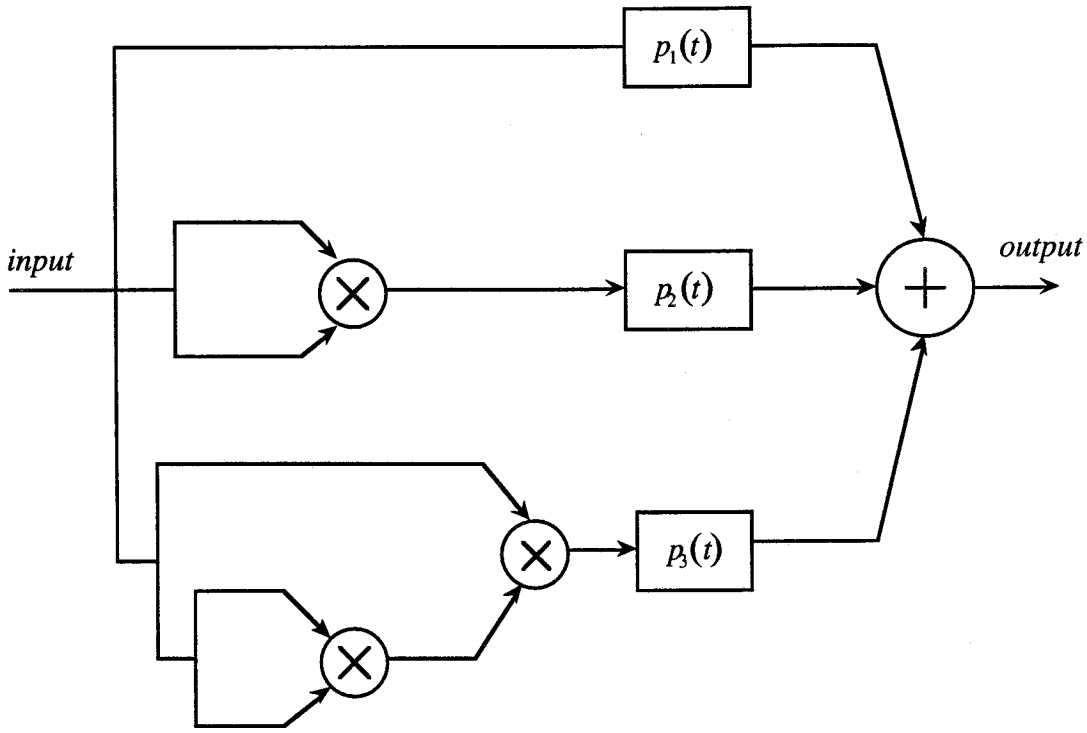

Figure 6.17 Realization of the predistortion block with Volterra series

The Laplace transfer functions (6.11), (6.12) and (6.13) are all of the form:

$$P(s) = a + bs + cs^2 \tag{6.14}$$

where $s = s, s_1 + s_2, s_1 + s_2 + s_3$ depending on the order of the function.

This corresponds to an amplifier with gain a, that is added to a differentiator with gain b, and a double differentiator with gain c.

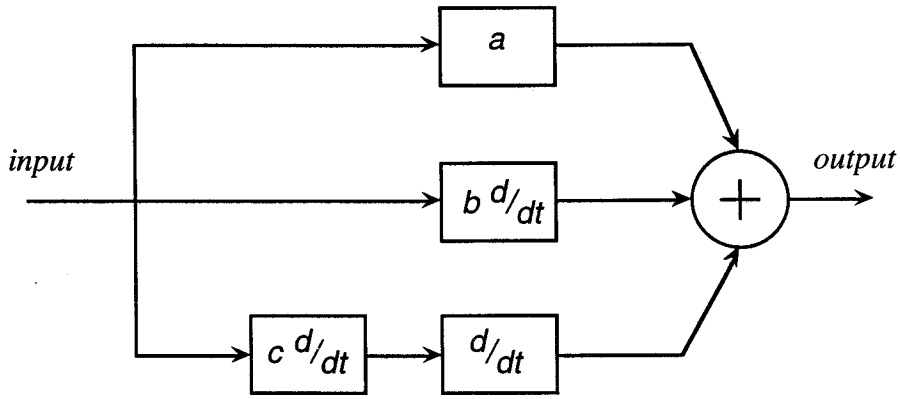

Figure 6.18 Realization of Laplace transfer function (6.14) in the time domain

Thus, the entire predistorter as represented by the transfer functions (6.8)-(6.10) and (6.11)-(6.13) can be represented in the time domain with the block diagram shown in Figure 6.19. The gain term S has been omitted from this figure but could be included in the gain terms shown.

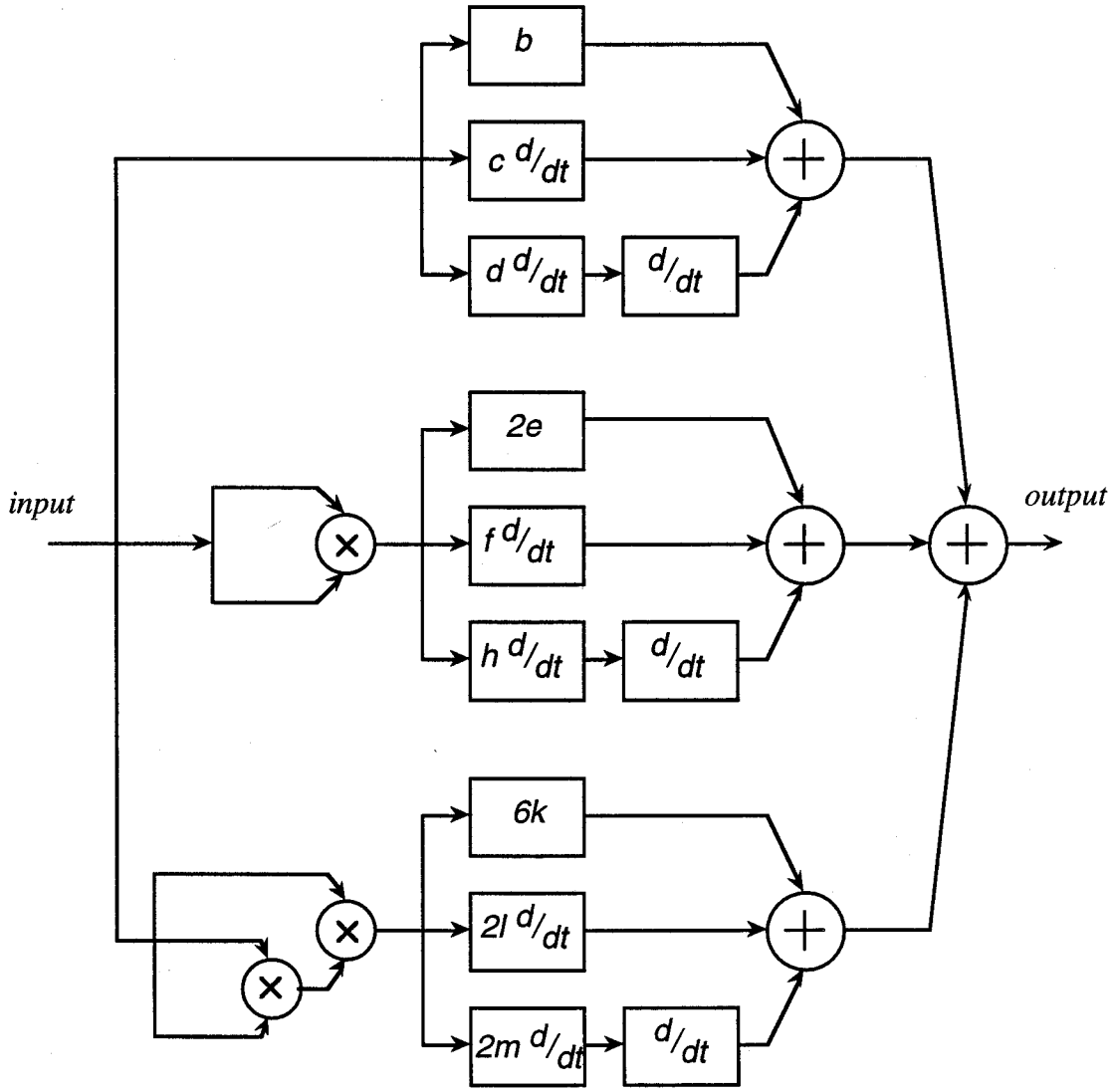

Figure 6.19 Predistortion block in the time domain

An important point to note about the predistorter is that it should be stable. It is known that any system with a given Laplace transform will be unstable if it has a pole on the right-hand side of the s-plane. The Laplace transforms for the predistorter (6.11)-

(6.13) have no poles, only zeros. Thus, the predistorter should be stable. Further, it can be seen that the predistorter is a causal system.

6.4 Summary and Discussion

In this chapter, a time domain model for the laser and a time domain model for the predistorter have been developed. The time domain model for the laser was based on an equivalent circuit model of the single-mode semiconductor laser rate equations. The circuit model was realized with the circuit simulation software package ECA-2. The time domain model for the predistorter was developed from the Volterra transfer functions of the predistorter shown in Chapter 4. The Volterra transfer functions are an approximation of the inverse of the laser characteristic. There are no direct rate equations that describe the operation of the predistorter.

The dc characteristics of the laser were included to verify the model for the laser and to demonstrate the extra simulating capabilities that the time domain model has over the frequency domain model. The threshold current shown in Figure 6.6 and the pulse response shown in Figure 6.11 agree with the results published by McGee [41]. Further, this time domain model differs from the time domain model presented in [41] and [47] in that this model uses a Zener diode in the circuit to represent the threshold carrier density as opposed to handling the term in the mathematics of a transfer function. Further, this model does not assume that the carrier density is constant, but rather keeps it a variable as defined in the rate equations.

The time domain models for the laser and the predistorter play an important role in predicting the distortion levels at the output of the laser (with and without predistortion).

7. HARMONIC AND INTERMODULATION PERFORMANCE OF TIME DOMAIN MODELS

As was previously mentioned in Chapter 2, any laser nonlinearities in an analog application will create frequency components in the output signal that were not present in the input signal. Two important methods of assessing nonlinear effects are based on the measurements of harmonic distortion and intermodulation distortion.

The harmonic and intermodulation distortion of laser model A and laser model B with and without predistortion is presented in this chapter. The purpose is to show that the harmonic and intermodulation distortion levels decrease when a predistortion block is added to the signal path prior to the laser.

7.1 Harmonic Performance of the Laser Diode and Predistorter

To carry out the simulations, the laser and predistorter were represented in the time domain. The laser was configured in ECA-2 by representing the rate equations in an equivalent circuit format as described in Chapter 6. The predistorter was also configured in ECA-2 as a modified version of the time domain model described in Chapter 6. The predistorter was cascaded in front of the laser and its transfer function was normalized so that the input and the output of the predistorter was current. This facilitates the comparison of the laser's output with and without predistortion.

To measure the harmonic distortion created by the laser, a time domain signal consisting of a sinusoid current was input to the laser and the output photon density was

measured. A FFT was performed on the output photon density and the ratio of the power in the second and third harmonics to the fundamental gave the resulting second and third order harmonic distortions respectively. To measure the harmonic distortion in the output of the laser when the predistorter was included, the input sinusoid current was first applied to the predistorter whose output was in turn applied to the input of the laser. Again, a FFT was performed on the output photon density and the ratio of the power in the second and third harmonics to the fundamental gave the resulting harmonic distortion.

A plot of the second order harmonic distortion for laser model A with and without predistortion is shown in Figure 7.1. A plot of the third order harmonic distortion for laser model A with and without predistortion is shown in Figure 7.2.

Laser model A uses the device parameters set out in Table 5.1 which were originally presented in [47]. Again, the bias current is 25 mA and the modulation index for the input current is 0.20.

A plot of the second order harmonic distortion for laser model B with and without predistortion is shown in Figure 7.3. A plot of the third order harmonic distortion for laser model B with and without predistortion is shown in Figure 7.4.

Laser model B uses the device parameters set out in Table 5.2 which were originally presented in [37]. Again, the bias current is 500 μA and the modulation index for the input current is 0.30.

For the purposes of comparing results to published ones, the modulation index m can be changed from 0.30 to 0.04 for the Device B parameters and the second order HD versus frequency can be plotted as shown in Figure 7.5. These results can be compared to the results shown in Figure 5.3 where the same device parameters were used.

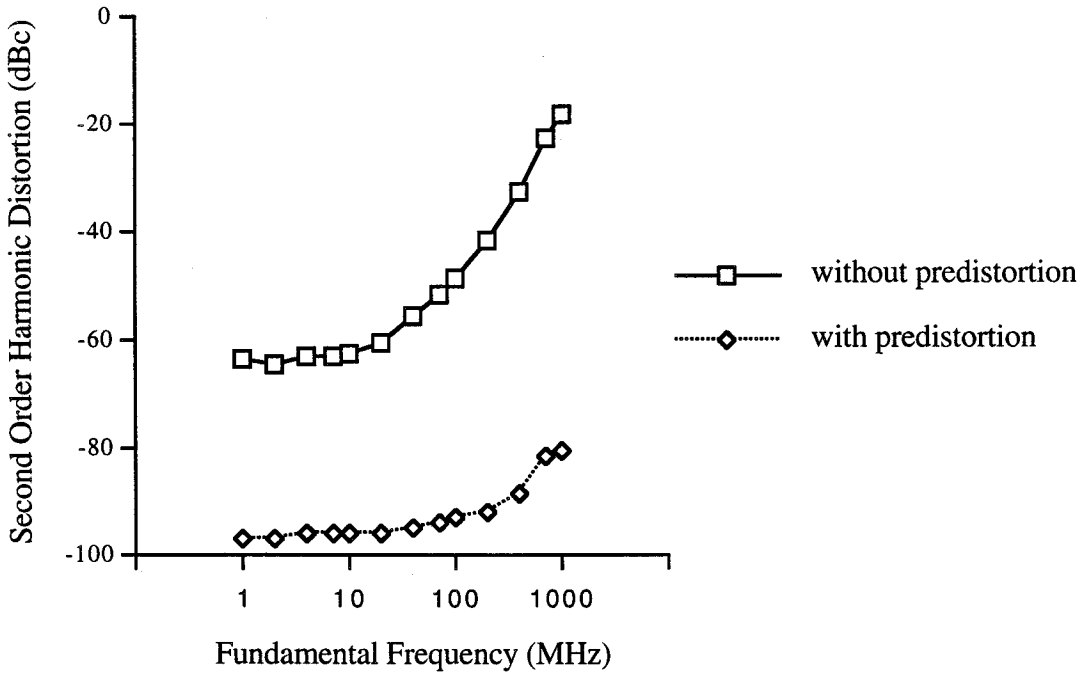

Figure 7.1 Second order HD of laser model A with and without predistortion

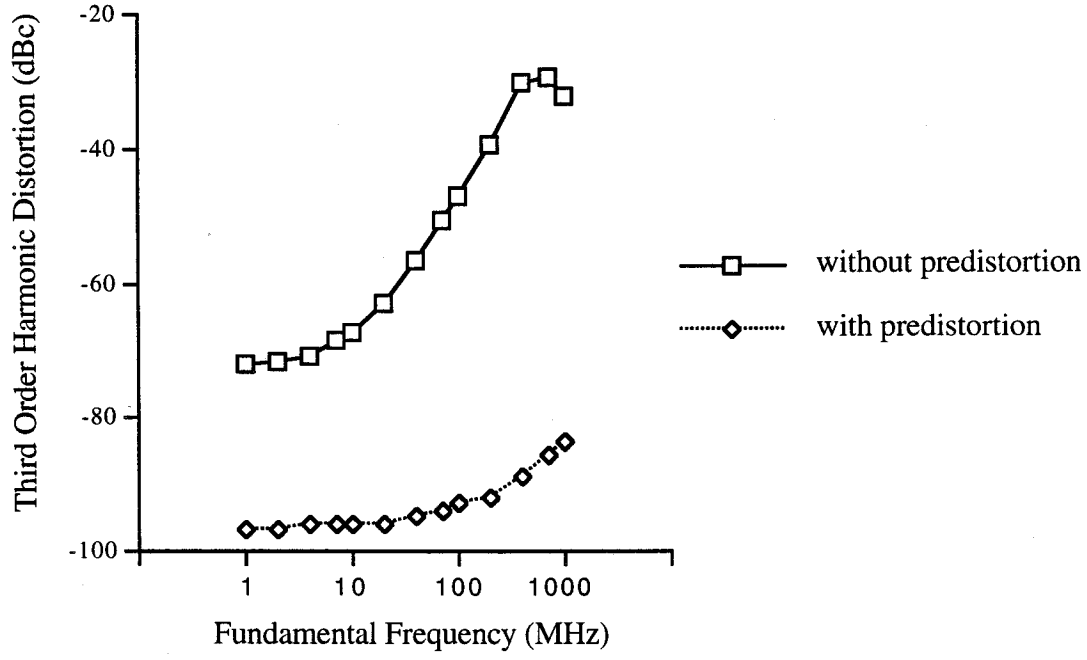

Figure 7.2 Third order HD of laser model A with and without predistortion

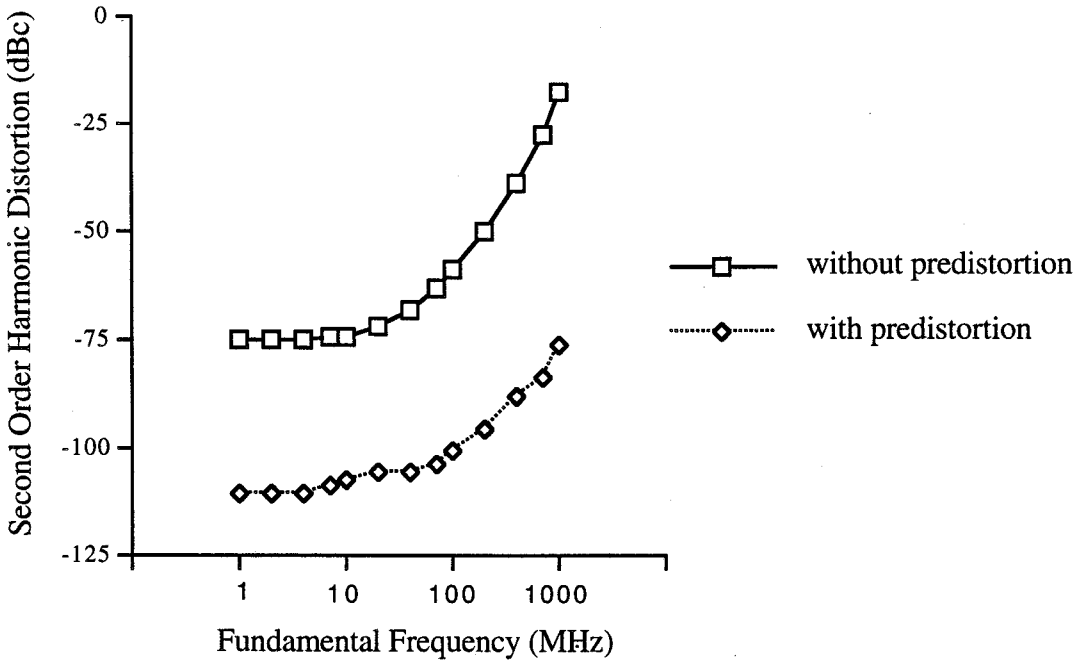

Figure 7.3 Second order HD of laser model B with and without predistortion

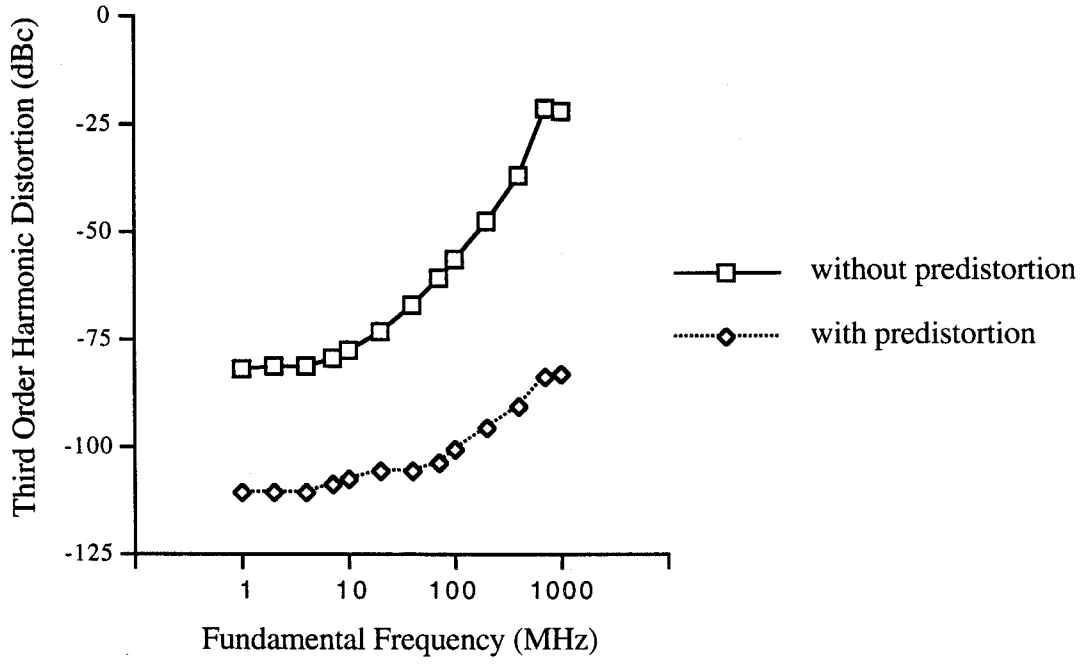

Figure 7.4 Third order HD of laser model B with and without predistortion

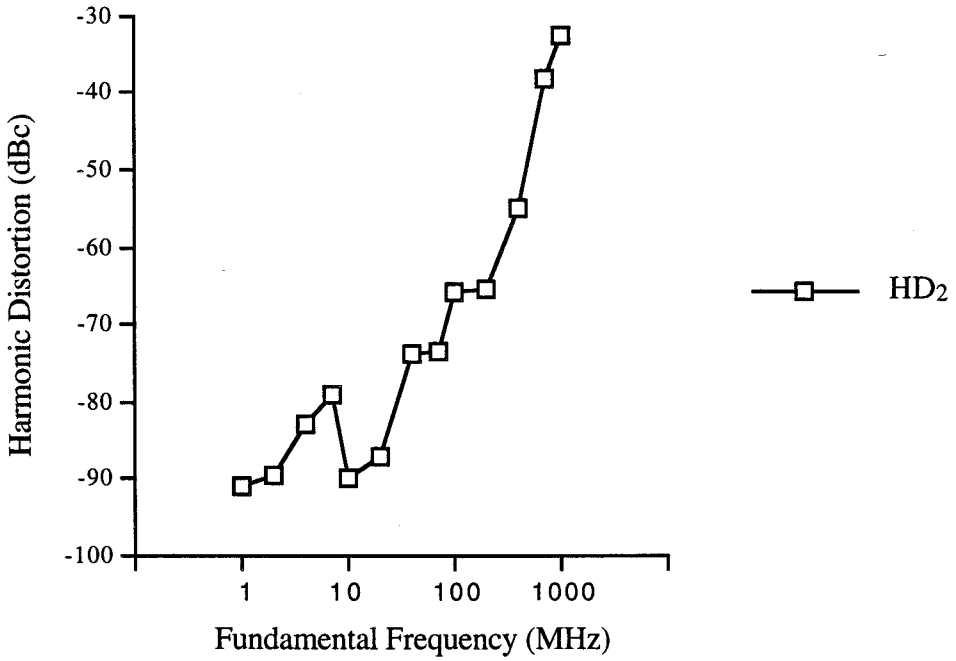

Figure 7.5 Second order HD of laser model B with modulation index 0.04

The circuit model for the laser can also be verified by comparing simulated results with experimentally measured results published by Way [47] for an actual laser. Device A parameters listed in Table 5.1 were determined for an Ortel LS-620 laser diode and were used by Way in his simulations. Figure 7.6 shows the second order harmonic distortion as a function of bias current for the experimentally measured and simulated results. The results in Figure 7.6 are for a modulating signal of 1 GHz and 11.2 mA peak-to-peak modulating current. Way lists a threshold current of 21 mA. From these results, it can be seen that there is a close agreement between the experimentally measured results and the simulated results. Simulations were also carried out for input frequencies of 2 GHz and a modulating current of 18 mA peak-to-peak. There was a close agreement between these results and the experimental results as well.

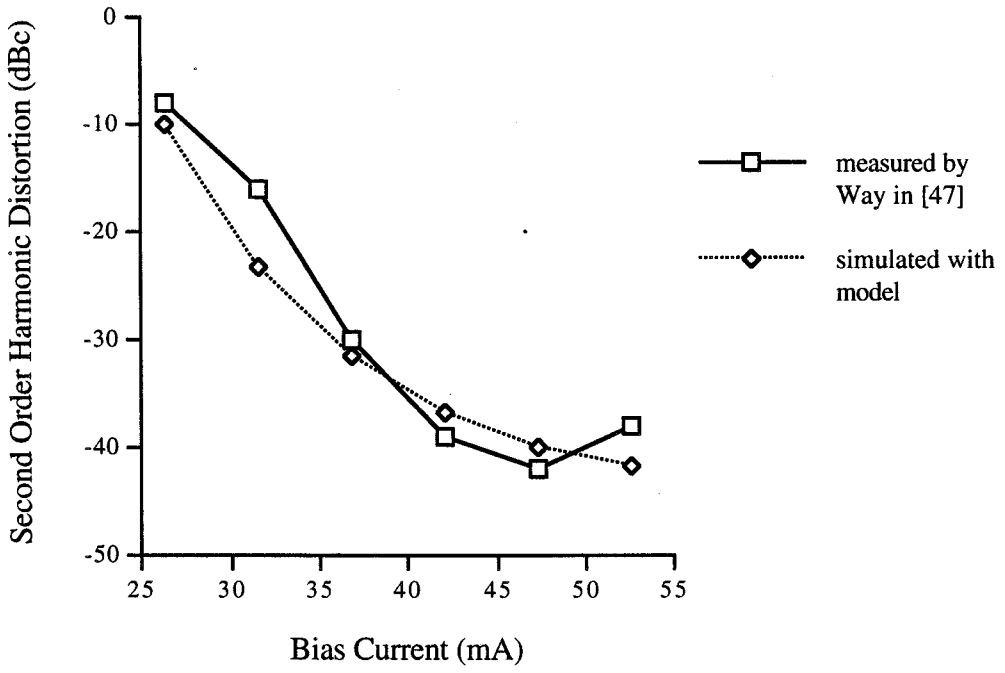

Figure 7.6 Second order HD versus bias current of laser model A with modulating current of 11.2 mA peak-to-peak

7.2 Intermodulation Performance of the Laser Diode and Predistorter

A plot of the third order intermodulation distortion for laser model A with and without predistortion is shown in Figure 7.7. For laser model A, the bias current is 25 mA and the modulation index is 0.20.

A plot of the third order intermodulation distortion for laser model B with and without predistortion is shown in Figure 7.8. For laser model B, the bias current is 500 μA and the modulation index is 0.30.

The frequency spacing between the two carriers is ten percent of the first carrier. For example, to measure the intermodulation products at 10 MHz, two carriers at frequencies 10 MHz and 11 MHz are combined at the input of the laser. The third order products will appear at 9 MHz and 12 MHz in the output.

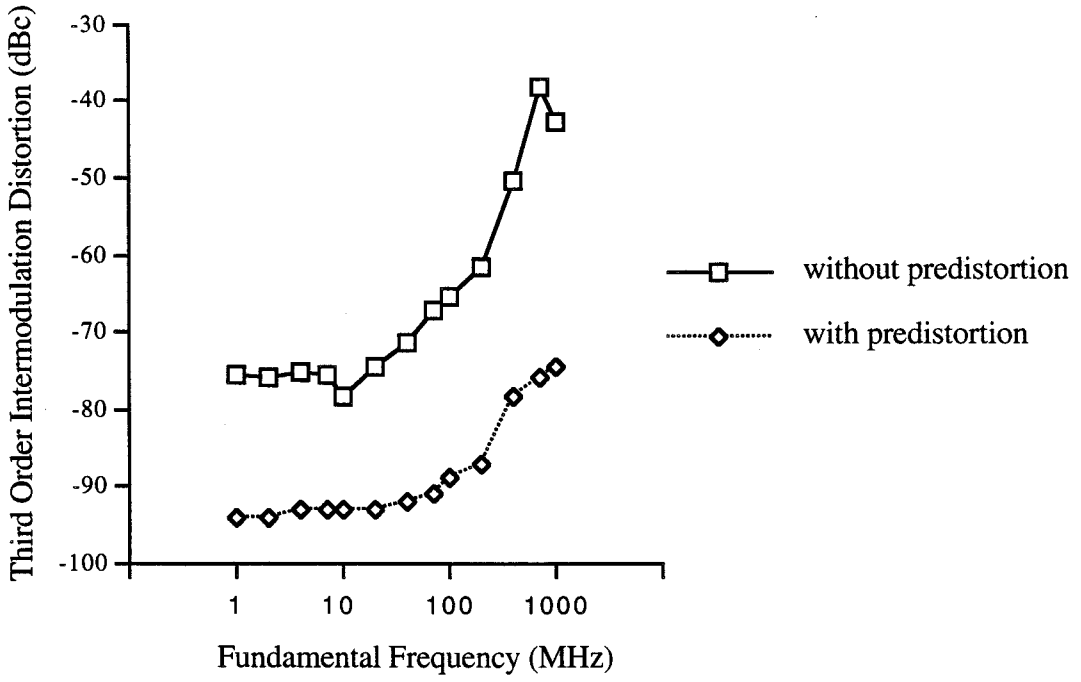

Figure 7.7 Third order IMD of laser model A with and without predistortion

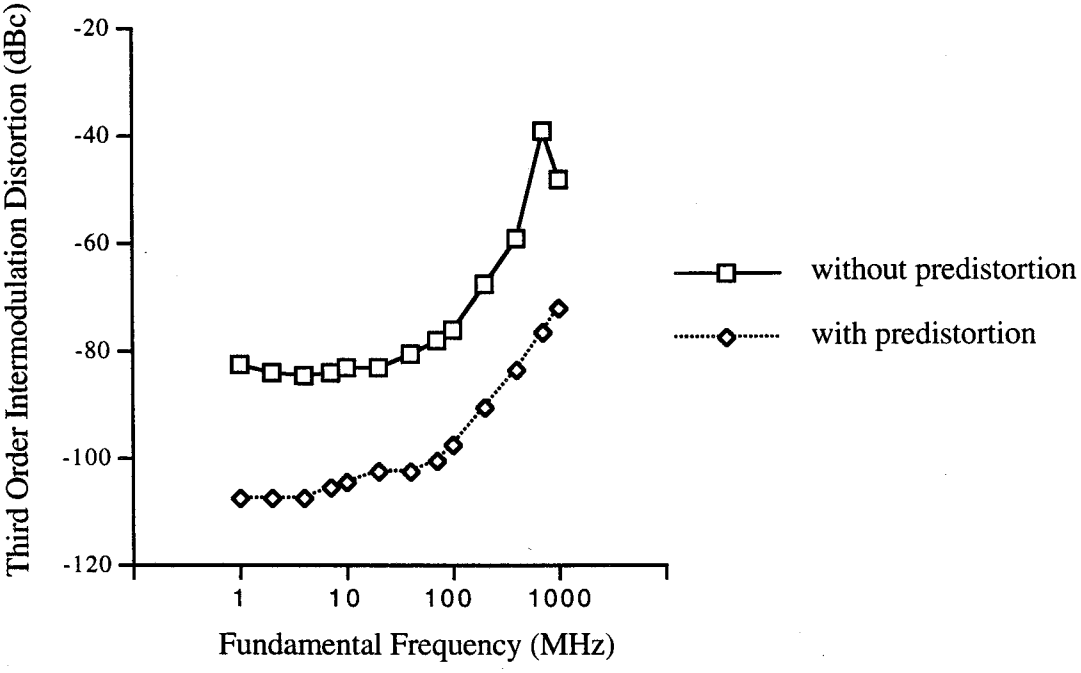

Figure 7.8 Third order IMD of laser model B with and without predistortion

7.3 Summary and Discussion

The intermodulation performance of the laser diode was not evaluated for fifth order products. The reason is that the fifth order product was small enough in most cases to be in, or just above, the noise floor of the FFT calculation in the output signal. Due to the numbers being represented with an 8-digit mantissa within ECA-2, the noise floor on an FFT calculation was approximately 100-110 dB below the carrier. Values around -100 dBc were measured at frequencies where the fifth order IMD would be, however, because the noise floor of the FFT calculation reached this level at neighboring frequencies, it is uncertain whether this value is power from the fifth order IMD or simply from noise.

As can be seen in Figures 7.1 through 7.5, 7.7 and 7.8, the nonlinear distortions increase with frequency as was predicted with the frequency domain models in Chapter 5. This is expected since nonlinear distortions increase as the fundamental frequency approaches the relaxation oscillation frequency, f_r, of the laser cavity. Way [46] expresses f_r as:

$$f_r = \frac{1}{2\pi}\left(\frac{N_o \Gamma g \tau_p + 1}{\tau_n \tau_p}\right)^{\frac{1}{2}}\left(\frac{J}{J_{th}} - 1\right)^{\frac{1}{2}} \tag{7.1}$$

where:

Γ = optical confinement factor
τ_s = spontaneous electron lifetime
τ_p = photon lifetime
N_o = transparent carrier density
g = optical power gain
J = bias current density above threshold
J_{th} = threshold current density

The relaxation oscillation frequency for the model A and model B lasers are approximately 3.1 GHz and 4.5 GHz respectively. Thus, the nonlinear distortions would continue to increase with frequency until the fundamental approached the relaxation oscillation frequency.

It can also be seen in Figures 7.1 through 7.5, 7.7 and 7.8 that the nonlinear distortion levels decrease when a predistortion block is incorporated prior to the laser. Again, the results shown in Chapter 5 are verified in principle. However, as can be seen in the same figures, the distortion levels are not reduced by 700 and 900 dB as in the cases in Chapter 5. There are two reasons for this. The first is due to the noise floor of the FFT calculation. The noise floor limits measurements to approximately -100 dBc. It is possible that the predistorter has reduced the distortion levels lower than the measured values if the measured value is a result of noise. Either way, it is obvious that the distortion level has been reduced to at least this value. The second reason is that the predistorters used here are only approximate inverses to the lasers and not exact mathematical inverses like the models in Chapter 5. In the time domain models, the laser is represented fairly accurately with the rate equations while the predistorter is approximated with a third order Volterra transfer function.

Finally, it can be seen in Figure 7.6 that the second order harmonic distortion increases as the bias current decreases. This is due to the modulating signal being clipped at the threshold current level.

8. REALIZATION OF PREDISTORTER IN HARDWARE

8.1 Predistorter Hardware Circuit

A hardware implementation of the Volterra based predistorter which was developed in Chapter 4 is presented in this chapter. Laboratory measurements have been conducted to demonstrate the improvement in linearity which can be obtained from using the predistorter. The predistorter was tested in conjunction with a General Optics model LANA-2013 Fabry-Perot laser diode. The predistorter circuit used in this chapter is based directly on the time domain model developed in Chapter 6. This time domain model was originally developed from the frequency domain model developed in Chapter 4.

To make the experimental work more manageable, the double differentiator paths were not implemented. The simplified predistorter block diagram is shown in Figure 8.1. If it was determined later that these paths would be effective, they could be added. However, as will be seen later, they were not required.

Once again, the predistorter transfer function is normalized so that the power of the signal input to the laser is the same with or without the predistorter.

The first step in building the predistorter, shown in Figure 8.1, is to recognize that five different functions must be realized in hardware. They are a squaring function, a cubing function, a differentiator, a straight gain, and a summer.

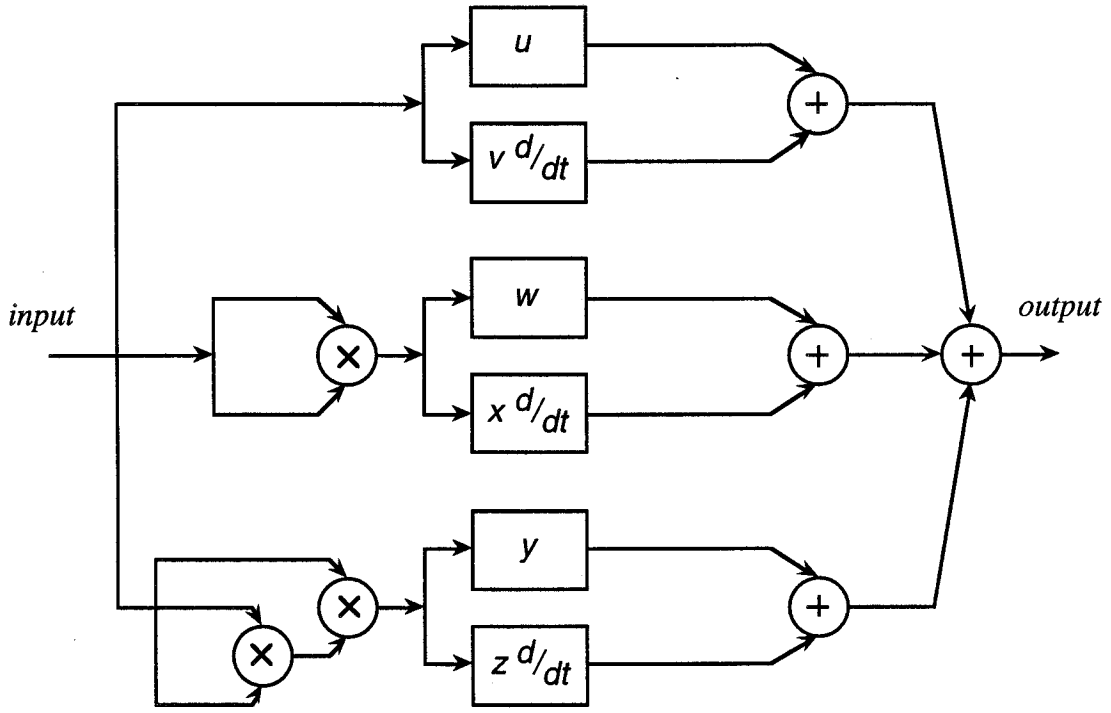

Figure 8.1 Time domain model of simplified predistorter

To begin with, the square and cube functions are realized using parallel and antiparallel diodes. Schottky diodes (M/A Com model MA40035) are used as the nonlinear elements. Basic circuit diagrams are shown in Figure 8.2 and Figure 8.3.

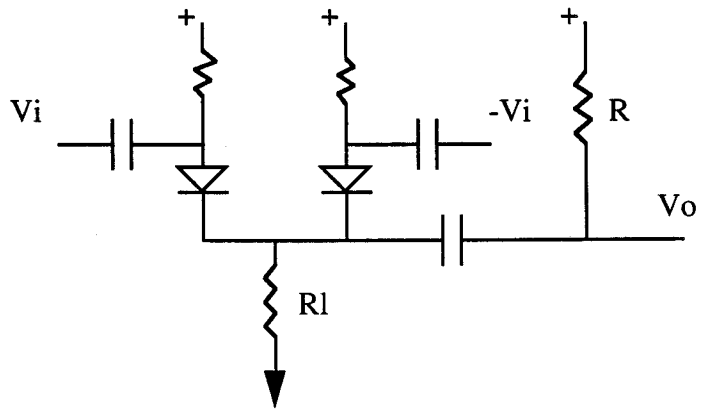

Figure 8.2 Square law circuit (Adapted from [74])

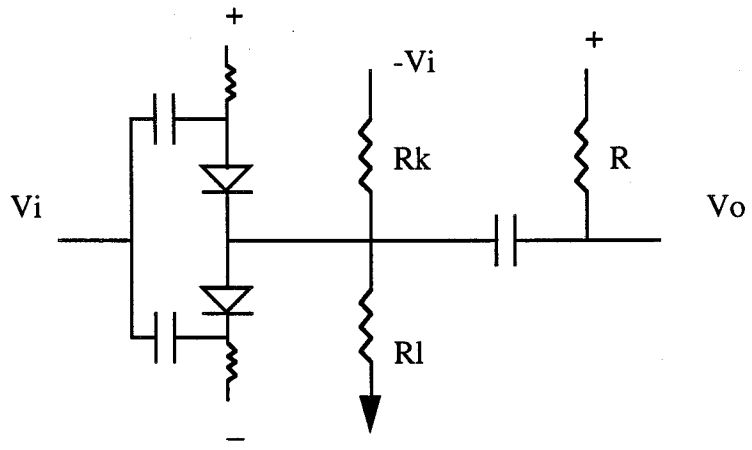

Figure 8.3 Cube law circuit (Adapted from [74])

In each circuit, the diodes are biased and operated under small signal conditions. The modulation depth is chosen such that one diode alone generates second, third, fourth, etc. order distortions. Two diodes are arranged in such a way that distortions of undesired order in the resulting output signal cancel each other. Thus, in the square law circuit, odd order terms cancel each other and in the cube law circuit, even order terms cancel. This is described in [74] and [75].

The differentiator is realized using an operational amplifier (Harris model HFA1100.) These amplifiers were chosen because of their high bandwidth capabilities. The basic circuit diagram is shown below in Figure 8.4.

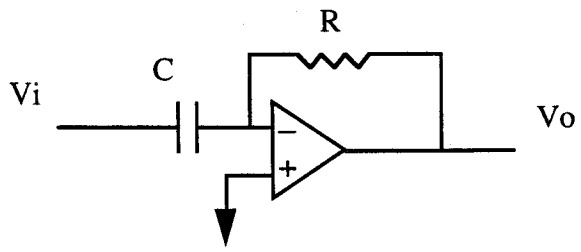

Figure 8.4 Differentiator circuit

The output voltage of the differentiator can be determined by the following equation:

$$Vo = -RC\frac{dVi}{dt} \tag{8.1}$$

A straight voltage gain is realized as well with an amplifier as shown in Figure 8.5.

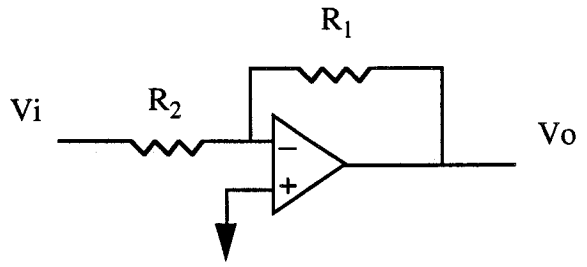

Figure 8.5 Voltage gain circuit

The output voltage can be determined by the following equation:

$$Vo = -\frac{R_1}{R_2} Vi \tag{8.2}$$

Figure 8.6 shows how a summer can be realized using an operational amplifier.

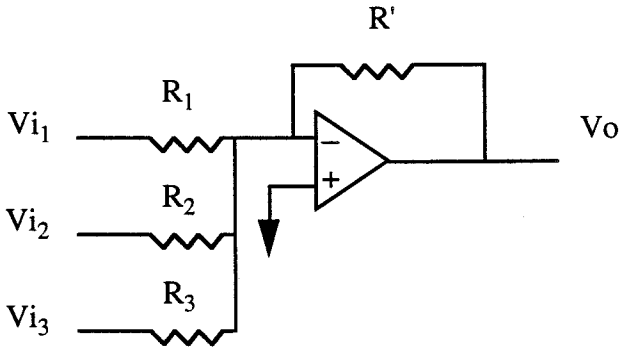

Figure 8.6 Voltage summer circuit

The output voltage can be determined by the following equation:

$$Vo = -\frac{R'}{R_1} Vi_1 - \frac{R'}{R_2} Vi_2 - \frac{R'}{R_3} Vi_3 \tag{8.3}$$

Utilizing all of these circuits to represent the various functions, the predistorter can be assembled. Figure 8.7 shows a detailed circuit diagram of the predistorter.

Notes: 1) All ⏚ represent ground termination unless otherwise specified
2) All op-amp power lines are decoupled with 22pF chip, .1uF ceramic and 10uF electrolytic capacitors
3) All non-variable resistors are chip resistors
4) All Schottky diodes are M/A Com MA40035
5) All op-amps are Harris HFA1100

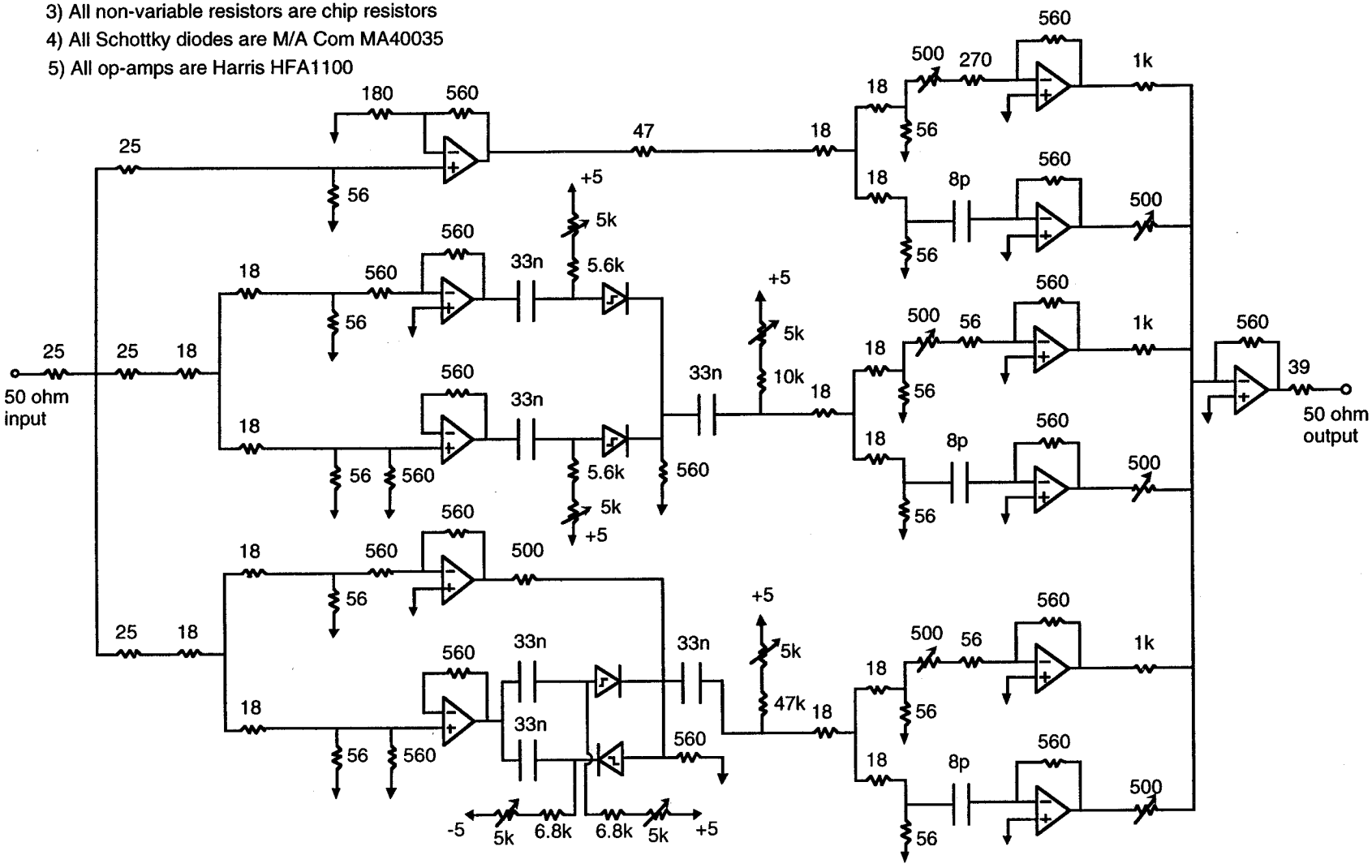

Figure 8.7 Detailed predistorter hardware circuit

One problem encountered in the design of the predistorter is determining the laser parameters. The laser parameters were not known for the General Optics model LANA-2013 laser. To help overcome the problem, adjustable resistor potentiometers were used to adjust the gain in various paths to obtain optimum performance.

The predistorter was tested with the experimental setup shown in Figure 8.8. To measure harmonic distortion, only one source is used. The power in the second and third order harmonics can be measured with the spectrum analyzer. This measurement can be made with and without the predistortion block in the path. To measure the third order intermodulation distortion, both sources are used. The sources are set at different frequencies and again, the spectrum analyzer is used to measure third order IMD with and without predistortion.

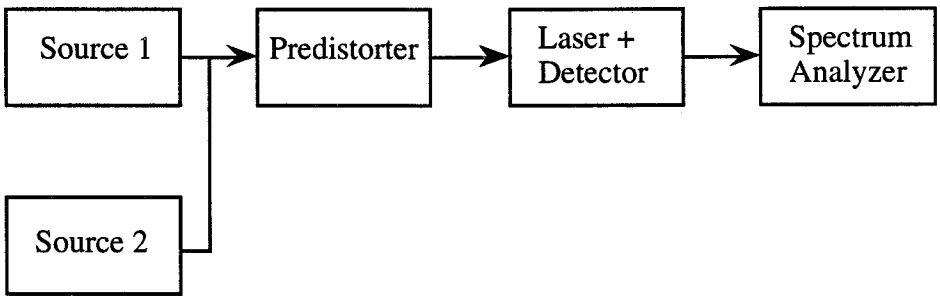

Figure 8.8 Experimental test circuit

8.2 Harmonic Performance of the Laser Diode and Predistorter

A plot of the second order harmonic distortion with and without predistortion is shown in Figure 8.9.

A plot of the third order harmonic distortion with and without predistortion is shown in Figure 8.10.

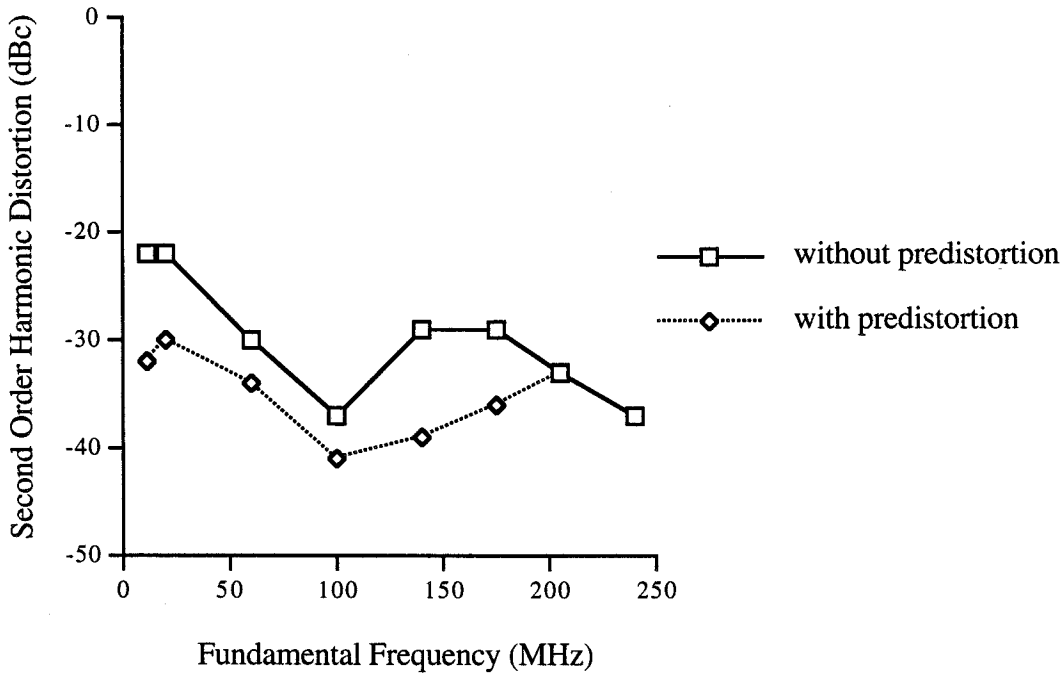

Figure 8.9 Second order HD of General Optics laser with and without predistortion

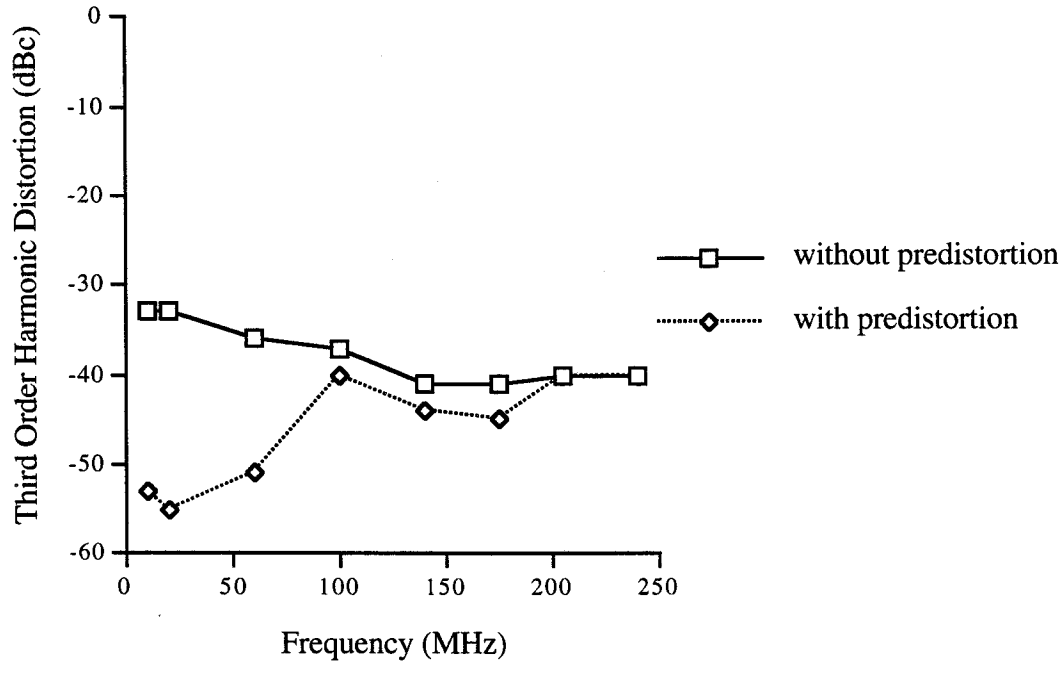

Figure 8.10 Third order HD of General Optics laser with and without predistortion

8.3 Intermodulation Performance of the Laser Diode and Predistorter

A plot of the third order intermodulation distortion with and without predistortion is shown in Figure 8.11.

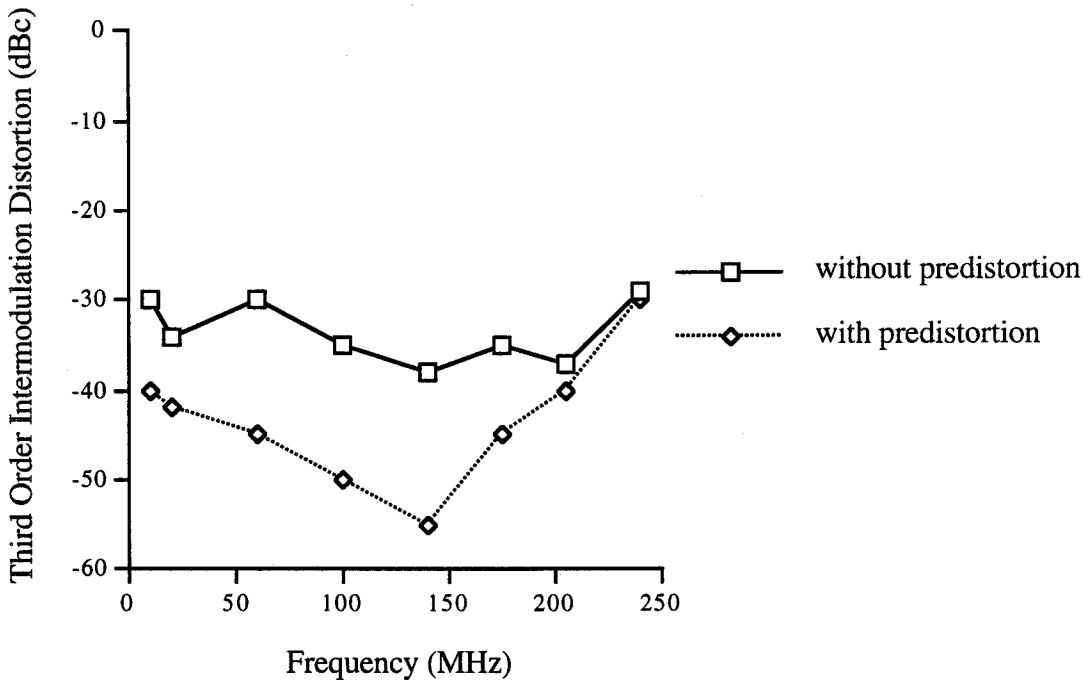

Figure 8.11 Third order IMD of General Optics laser with and without predistortion

Above 175 MHz, the predistortion block is providing less than 10 dB improvement in the laser output distortion.

8.4 Summary and Discussion

To this point, it is assumed that the only nonlinear element is the laser, however, it is important to note that the predistorter can be used to linearize more than just the laser. The predistorter could be used to linearize the distortion introduced by any of the

following: laser drive circuitry, laser, fiber, or photodetector circuitry. Since all of these components are required in the experiment, it is not certain that the laser is the only nonlinear component although it is generally assumed that it is the most nonlinear element in the system.

From Figures 8.9 through 8.11, it can be seen that the predistorter block has reduced the harmonic and intermodulation distortion output by the laser. However, there are some downfalls with the circuit. First of all, the predistorter only reduced the distortion levels up to 175 MHz. This was due to the bandwidth limitation of the square and cube law circuits. Above 175 MHz, the square and cube law circuits did not operate properly. This in turn can be attributed to the phase delay introduced by the operational amplifier. Although the HFA1100 has a unity gain bandwidth of 850 MHz, the phase lag of this amplifier becomes significant for this application around 200 MHz. Because the square and cube law circuits are based on adding in phase components and canceling out of phase components, the phase lag of the operational amplifier is an important parameter.

As a result of this limited bandwidth, the effect of the differentiator paths never played a role in reducing distortion products at higher frequencies as expected. Results in the previous chapters showed that the distortion levels are frequency dependent and that additional compensation is required at higher frequencies. However, the extra compensation which was to be added by the differentiating path was never tested because the bandwidth of the circuit was limited by the square and cube law circuits to be below 200 MHz.

Second, it is not evident from the results in Figures 8.9 through 8.11 but while the predistorter decreases the power in the second and third order harmonics, it also increased the power in the fourth and fifth order products at some frequencies. The square law circuit is not perfect. It generates not just second order products but fourth, sixth, eighth, etc. as well. The power in the higher order terms is generally negligible but at times the

fourth order term is significant. The same can be said about the fifth order term generated from the cube law circuit.

Third, assuming that the 175 MHz was a wide enough bandwidth for a CATV application, the predistorter does not linearize the laser enough to meet the CATV distortion requirements for CSO and CTB within the 175 MHz bandwidth.

Consequently, it appears that this predistortion circuit needs to be improved if it is to be used in a practical CATV application. The first step in improving the operation of the predistorter would be to design better square law and cube law functions. The goal would be to eliminate the fourth and fifth order products generated by these circuits and to increase the bandwidth of these circuits. This seems to suggest that a broadband linear amplifier with zero phase delay is required to build a circuit to linearize a laser. The problem is that amplifiers suffer from nonlinearities as well and compensation circuits similar to the ones for lasers are being developed to increase their linearity. The situation appears to be a *Catch 22*.

The results in Figures 8.9 through 8.11 show that this laser is extremely nonlinear if it were to be considered for a CATV application. To determine the effect the predistorter would have on a high quality laser, the predistorter was tested on a Northern Telecom model NT8L58CC Fabry-Perot laser. This laser is linear enough to be considered for a CATV application. What the results showed is that the predistorter had no positive effect on the distortion levels at the output. So essentially the predistorter appears to work only in applications with poor lasers and not in ones with good lasers. Darcie [23] found the same results in tests with his predistorter. His predistorter worked for lasers with relatively large sublinearity of the L-I characteristic but had little improvement for good lasers biased at an optimum level.

In summary, the technique has been shown to be valid despite the implementation needing some improvements. Further, the entire component cost for the predistorter is less than $200. This is less than the price of the laser it is linearizing. Although this implementation does not perform as well as the $10,000 Ortel laser and linearizer system [61], it is significantly less expensive.

9. CONCLUSION

There were four main objectives of the research described in this thesis. The first objective was to review the techniques available for improving the linearity of semiconductor lasers in analog applications and, based on this review, to select the most appropriate technique for this research. The second objective was to model the single-mode semiconductor laser rate equations and thereby demonstrate the frequency dependence of the laser nonlinearities. The third objective was to develop the linearization scheme selected for this research in software. The final objective was to attempt to build a hardware prototype of the linearization circuit and test it with a laser diode.

Based on this review, predistortion was selected as the most appropriate linearization technique. Predistortion was chosen over other linearization techniques such as optical feedforward and electrical feedback because it appears to offer high bandwidth compensation at low cost. The predistortion block is incorporated prior to the laser with the intent that its characteristics be the inverse to those of the laser.

Two models of a single-mode Fabry-Perot semiconductor laser were developed in order to predict the laser's performance in analog transmission. The first model was based on an analysis of the single-mode semiconductor laser rate equations in the frequency domain. The laser was modeled with Volterra kernels. The Volterra kernels for the laser were developed from the Volterra kernels for the predistorter. The kernels for the predistorter were developed from the rate equations first because of algebraic simplicity. The second model for the laser was developed in the time domain, also from the rate

equations. This new model for the laser was based on a time domain simulation of the rate equations using the circuit simulation software package ECA-2.

The frequency domain model for the predistorter, which was represented by Volterra kernels, was used to develop a time domain model for the predistorter. The frequency domain transfer functions were transformed to their time domain equivalent.

After the models had been developed, the frequency domain model for the laser was tested individually and also in cascade with the frequency domain model for the predistorter. In addition, the time domain model for the laser was tested individually and also in cascade with the time domain model for the predistorter.

This modeling demonstrated two important points. First, that the harmonic and intermodulation distortions generated at the output of the semiconductor laser are frequency dependent and that these distortions increase with frequency. Further, based on the laser parameters simulated, compensation that is frequency dependent would be required if the lasers were to be used in broadband CATV applications. Second, predistortion developed from a Volterra Series approach could provide proper frequency dependent compensation.

A prototype predistorter design was built in hardware and tested using a General Optics model LANA-2013 semiconductor laser. The results showed that the predistorter can reduce the harmonic and intermodulation distortion at the laser output on the average of 10 dB at frequencies up to 175 MHz. The bandwidth limitation was attributed to the phase limitations of the operational amplifiers used in the predistorter circuit.

Future work can be conducted in several areas. One area would involve designing a predistorter circuit with linear amplifiers that have a wider bandwidth. The importance lies in designing effective wideband square and cube law circuits.

Another area for future work is modeling the predistorter in terms of hardware components in ECA-2. Currently, the time domain model for the predistorter is modeled with ideal square law, cube law and gain functions in ECA-2. By modeling the predistorter with nonideal hardware components, the functions become less than ideal and a model that performs closer to the actual predistorter could be tested.

Modeling an adaptive predistorter in software and later hardware is another option. Adaptive predistortion offers the additional advantage of compensating for change in laser nonlinearities due to temperature fluctuations, product variances and aging.

Work could be extended further in the software modeling area. The current models are based solely on the two single-mode semiconductor rate equations. Nonlinearities in the laser output can originate from other sources such as facet reflections and spatial hole burning. Implementing these effects into the model would improve the models accuracy of predicting nonlinear distortions. Modeling quantum-well lasers with the circuit simulation software package is another possibility. Quantum-well lasers can be represented with three rate equations depending on the nature of the wells. A time domain simulation of a quantum-well laser could be done on ECA-2 in a similar manner to the model constructed for the Fabry-Perot laser.

Finally, the time domain software model could be used in matching modeled results with those from real lasers. The model can be used to perform a sensitivity analysis of the laser parameters that characterize the laser output. Further, the model could be used to estimate unknown laser parameters by modifying an unknown parameter until the output of the model matched that of the real laser.

REFERENCES

[1] W. B. Jones, Jr., *Introduction to optical fiber communication systems,* New York, NY: Holt, Rinehart and Winston, 1988.

[2] D. Hondros, P. Debye, "Elektromagnetische wellen an dielectrischen draehten," *Ann. Phys.,* vol. 32, pp. 465-476, 1910.

[3] F. P. Kapron, D. B. Keck, R. D. Maurer, "Radiation losses in glass optical waveguides," *Applied Physics Letters,* vol. 17, pp. 423-425, Nov. 1970.

[4] J. S. Cook, O. I. Szentesi, "North American field trials and early applications in telephony," *IEEE Journal on Selected Areas in Communications,* vol. SAC-1, pp. 393-397, Apr. 1983.

[5] P. H. Chouinard, "Description and performance review of the Yorkville integrated services fiber optic trial," *Proceedings of the International Conference on Communications*, pp. 28.3-28.6, June 1979.

[6] J. R. Stauffer, "FT3C-A lightwave system for metropolitan and intercity applications," *IEEE Journal on Selected Areas in Communications,* vol. SAC-1, pp. 413-419, Apr. 1983.

[7] A. Moncalvo, F. Tosco, "European field trials and early applications in telephony," *IEEE Journal on Selected Areas in Communications,* vol. SAC-1, pp. 398-403, Apr. 1983.

[8] E. Iwahashi, "Trends in long-wavelength single-mode transmission systems and demonstrations in Japan," *IEEE Journal on Quantum Electronics*, vol. QE-17, pp. 890-896, June 1981.

[9] H. Ishio, "Japanese field trials and applications in telephony," *IEEE Journal on Selected Areas in Communications,* vol. SAC-1, pp. 404-412, Apr. 1983.

[10] O'Neill, E. F., ed., *A History of Science and Engineering in the Bell System,* AT&T Bell Laboratories, 1985.

[11] T. E. Darcie, P. P. Iannone, B. L. Kasper, J. R. Talman, C. A. Burrus, T. A. Baker, "Wideband lightwave distribution system using subcarrier multiplexing," *IEEE Journal of Lightwave Technology,* vol. 7, no. 6, pp. 997-1005, June 1989.

[12] P. Hill, R. Olshansky, "Twenty channel FSK subcarrier multiplexed optical communication system for video distribution," *Electronic Letters,* vol. 24, no. 14, pp. 892-894, 1988.

[13] N. Kanno, K. Ito, "Fiber-optic subcarrier multiplexing video transport employing multilevel QAM," *IEEE Journal on Selected Areas in Communications,* vol. 8, no. 7, pp. 1313-1319, Sept. 1990.

[14] M. Kavehrad, E. Savov, "Fiber-optic transmission of microwave 64-QAM signals," *IEEE Journal on Selected Areas in Communications,* vol. 8, no. 7, pp. 1320-1326, Sept. 1990.

[15] F. V. C. Mendis, T. T. Tjhung, B. Selvan, "20 km single-mode optical fibre system for multichannel video," *Electronics Letters*, vol. 24, no. 7, pp. 442-443, Mar. 1988.

[16] R. Olshansky, V. A. Lanzisera, "60-Channel FM video subcarrier multiplexed optical communication system," *Electronics Letters*, vol. 23, no. 22, pp. 1196-1198, Oct. 1987.

[17] W. Way, C. E. Zah, C. Caneau, S. G. Menocal, F. Favire, F. K. Shokoohi, N. K. Cheung, T. P. Lee, "Multichannel FM video transmission using traveling wave amplifiers for subscriber distribution," *Electronic Letters,* vol. 24, no. 22, p. 1370-1372, 1988.

[18] S. D. Walker, M. Li, A. C. Boucouvalas, D. G. Cunningham, A. N. Coles, "Design techniques for subcarrier multiplexed broadcast optical networks," *IEEE Journal on Selected Areas in Communications,* vol. 8, no. 7, pp. 1276-1284, Sept. 1990.

[19] R. Olshansky, R. Gross, M. Schmidt, "Subcarrier multiplexed coherent lightwave systems for video distribution," *IEEE Journal on Selected Areas in Communications,* vol. 8, no. 7, pp. 1268-1275, Sept. 1990.

[20] T. E. Darcie, "Subcarrier multiplexing for lightwave networks and video distribution systems," *IEEE Journal on Selected Areas in Communications,* vol. 8, no. 7, pp. 1240-1248, Sept. 1990.

[21] R. Olshansky, V. A. Lanzisera, P. M. Hill, "Subcarrier multiplexed lightwave systems for broadband distribution," *IEEE Journal of Lightwave Technology*, vol. 7, no. 9, pp. 1329-1341, Sept. 1989.

[22] J. A. Chiddix, H. Laor, D. M. Pangrac, L. D. Williamson, R. Wolfe, "AM video on fiber in CATV systems: need and implementation," *IEEE Journal on Selected Areas in Communications,* vol. 8, no. 7, pp. 1229-1239, Sept. 1990.

[23] T. E. Darcie, J. Lipson, C. B. Roxlo, C. J. Mcgrath, "Fiber optic device technology for broadband analog video systems," *IEEE LCS,* vol. 1, no. 1, pp. 46-52, Feb. 1990.

[24] T. E. Darcie, G. E. Bodeep, "Lightwave subcarrier CATV transmission systems," *IEEE Transactions on Microwave Theory and Techniques*, vol. 38, no. 5, pp. 524-533, May 1990.

[25] G. M. Hart, N. F. Hamilton-Piercy, "A broadband urban hybrid coaxial/fiber telecommunications network," *IEEE LCS,* vol. 1, no. 1, pp. 38-45, Feb. 1990.

[26] G. P. Agrawal, "Gain nonlinearities in semiconductor lasers: theory and application to distributed feedback lasers," *IEEE Journal of Quantum Electronics*, vol. QE-23, no. 6, pp. 860-868, June 1987.

[27] K. Alameh, R. A. Minasian, "Optimum optical modulation index of laser transmitters in SCM systems," *Electronics Letters*, vol. 26, no. 16, pp. 1273-1275, Aug. 1990.

[28] K. Alameh, R. A. Minasian, "Ultimate limits of subcarrier multiplexed lightwave transmission," *Electronics Letters*, vol. 27, no. 14, pp. 1260-1262, July 1991.

[29] J. H. Angenent, "Simple model for calculation of distortion in an optical analog subcarrier multiplexed CATV system," *Electronics Letters*, vol. 26, no. 24, pp. 2049-2050, Nov. 1990.

[30] C. J. Chung, I. Jacobs, "Practical TV channel capacity of lightwave multichannel AM SCM systems limited by the threshold nonlinearity of laser diodes," *IEEE Photonics Technology Letters*, vol. 4, no. 3, pp. 289-292, Mar. 1992.

[31] C. J. Chung, I. Jacobs, "Simulation of the effects of laser clipping on the performance of AM SCM lightwave systems," *IEEE Photonics Technology Letters*, vol. 3, no. 11, pp. 1034-1036, Nov. 1991.

[32] A. Czylwik, "Nonlinear system modeling of semiconductor lasers based on Volterra series," *Journal of Optical Communications*, vol. 3, pp. 104-114, July 1986.

[33] T. E. Darcie, R. S. Tucker, "Intermodulation and harmonic distortion in InGaAsP lasers," *Electronics Letters*, vol. 21, no. 16, pp. 665-666, Aug. 1985, erratum, *ibid.*, vol. 22, no. 11, p. 619, May 1986.

[34] S. Huang, L. Chainulu Upadhyayula, J. Lipson, E. J. Flynn, C. B. Roxlo, "Frequency-dependent distortions of composite triple beat in lightwave CATV transmission systems," *IEEE Journal on Selected Areas in Communications*, vol. 8, no. 7, pp. 1365-1368, Sept. 1990.

[35] P. Iannone, T. E. Darcie, "Multichannel intermodulation distortion in high-speed GaInAsP lasers," *Electronics Letters*, vol. 23, no. 25, pp. 1361-1362, Dec. 1987.

[36] H. Kawamura, K. Kamite, H. Yonetani, S. Ogita, H. Soda, H. Ishikawa, "Effect of varying threshold gain on second order intermodulation distortion in distributed feedback lasers," *Electronics Letters*, vol. 26, no. 20, Sept. 1990.

[37] C. Y. Kuo, "Fundamental second-order nonlinear distortions in analog AM CATV transport systems based on single frequency semiconductor lasers," *Journal of Lightwave Technology*, vol. 10, no. 2, pp. 235-243, Feb. 1992.

[38] K. Y. Lau, A. Yariv, "Intermodulation distortion in a directly modulated semiconductor injection laser," *Applied Physics Letters*, vol. 45, no. 10, pp. 1034-1036, Nov. 1984.

[39] J. LeBihan, G. Yabre, J. Debeau, E. LeCoquil, "Bessel function analysis of harmonic distortion in semiconductor lasers," *Electronics Letters*, vol. 29, no. 10, pp. 834-835, May 1993.

[40] G. Morthier, F. Libbrecht, K. David, P. Vanwikelberge, R. G. Baets, "Theoretical investigation of the second-order harmonic distortion in the AM response of 1.55 um F-P and DFB lasers," *IEEE Journal of Quantum Electronics*, vol. 27, no. 8, pp. 1990-2002, Aug. 1991.

[41] P. Neusy, W. F. McGee, "Effects of laser nonlinearities on TV distribution using subcarrier multiplexing," *Proceedings of Canadian Conference on Electrical and Computer Engineering*, Montreal, PQ, Sept. 1989, pp. 833-836.

[42] K. Peterman, G. Arnold, "Noise and distortion characteristics of semiconductor lasers in optical fiber communication systems," *IEEE Journal of Quantum Electronics*, vol. QE-18, no. 4, pp. 543-555, Apr. 1982.

[43] A. A. M. Saleh, "Fundamental limit on the number of channels in subcarrier-multiplexed lightwave CATV system," *Electronics Letters*, vol. 25, no. 12, pp. 776-777, June 1989.

[44] K. Stubkjaer, M. Danielsen, "Nonlinearities of GaAlAs lasers - harmonic distortion," *IEEE Journal of Quantum Electronics*, vol. QE-16, no. 5, pp. 531-537, May 1980.

[45] A. Takemoto, H. Watanabe, Y. Nakajima, Y. Sakakibara, S. Kakimoto, J. Yamashita, T. Hatta, Y. Miyake, "Distributed feedback laser diode and module for CATV systems," *IEEE Journal on Selected Areas in Communications*, vol. 8, no. 7, pp. 1359-1364, Sept. 1990.

[46] S. J. Wang, A. B. Piccirilli, Y. J. Wang, N. K. Dutta, "Temperature dependence of the second harmonic distortion of buried heterostructure distributed feedback lasers," *Electronics Letters*, vol. 26, no. 14, pp. 1095-1097, July 1990.

[47] W. I. Way, "Large signal nonlinear distortion prediction for a single-mode laser diode under microwave intensity modulation," *IEEE Journal of Lightwave Technology*, vol. LT-5, no. 3, pp. 305-315, Mar. 1987.

[48] G. E. Bodeep, T. E. Darcie, "Semiconductor lasers versus external modulators: a comparison of nonlinear distortion for lightwave subcarrier CATV applications," *IEEE Photonics Technology Letters*, vol. 1, no. 11, pp. 401-403, Nov. 1989.

[49] L. Adnet, H. Mionet, W. Schmid, "Optoelectonics in the subscriber loop," *Alcatel technical journal: Electrical Communication,* 4th Quarter, 1992, pp. 58-65.

[50] M. Balmes, J. Bourne, J. Mar, "Fiber to the home: the technology behind Heathrow," *IEEE LCS,* vol. 1, no. 3, pp. 25-29, Aug. 1990.

[51] T. S. Rzeszewski, "A two-layer fiber network for broadband integrated services," *IEEE LCS,* vol. 1, no. 1, pp. 77-80, Feb. 1990.

[52] J. Wilson, *Optoelectronics: an introduction,* Englewood Cliffs, NJ: Prentice-Hall, 1983.

[53] G. Keiser, *Optical fiber communications*, New York, NY: McGraw-Hill Inc., 1991.

[54] K. Furuya, Y. Suematsu, T. Hong, "Reduction of resonance like peak in direct modulation due to carrier diffusion in injection laser," *Applied Optics*, vol. 17, p. 1949, 1978.

[55] R. S. Tucker, D. J. Pope, "Circuit modeling of the effect of diffusion on damping in a narrow-stripe semiconductor laser," *IEEE Journal of Quantum Electronics*, vol. QE-19, no. 7, pp. 1179-1183, July 1983.

[56] D. Wilt, K. Y. Lau, A. Yariv, "The effect of lateral carrier diffusion on the modulation response of a semiconductor laser," *Journal of Applied Physics* , vol. 52, p. 4970, 1981.

[57] M. P. Kesler, E. P. Ippen, "Subpicosecond gain dynamics in GaAlAs laser diodes," *Applied Physics Letters* , vol. 51, no. 22, p. 1765, 1987.

[58] K. Petermann, *Laser Diode Modulation and Noise,* Dordrecht, The Netherlands: Kluwer Academic Publishers, 1988.

[59] C. H. Henry , "Properties of harmonic distortion of laser diodes with reflected waves," *Journal of Optical Communications*, vol. 3, no. 4, pp. 129-132, 1982.

[60] H. Kressel, J. K. Butler, *Semiconductor lasers and heterojunction LED's*, New York, NY: Academic Press, 1977.

[61] H. A. Blauvelt, *Predistorter for linearization of electronic and optical signals*, Ortel Corporation, Alhambra, CA: US Patent Number: 5252930, Oct. 1993.

[62] M. Sekita, T. Kawamura, K. Ito, S. Fujita, M. Ishii, V. Mirjake, "TV video transmission by analog baseband modulation of 1.3 um band laser diode," *6th European Conference Opt. Comm.*, pp. 394-396, York, 1980.

[63] A. Van de Grijp, J. C. Koopman, L. J. Meuleman, A. Nicia, E. Roza, J. Van Heuven, "Novel electro-optical feedback technique for noise and distortion reduction in high-quality analog optical transmission video signals," *Electronics Letters*, vol. 17, pp. 361-362, May 1981.

[64] Y. Ueno, M. Kajitani, "Color TV transmission using light emitting diode," *NEC Research and Development*, no. 35, pp. 15-20, Oct. 1974.

[65] J. Strauss, O. I. Szentesi, "Linearized transmitters for optical communications," *Proc. IEEE Int. Symp. on Circuits and Systems*, Apr. 25-27, Phoenix, Arizona, pp. 288-292.

[66] R. E. Patterson, J. Straus, G. Blenman, T. Witkowicz, "Linearization of multichannel analog optical transmitters by quasi-feedforward compensation technique," *IEEE Transactions on Communications*, vol. COM-27, no. 3, pp. 582-588, Mar. 1979.

[67] D. Hassin, R. Vahldieck, "Feedforward linearization of analog modulated laser diodes - theoretical analysis and experimental verification," *IEEE Transactions on Microwave Theory and Techniques*, pp. 2376-2382, Dec. 1993.

[68] L. S. Fock, R. S. Tucker, "Simultaneous reduction of intensity noise and distortion in semiconductor lasers by feedforward compensation," *Electronics Letters*, vol. 27, no. 14, pp. 1297-1299, July 1991.

[69] A. Lidgard, N. A. Olsson, "Generation and cancellation of second-order harmonic distortion in analog optical systems by interferometric FM-AM conversion," *IEEE Photonics Technology Letters*, vol. 2, no. 7, pp. 519-521, July 1990.

[70] K. Asatani, T. Kimura, "Linearization of LED nonlinearity by predistortions," *IEEE Transactions on Electron Devices*, vol. ED-25, no. 2, pp. 207-212, Feb. 1978.

[71] R. B. Childs, V. A. O'Byrne, "Predistortion linearization of directly modulated DFB lasers and external modulators for AM video transmission," *Proceedings Optical Fiber Communications Conference*, San Francisco, CA, Jan. 1990.

[72] S. M. Mysore, *Analysis and compensation of semiconductor laser nonlinearity for analog video transmission*, M. Sc. thesis submitted to the Department of Electrical Engineering, University of Alberta, Edmonton, AB, Fall 1984.

[73] N. Tayebi, *Laser nonlinearity compensation for subcarrier multiplexed optical transmission systems,* M. Sc. thesis submitted to the Department of Electrical Engineering, University of Ottawa, Ottawa, ON, Nov. 1992.

[74] M. Bertelsmeier, W. Zschunke, "Linearization of broadband optical transmission systems by adaptive predistortion," *Frequenz*, vol. 38, no. 9, pp. 206-212, 1984.

[75] S. A. Maas, *Nonlinear microwave circuits*, Norwood, MA: Artech House, Inc., 1988.

[76] M. Schetzen, *The Volterra and Wiener theories of nonlinear systems,* New York, NY: John Wiley and Sons, Inc., 1980.

[77] T. K. Biswas, W. F. McGee, "Volterra series analysis of semiconductor laser diode," *IEEE Photonics Technology Letters*, vol. 3, no. 8, pp. 706-708, Aug. 1991.

[78] T. Davis, *ECA-2: Electronic circuit analysis,* version 2.65, Ann Arbor, MI: Tatum Labs Inc., 1993.

[79] R. S. Tucker, "Large-signal circuit model for simulation of injection-laser modulation dynamics," *Proceedings of IEE*, vol. 128, pt. I, no. 5, pp. 180-184, Oct. 1981.

[80] R. S. Tucker, I. P. Kaminow, "High-frequency characteristics of directly modulated InGaAsP ridge waveguide and buried heterostructure lasers," *IEEE Journal of Lightwave Technology*, vol. LT-2, no. 4, pp. 385-393, Aug. 1984.

APPENDIX A

Derivation of the Volterra Model for the Predistorter

Based on the rate equations (2.8) and (2.9) initially presented in Chapter 2, the Volterra transfer functions for the predistorter can be derived. This derivation is outlined below in detail.

For a single-mode laser, the two rate equations are:

$$\frac{dN}{dt} = \frac{I}{V} - \frac{N}{\tau_s} - g(N - N_o)(1 - \varepsilon S)S \tag{A.1}$$

$$\frac{dS}{dt} = \Gamma g(N - N_o)(1 - \varepsilon S)S - \frac{S}{\tau_p} + \Gamma\beta\frac{N}{\tau_s} \tag{A.2}$$

The variable parameters in the equations are:

S = density of photons in lasing mode

N = density of electrons in the conduction band of the semiconductor

I = injection current

The constant parameters in the equations are:

Γ = optical confinement factor

τ_s = spontaneous electron lifetime

τ_p = photon lifetime

N_o = transparent carrier density

g = optical power gain

ε = power gain compression parameter

β = probability of spont. emission of a photon in phase with lasing mode

V = volume of active laser region times electronic charge

Equation (A.2) can be rearranged to give (A.3) and from this N can be solved for as shown in (A.4):

$$\frac{dS}{dt} = \left[\Gamma g(1-\varepsilon S)S + \frac{\Gamma\beta}{\tau_s}\right]N - \Gamma g(1-\varepsilon S)SN_o - \frac{S}{\tau_p} \tag{A.3}$$

$$N = \frac{\dfrac{dS}{dt} + \dfrac{S}{\tau_p} + \Gamma g(1-\varepsilon S)SN_o}{\Gamma g(1-\varepsilon S)S + \dfrac{\Gamma\beta}{\tau_s}} \tag{A.4}$$

Substituting $S_b + s = S$, where S_b is the bias term and s is the ac term, into (A.4) and expanding terms gives:

$$N = \frac{s' + \left[\dfrac{1}{\tau_p} + \Gamma g N_o - 2S_b\Gamma g N_o\varepsilon\right]s + \left[-\Gamma g N_o\varepsilon\right]s^2 + \left[\dfrac{S_b}{\tau_p} + S_b\Gamma g N_o - S_b^2\Gamma g N_o\varepsilon\right]}{\left[-\Gamma g\varepsilon\right]s^2 + \left[\Gamma g - 2\Gamma g\varepsilon S_b\right]s + \left[\Gamma g S_b - \Gamma g\varepsilon S_b^2 + \dfrac{\Gamma\beta}{\tau_s}\right]} \tag{A.5}$$

where: $s' = \dfrac{ds}{dt}$

The second order denominator in (A.5) can be represented by a third order numerator term:

$$\text{i.e.:}\ \frac{1}{\rho s^2 + \sigma s + \alpha} = A + Bs + Cs^2 + Ds^3 \tag{A.6}$$

where:

$$A = \frac{1}{\alpha}$$

$$B = \frac{-\sigma}{\alpha^2}$$

$$C = \frac{\sigma^2}{\alpha^3} - \frac{\rho}{\alpha^2}$$

$$D = \frac{2\rho\sigma}{\alpha^3} - \frac{\sigma^3}{\alpha^4}$$

Thus, (A.5) can be represented as:

$$N = \left[s' + Es + Fs^2 + G\right]\left[A + Bs + Cs^2 + Ds^3\right] \tag{A.7}$$

where:

$$A = \frac{1}{\alpha}$$

$$B = \frac{-\sigma}{\alpha^2}$$

$$C = \frac{\sigma^2}{\alpha^3} - \frac{\rho}{\alpha^2}$$

$$D = \frac{2\rho\sigma}{\alpha^3} - \frac{\sigma^3}{\alpha^4}$$

$$E = \frac{1}{\tau_p} + \Gamma g N_o - 2S_b \Gamma g N_o \varepsilon$$

$$F = -\Gamma g N_o \varepsilon$$

$$G = \frac{S_b}{\tau_p} + S_b \Gamma g N_o - S_b^2 \Gamma g N_o \varepsilon$$

$$\alpha = \Gamma\left(g S_b - g\varepsilon S_b^2 + \beta/\tau_s\right)$$

$$\sigma = \Gamma g\left(1 - 2\varepsilon S_b\right)$$

$$\rho = -\Gamma\varepsilon g$$

Expanding the product terms in (A.1) gives:

$$\frac{I}{V} = \frac{dN}{dt} + \frac{N}{\tau_s} + gNS - gN\varepsilon S^2 - gN_o S + gN_o\varepsilon S^2 \tag{A.8}$$

Substituting $S_b + s = S$ into (A.8) and expanding terms gives:

$$\frac{I}{V} = \frac{dN}{dt} + \frac{N}{\tau_s} + gNS_b + gNs - gN\varepsilon S_b^{\,2} - 2gN\varepsilon S_b s - gN\varepsilon s^2 - gN_o S_b - gN_o s + gN_o \varepsilon S_b^{\,2} + 2gN_o \varepsilon S_b s + gN_o \varepsilon s^2 \quad \text{(A.9)}$$

Rearranging (A.9) gives:

$$\frac{I}{V} = \frac{dN}{dt} + \left[\left(\frac{1}{\tau_s} + gS_b - g\varepsilon S_b^2\right) + \left(g - 2g\varepsilon S_b\right)s - \left(g\varepsilon\right)s^2\right]N + \left(gN_o\varepsilon\right)s^2 + \left(2gN_o\varepsilon S_b - gN_o\right)s + \left(gN_o\varepsilon S_b^2 - gN_o S_b\right) \quad \text{(A.10)}$$

Equation (A.10) can be written as:

$$\frac{I}{V} = \frac{dN}{dt} + \left[H + Is + Js^2\right]N + Ks^2 + Ls + M \quad \text{(A.11)}$$

where:

$$H = \frac{1}{\tau_s} + gS_b - g\varepsilon S_b^2$$
$$I = g - 2g\varepsilon S_b$$
$$J = -g\varepsilon$$
$$K = gN_o\varepsilon$$
$$L = 2gN_o\varepsilon S_b - gN_o$$
$$M = gN_o\varepsilon S_b^2 - gN_o S_b$$

Substituting (A.7) into (A.11) gives:

$$\frac{I}{V} = \frac{d}{dt}\left\{\left[\frac{ds}{dt} + Es + Fs^2 + G\right]\left[A + Bs + Cs^2 + Ds^3\right]\right\} + \left[H + Is + Js^2\right]\left[\frac{ds}{dt} + Es + Fs^2 + G\right]\left[A + Bs + Cs^2 + Ds^3\right] + Ks^2 + Ls + M \quad \text{(A.12)}$$

Expanding terms in (A.12):

$$\frac{I}{V} = [s'' + Es' + 2Fss'][A + Bs + Cs^2 + Ds^3]$$
$$+[s' + Es + Fs^2 + G][Bs' + 2Css' + 3Ds^2 s']$$
$$+[H + Is + Js^2][s' + Es + Fs^2 + G][A + Bs + Cs^2 + Ds^3] + Ks^2 + Ls + M$$

(A.13)

(A.13) can be expanded further to give (A.14):

$$\frac{I}{V} = As'' + EAs' + 2AFss' + Bss'' + EBss' + 2FBs^2 s' + Cs^2 s'' + ECs^2 s' + 2FCs^3 s' + Ds^3 s''$$
$$+EDs^3 s' + 2FDs^4 s' + Bs' s' + EBss' + FBs^2 s' + GBs' + 2Css' s' + 2CEs^2 s' + 2CFs^3 s'$$
$$+2CGss' + 3Ds^2 s' s' + 3DEs^3 s' + 3DFs^4 s' + 3DGs^2 s' + HAs' + AIss' + AJs^2 s'$$
$$+AEHs + AEIs^2 + AEJs^3 + AFHs^2 + AFIs^3 + AFJs^4 + AGH + AGIs$$
$$+AGJs^2 + HBs' s + IBs^2 s' + BJs^3 s' + BEHs^2 + BEIs^3 + BEJs^4 + BFHs^3$$
$$+BFIs^4 + BFJs^5 + GBHs + GBIs^2 + GBJs^3 + CHs^2 s' + CIs^3 s' + CJs^4 s'$$
$$+CEHs^3 + CEIs^4 + CEJs^5 + CFHs^4 + CFIs^5 + CFJs^6 + CGHs^2 + CGIs^3$$
$$+CGJs^4 + DHs^3 s' + DIs^4 s' + DJs^5 s' + DEHs^4 + DEIs^5 + DEJs^6 + DFHs^5$$
$$+DFIs^6 + DFJs^7 + DHGs^3 + DIGs^4 + DJGs^5 + Ks^2 + Ls + M$$

(A.14)

The terms above third order in (A.14) are not valid since a third order truncation was performed in (A.6).

Substituting $I_b + i = I$ into (A.14):

$$\frac{i}{V} = \left(AGH + M - {}^{I_b}\!/_{V}\right) + (AEH + AGI + GBH + L)s + (EA + GB + AH)s' + (A)s''$$
$$+(AEI + AFH + AGJ + BEH + GBI + CGH + K)s^2$$
$$+(2AF + 2EB + 2CG + AI + HB)ss' + (B)s' s' + (B)ss''$$
$$+(AEJ + AFI + BEI + BFH + GBJ + CEH + CGI + DHG)s^3$$
$$+(3FB + 3CE + 3DG + AJ + IB + CH)s^2 s' + (C)s^2 s'' + (2C)ss' s'$$

(A.15)

Simplifying the expression in (A.15) results in:

$$i = a + bs + cs' + ds'' + es^2 + fss' + gs's' + hss'' + ks^3 + ls^2s' + ms^2s'' + nss's' \qquad \text{(A.16)}$$

The constants *a, b, c, ...* correlate to the coefficients in equation (A.15) and are expressed totally in terms of the laser parameters and the bias current.

To derive the Volterra transfer functions for the predistortion block we treat s or $s(t)$ as the input and i or $i(t)$ as the output of the system. In the truest sense, this is the derivation for a postdistorter since the output of the laser which is S is being used as the input to this system. However, this system will be placed in front of the laser so that ultimately, it will act as a predistorter.

The first order Volterra transfer function is obtained by substituting $s(t) = Se^{j\omega t}$, where S is an arbitrary bias level of photons and $e^{j\omega t}$ is a unit phasor, into equation (A.16) and taking the coefficients of $e^{j\omega t}$ to get $P_1(\omega)$. The term S is optional. If the input to the predistorter is photon density, the S term is not required. However, if the input to the predistorter is current, as will be the case in later simulations, the S term is required to normalize the predistorter transfer functions. It is included here. In equation (A.16), only the first order terms will create output terms of the form $e^{j\omega t}$. Thus:

$$P_1(\omega) = \left(b + cj\omega - d\omega^2\right)S \qquad \text{(A.17)}$$

To derive the second order Volterra transfer function, $s(t) = S\left(e^{j\omega_1 t} + e^{j\omega_2 t}\right)$ is substituted into equation (A.16) and the coefficients of $e^{j(\omega_1+\omega_2)t}$ form $P_2(\omega_1, \omega_2)$. This time, only second order terms in (A.16) will contribute terms of the form $e^{j(\omega_1+\omega_2)t}$ to the output. Thus:

$$P_2(\omega_1,\omega_2)=\left(2e+fj(\omega_1+\omega_2)-h(\omega_1+\omega_2)^2\right)S^2 \qquad \text{(A.18)}$$

In a similar way $P_3(\omega_1,\omega_2,\omega_3)$ is derived by substituting $s(t)=S\left(e^{j\omega_1 t}+e^{j\omega_2 t}+e^{j\omega_3 t}\right)$ into (A.16) and taking the coefficients of the term $e^{j(\omega_1+\omega_2+\omega_3)t}$ to get $P_3(\omega_1,\omega_2,\omega_3)$.

$$P_3(\omega_1,\omega_2,\omega_3)=\left(6k+2lj(\omega_1+\omega_2+\omega_3)-2m(\omega_1+\omega_2+\omega_3)^2\right)S^3 \qquad \text{(A.19)}$$

These three functions (A.17), (A.18) and (A.19) represent the Volterra transfer functions for the predistorter.

APPENDIX B

Derivation of the Volterra Model for the Laser

The derivation of the Volterra transfer functions for the laser are outlined below. The transfer functions describing the laser will be derived by determining the inverse of the predistorter functions. The first, second and third order transfer functions representing the predistorter are:

$$P_1(\omega) = \left(b + cj\omega - d\omega^2\right)S \tag{B.1}$$

$$P_2(\omega_1, \omega_2) = \left(2e + fj(\omega_1 + \omega_2) - h(\omega_1 + \omega_2)^2\right)S^2 \tag{B.2}$$

$$P_3(\omega_1, \omega_2, \omega_3) = \left(6k + 2lj(\omega_1 + \omega_2 + \omega_3) - 2m(\omega_1 + \omega_2 + \omega_3)^2\right)S^3 \tag{B.3}$$

The transfer functions describing the laser are determined as follows:

1) First Order

The first order functions have a simple relation:

$$L_1(\omega) = \frac{1}{P_1(\omega)} \tag{B.4}$$

2) Second Order

The second order function, $L_2(\omega_1, \omega_2)$, is obtained by applying an input equal to $e^{j\omega_1 t} + e^{j\omega_2 t}$ to the system and then canceling the terms of $e^{j(\omega_1+\omega_2)t}$ which correspond to the operation of the second order system.

The input to the predistorter is:

$$a(t) = e^{j\omega_1 t} + e^{j\omega_2 t} \tag{B.5}$$

The output of the predistorter is:

$$y(t) = P_1(\omega_1)e^{j\omega_1 t} + P_1(\omega_2)e^{j\omega_2 t} + P_2(\omega_1,\omega_2)e^{j(\omega_1+\omega_2)t} \tag{B.6}$$

Using (B.6) as the input to the laser, the output of the laser becomes:

$$\begin{aligned} x(t) = {} & L_1(\omega_1)P_1(\omega_1)e^{j\omega_1 t} + L_1(\omega_2)P_1(\omega_2)e^{j\omega_2 t} + L_1(\omega_1+\omega_2)P_2(\omega_1,\omega_2)e^{j(\omega_1+\omega_2)t} \\ & + L_2(\omega_1,\omega_2)P_1(\omega_1)P_1(\omega_2)e^{j(\omega_1+\omega_2)t} \\ & + L_2(\omega_1,\omega_1+\omega_2)P_1(\omega_1)P_2(\omega_1,\omega_2)e^{j(2\omega_1+\omega_2)t} \\ & + L_2(\omega_2,\omega_1+\omega_2)P_1(\omega_2)P_2(\omega_1,\omega_2)e^{j(\omega_1+2\omega_2)t} \end{aligned} \tag{B.7}$$

The coefficients of $e^{j(\omega_1+\omega_2)t}$ should be zero. Thus, with the use of (B.4):

$$L_2(\omega_1,\omega_2) = \frac{-P_2(\omega_1,\omega_2)}{P_1(\omega_1)P_1(\omega_2)P_1(\omega_1+\omega_2)} \tag{B.8}$$

3) Third Order

The third order function, $L_3(\omega_1,\omega_2,\omega_3)$, is determined in a similar way. The input in this case consists of three tones, $e^{j\omega_1 t} + e^{j\omega_2 t} + e^{j\omega_3 t}$.

The input to the predistorter is:

$$a(t) = e^{j\omega_1 t} + e^{j\omega_2 t} + e^{j\omega_3 t} \tag{B.9}$$

The output of the predistorter is:

$$y(t) = P_1(\omega_1)e^{j\omega_1 t} + P_1(\omega_2)e^{j\omega_2 t} + P_1(\omega_3)e^{j\omega_3 t} + P_2(\omega_1,\omega_2)e^{j(\omega_1+\omega_2)t} + P_2(\omega_1,\omega_3)e^{j(\omega_1+\omega_3)t} + P_2(\omega_2,\omega_3)e^{j(\omega_2+\omega_3)t} + P_3(\omega_1,\omega_2,\omega_3)e^{j(\omega_1+\omega_2+\omega_3)t} \quad \text{(B.10)}$$

Using (B.10) as the input to the laser, the output of the laser becomes:

$$\begin{aligned} x(t) = {} & L_1(\omega_1)P_1(\omega_1)e^{j\omega_1 t} + L_1(\omega_2)P_1(\omega_2)e^{j\omega_2 t} + L_1(\omega_3)P_1(\omega_3)e^{j\omega_3 t} \\ & + L_1(\omega_1+\omega_2)P_2(\omega_1,\omega_2)e^{j(\omega_1+\omega_2)t} + L_1(\omega_1+\omega_3)P_2(\omega_1,\omega_3)e^{j(\omega_1+\omega_3)t} \\ & + L_1(\omega_2+\omega_3)P_2(\omega_2,\omega_3)e^{j(\omega_2+\omega_3)t} \\ & + L_1(\omega_1+\omega_2+\omega_3)P_3(\omega_1,\omega_2,\omega_3)e^{j(\omega_1+\omega_2+\omega_3)t} \\ & + L_2(\omega_1,\omega_2+\omega_3)P_1(\omega_1)P_2(\omega_2,\omega_3)e^{j(\omega_1+\omega_2+\omega_3)t} \\ & + L_2(\omega_2,\omega_1+\omega_3)P_1(\omega_2)P_2(\omega_1,\omega_3)e^{j(\omega_1+\omega_2+\omega_3)t} \\ & + L_2(\omega_3,\omega_1+\omega_2)P_1(\omega_3)P_2(\omega_1,\omega_2)e^{j(\omega_1+\omega_2+\omega_3)t} + \cdots \\ & + L_3(\omega_1,\omega_2,\omega_3)P_1(\omega_1)P_1(\omega_2)P_1(\omega_3)e^{j(\omega_1+\omega_2+\omega_3)t} + \cdots \end{aligned} \quad \text{(B.11)}$$

The coefficients of $e^{j(\omega_1+\omega_2+\omega_3)t}$ should be zero. Thus:

$$\begin{aligned} L_3(\omega_1,\omega_2,\omega_3) = {} & \frac{-L_1(\omega_1+\omega_2+\omega_3)P_3(\omega_1,\omega_2,\omega_3)}{P_1(\omega_1)P_1(\omega_2)P_1(\omega_3)} - \frac{L_2(\omega_1,\omega_2+\omega_3)P_1(\omega_1)P_2(\omega_2,\omega_3)}{P_1(\omega_1)P_1(\omega_2)P_1(\omega_3)} \\ & - \frac{L_2(\omega_2,\omega_1+\omega_3)P_1(\omega_2)P_2(\omega_1,\omega_3)}{P_1(\omega_1)P_1(\omega_2)P_1(\omega_3)} - \frac{L_2(\omega_3,\omega_2+\omega_1)P_1(\omega_3)P_2(\omega_2,\omega_1)}{P_1(\omega_1)P_1(\omega_2)P_1(\omega_3)} \end{aligned} \quad \text{(B.12)}$$

$$\begin{aligned} L_3(\omega_1,\omega_2,\omega_3) = {} & \frac{-1}{P_1(\omega_1+\omega_2+\omega_3)P_1(\omega_1)P_1(\omega_2)P_1(\omega_3)} \\ & \times \left[P_3(\omega_1,\omega_2,\omega_3) - \frac{P_2(\omega_1,\omega_2+\omega_3)P_2(\omega_2,\omega_3)}{P_1(\omega_2+\omega_3)} - \frac{P_2(\omega_2,\omega_1+\omega_3)P_2(\omega_1,\omega_3)}{P_1(\omega_1+\omega_3)} - \right. \\ & \left. \frac{P_2(\omega_3,\omega_1+\omega_2)P_2(\omega_1,\omega_2)}{P_1(\omega_1+\omega_2)} \right] \end{aligned} \quad \text{(B.13)}$$

The functions (B.4), (B.8) and (B.13) represent the Volterra transfer functions for the laser.

APPENDIX C

Response of the Laser and Predistorter to a Tone Input

The response of the predistorter and laser diode in cascade to a single frequency tone can be calculated. To proceed with the analysis, a frequency domain approach is used.

The output of a *p-th* order Volterra system in the frequency domain is:

$$Y_p(\omega) = \frac{1}{(2\pi)^{p-1}} \int_{-\infty}^{\infty}\int_{-\infty}^{\infty}\cdots\int_{-\infty}^{\infty} H_p\left(\omega-\omega_1-\omega_2-\cdots-\omega_{p-1},\omega_1,\omega_2,\cdots\omega_{p-1}\right) X\left(\omega-\omega_1-\omega_2-\cdots-\omega_{p-1}\right)X(\omega_1)X(\omega_2)\cdots X\left(\omega_{p-1}\right)d\omega_1 d\omega_2\cdots d\omega_{p-1} \tag{C.1}$$

If we consider a system that is modeled with three Volterra systems: first order, second order and third order, then the output of the system is the sum of the output of each Volterra operator. In the frequency domain this can be expressed in the following form:

$$Y(\omega) = H_1(\omega)X(\omega) + \frac{1}{2\pi}\int_{-\infty}^{\infty} H_2(\omega-\omega_1,\omega_1)X(\omega-\omega_1)X(\omega_1)d\omega_1 + \frac{1}{(2\pi)^2}\int_{-\infty}^{\infty}\int_{-\infty}^{\infty} H_3(\omega-\omega_1-\omega_2,\omega_1,\omega_2)X(\omega-\omega_1-\omega_2)X(\omega_1)X(\omega_2)d\omega_1 d\omega_2 \tag{C.2}$$

If a single frequency tone, $X(\omega) = \delta(\omega-\omega_o)$, is applied to the predistortion block with Fourier transforms P_1, P_2 and P_3, the frequency domain output of the predistorter is:

$$Y(\omega) = P_1(\omega)\delta(\omega-\omega_o) + \frac{1}{2\pi}\int_{-\infty}^{\infty} P_2(\omega-\omega_1,\omega_1)\delta(\omega-\omega_1-\omega_o)\delta(\omega_1-\omega_o)d\omega_1$$
$$+\frac{1}{(2\pi)^2}\int_{-\infty-\infty}^{\infty\infty} P_3(\omega-\omega_1-\omega_2,\omega_1,\omega_2)\delta(\omega-\omega_1-\omega_2-\omega_o)\delta(\omega_1-\omega_o)\delta(\omega_2-\omega_o)d\omega_1 d\omega_2 \quad (C.3)$$

which becomes:

$$Y(\omega) = P_1(\omega_o)\delta(\omega-\omega_o) + \frac{1}{2\pi}P_2(\omega_o,\omega_o)\delta(\omega-2\omega_o)$$
$$+\frac{1}{(2\pi)^2}P_3(\omega_o,\omega_o,\omega_o)\delta(\omega-3\omega_o) \quad (C.4)$$

Now, $Y(\omega)$ is the input to the laser transfer functions described by L_1, L_2 and L_3. Again, the laser is modeled by three Volterra operators. The output of the laser is:

$$R(\omega) = L_1(\omega)Y(\omega) + \frac{1}{2\pi}\int_{-\infty}^{\infty} L_2(\omega-\omega_1,\omega_1)Y(\omega-\omega_1)Y(\omega_1)d\omega_1$$
$$+\frac{1}{(2\pi)^2}\int_{-\infty-\infty}^{\infty\infty} L_3(\omega-\omega_1-\omega_2,\omega_1,\omega_2)Y(\omega-\omega_1-\omega_2)Y(\omega_1)Y(\omega_2)d\omega_1 d\omega_2 \quad (C.5)$$

We calculate the output of each Volterra operator separately and determine the total output as the sum of the output of each operator:

$$R(\omega) = R_1(\omega) + R_2(\omega) + R_3(\omega) \quad (C.6)$$

with:

$$R_1(\omega) = L_1(\omega)Y(\omega) \quad (C.7)$$

$$R_2(\omega) = \frac{1}{2\pi}\int_{-\infty}^{\infty} L_2(\omega-\omega_1,\omega_1)Y(\omega-\omega_1)Y(\omega_1)d\omega_1 \quad (C.8)$$

$$R_3(\omega) = \frac{1}{(2\pi)^2} \int_{-\infty}^{\infty} \int_{-\infty}^{\infty} L_3(\omega - \omega_1 - \omega_2, \omega_1, \omega_2) Y(\omega - \omega_1 - \omega_2) Y(\omega_1) Y(\omega_2) d\omega_1 d\omega_2 \tag{C.9}$$

Now, we substitute equation (C.4) into (C.7) through (C.9) to determine the output:

$$R_1(\omega) = L_1(\omega)\Big[P_1(\omega_o)\delta(\omega - \omega_o) + \frac{1}{2\pi} P_2(\omega_o, \omega_o)\delta(\omega - 2\omega_o) + \frac{1}{(2\pi)^2} P_3(\omega_o, \omega_o, \omega_o)\delta(\omega - 3\omega_o) \Big] \tag{C.10}$$

Expanding (C.10) gives (C.11):

$$R_1(\omega) = L_1(\omega_o)P_1(\omega_o)\delta(\omega - \omega_o) + \frac{1}{2\pi} L_1(2\omega_o)P_2(\omega_o, \omega_o)\delta(\omega - 2\omega_o) + \frac{1}{(2\pi)^2} L_1(3\omega_o)P_3(\omega_o, \omega_o, \omega_o)\delta(\omega - 3\omega_o) \tag{C.11}$$

The same method is used for $R_2(\omega)$:

$$\begin{aligned} R_2(\omega) = \frac{1}{2\pi} \int_{-\infty}^{\infty} L_2(\omega - \omega_1, \omega_1) \Big[& P_1(\omega_o)\delta(\omega - \omega_1 - \omega_o) \\ & + \frac{1}{2\pi} P_2(\omega_o, \omega_o)\delta(\omega - \omega_1 - 2\omega_o) + \frac{1}{(2\pi)^2} P_3(\omega_o, \omega_o, \omega_o)\delta(\omega - \omega_1 - 3\omega_o) \Big] \\ & \times \Big[P_1(\omega_o)\delta(\omega_1 - \omega_o) + \frac{1}{2\pi} P_2(\omega_o, \omega_o)\delta(\omega_1 - 2\omega_o) \\ & + \frac{1}{(2\pi)^2} P_3(\omega_o, \omega_o, \omega_o)\delta(\omega_1 - 3\omega_o) \Big] d\omega_1 \end{aligned} \tag{C.12}$$

Expanding (C.12) gives (C.13):

$$R_2(\omega)=\frac{1}{2\pi}L_2(\omega_o,\omega_o)P_1^{\,2}(\omega_o)\delta(\omega-2\omega_o)$$
$$+\frac{1}{(2\pi)^2}L_2(2\omega_o,\omega_o)P_2(\omega_o,\omega_o)P_1(\omega_o)\delta(\omega-3\omega_o) \qquad \text{(C.13)}$$
$$+\frac{1}{(2\pi)^2}L_2(\omega_o,2\omega_o)P_1(\omega_o)P_2(\omega_o,\omega_o)\delta(\omega-3\omega_o)$$

The terms above third order in (C.13) are not valid because of the third order truncation in (A.6) and so they are not shown.

The same method is used for $R_3(\omega)$:

$$R_3(\omega)=\frac{1}{(2\pi)^2}\int_{-\infty}^{\infty}\int_{-\infty}^{\infty}L_3(\omega-\omega_1-\omega_2,\omega_1,\omega_2)\Big[P_1(\omega_o)\delta(\omega-\omega_1-\omega_2-\omega_o)$$
$$+\frac{1}{2\pi}P_2(\omega_o,\omega_o)\delta(\omega-\omega_1-\omega_2-2\omega_o)+\frac{1}{(2\pi)^2}P_3(\omega_o,\omega_o,\omega_o)\delta(\omega-\omega_1-\omega_2-3\omega_o)\Big]$$
$$\times\Big[P_1(\omega_o)\delta(\omega_1-\omega_o)+\frac{1}{2\pi}P_2(\omega_o,\omega_o)\delta(\omega_1-2\omega_o)+\frac{1}{(2\pi)^2}P_3(\omega_o,\omega_o,\omega_o)\delta(\omega_1-3\omega_o)\Big]$$
$$\times\Big[P_1(\omega_o)\delta(\omega_2-\omega_o)+\frac{1}{2\pi}P_2(\omega_o,\omega_o)\delta(\omega_2-2\omega_o)$$
$$+\frac{1}{(2\pi)^2}P_3(\omega_o,\omega_o,\omega_o)\delta(\omega_2-3\omega_o)\Big]d\omega_1 d\omega_2$$

(C.14)

The coefficients of the δ-functions can be computed by calculating this double integral.

The third order coefficients are combined with the coefficients of the first and second order computations to determine the output of the laser. These coefficients represent the entire response of the cascaded predistorter and laser to a tone input $\left(e^{j\omega t}\right)$. The coefficients are listed below:

$\delta(\omega-\omega_o)$:

$$L_1(\omega_o)P_1(\omega_o)=1 \qquad \text{(C.15)}$$

$\delta(\omega - 2\omega_o)$:

$$\frac{1}{2\pi}\left[L_1(2\omega_o)P_2(\omega_o,\omega_o) + L_2(\omega_o,\omega_o)P_1^2(\omega_o)\right] \tag{C.16}$$

$\delta(\omega - 3\omega_o)$:

$$\begin{aligned}&\frac{1}{(2\pi)^2}\left[L_1(3\omega_o)P_3(\omega_o,\omega_o,\omega_o) + L_2(2\omega_o,\omega_o)P_2(\omega_o,\omega_o)P_1(\omega_o)\right.\\&\left.+L_2(\omega_o,2\omega_o)P_1(\omega_o)P_2(\omega_o,\omega_o) + L_3(\omega_o,\omega_o,\omega_o)P_1^3(\omega_o)\right]\end{aligned} \tag{C.17}$$

APPENDIX D

ECA-2 Circuit Listing for Laser Model A

1	Vo	0	0	1.		
2	Ro	9	0	1.u		
3	Roo	9	0	1.M		
4	I1	9	0	69.44E+33		
5	Gd1	1	0	0.		
6	R1a	1	3	3.32n		
7	R1b	3	0	400.p		
8	C1	1	0	1.		
9	D1	2	1	1.G	F	0.
10	+			10.E-21	Z	4.6E+24
11	Mv	6	0	1.		
12	Gv	2	4	1.p		
13	Gvm	4	0	1.T		
14	Rq	2	4	100.E+48		
15	I2	3	0	1.615M		
16	Gd2	5	0	0.		
17	I3	4	0	646.G		
18	Gd3	5	0	0.		
19	R2	5	0	2.p		
20	C2	5	0	1.		
21	I4	5	0	1.		
22	Gd4	6	0	0.		
23	R3	6	0	1.	P1	
24	+			-38.E-24	P2	

ECA-2 Circuit Listing for Laser Model B

1	Vo	0	0	1.		
2	Ro	9	0	1.u		
3	Roo	9	0	1.M		
4	I1	9	0	1.7361E+36		
5	Gd1	1	0	0		
6	R1a	1	3	2.6n		
7	R1b	3	0	400.p		
8	C1	1	0	1.		
9	D1	2	1	1.G	F	0
10	+			10.E-21	Z	1.E+24
11	Mv	6	0	1		
12	Gv	2	4	3.p		
13	Gvm	4	0	1.T		
14	Rq	2	4	100.E+48		
15	I2	3	0	850.K		
16	Gd2	5	0	0		
17	I3	4	0	340.G		
18	Gd3	5	0	0		
19	R2	5	0	2.p		
20	C2	5	0	1		
21	I4	5	0	1		
22	Gd4	6	0	0		
23	R3	6	0	1.	P1	
24	+			-30.E-24	P2	